Brazil Oil & Gas, tt_nrg and Norway Oil & Gas

EPRASHEED
signature series

2012 – Issue 27

Saudi Arabia oil & gas

Saudi Arabia Oil & Gas (Print) ISSN 2045-6670
www.saudiarabiaoilandgas.com
Saudi Arabia Oil & Gas (Online) ISSN 2045-6689

Maximising the Value of the Intelligent Field

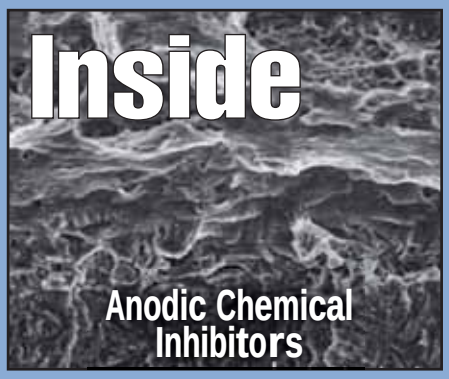

Inside

Anodic Chemical Inhibitors

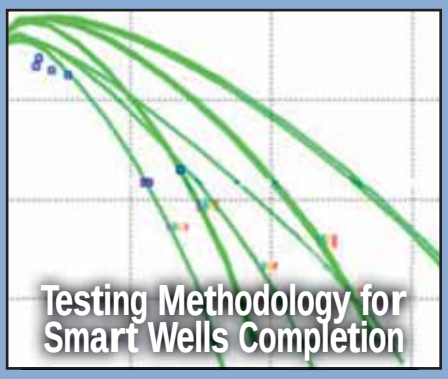

Testing Methodology for Smart Wells Completion

Want sealed frameworks from geological and geophysical data in minutes, not weeks? **Speed Up**

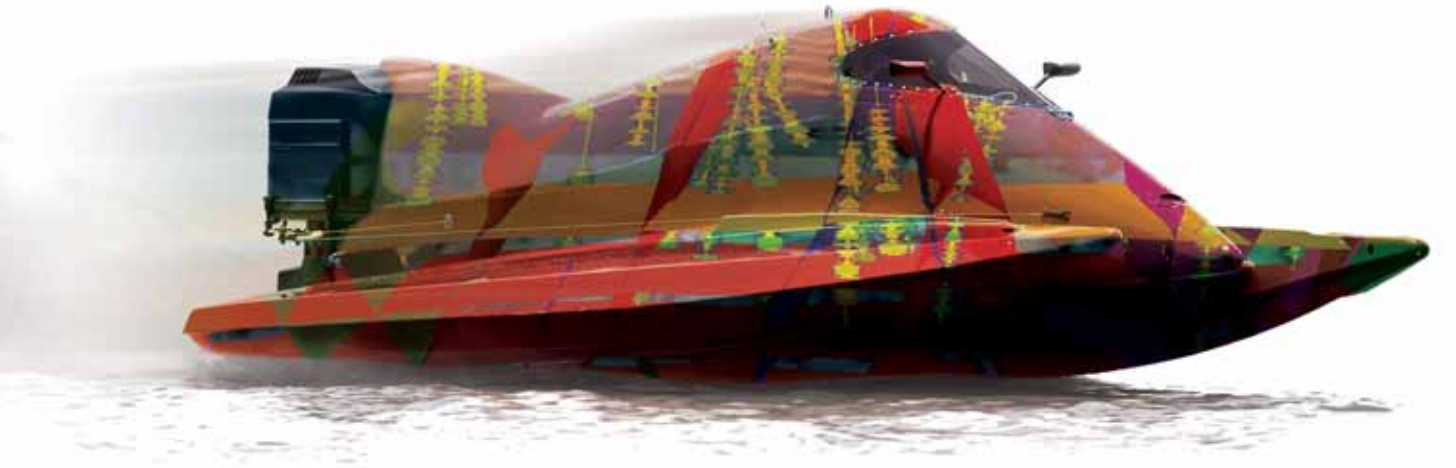

DecisionSpace® Desktop software automatically generates accurate sealed frameworks in about a minute.

As geoscientists interpret data, Landmark's new unified DecisionSpace® Desktop software automatically constructs fault networks, seals horizons against the fault network and generates a sealed framework. When geologists make picks or geophysicists interpret sections, watch live updates ripple through the framework and then create accurate, report-quality maps instantly. What once took hours, or even days, now takes just a minute.

So speed up your cycle time. Get better answers faster. Visit halliburton.com/decisionspacedesktop.

High Science Simplified®

HALLIBURTON | Landmark Software & Services

Who is going to help discover the energy for a global population expected to grow 20% by 2025?

Join us, and you will.

At Chevron, we're dedicated to providing the energy the world needs to keep moving forward. Here you can be part of a diverse team of professionals from different disciplines and skill sets working together. A team that welcomes tomorrow's challenges and believes the best way to solve them is through collaboration. So no matter what your expertise, you'll have the tools and support to make a difference every day. Find out how far your skills and talents can take you. For local and global opportunities, visit us online today.

Chevron

Human Energy®

An equal opportunity employer that values diversity and fosters a culture of inclusion.

مدينة الملك عبدالعزيز
للعلوم والتقنية KACST

Oil and Gas Research Institute

Hydrocarbon resources (crude oil and gas) are the main source of world energy, and as the international demand increases, the technical challenges increase to meet that demand. Hydrocarbon production optimization at minimum cost and the need to serve the national petroleum industry has been the driving force behind the establishment of the Oil and Gas Research Institute (OGRI) at King Abdulaziz City for Science and Technology (KACST). OGRI is a governmental research and development entity. Its applied research activities concentrate on the upstream sector of the petroleum industry. Fields of interest cover most of the petroleum science and engineering aspects through four main divisions:

- Reservoir Characterization and Numerical Simulation,
- Drilling Engineering,
- Rock Mechanics,
- Production and Enhanced Recovery.

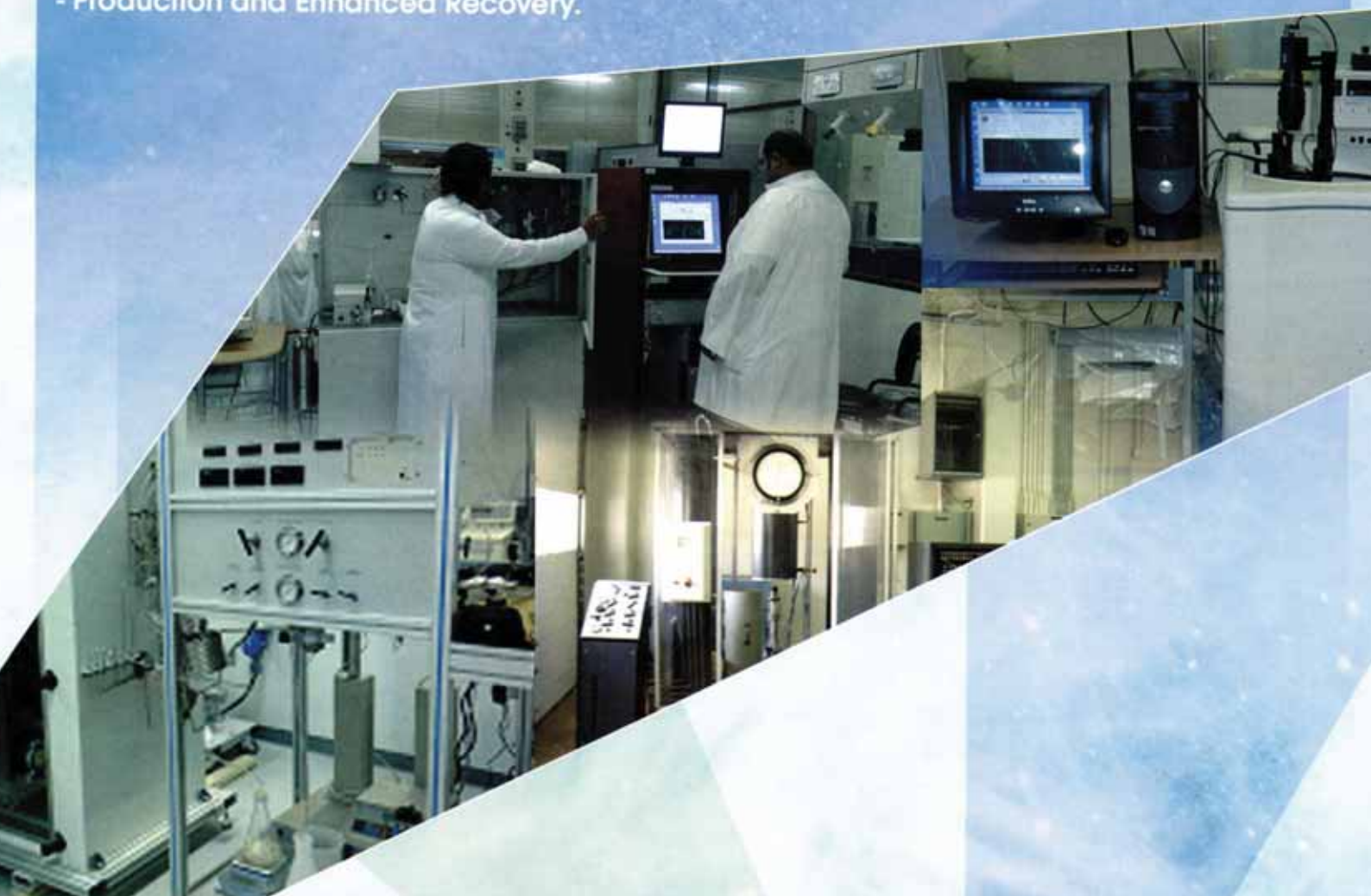

Services Provided

Service	Techniques
CONVENTIONAL CORE ANALYSIS	➤ Helium Porosity (Ambient Conditions) ➤ Gas Permeability & Porosity (Low and Reservoir Overburden Stress) ➤ Klinkenberg Correction ➤ Liquid Permeability (Reservoir Conditions)
SPECIAL CORE ANALYSIS (SCAL)	**CAPILLARY PRESSURE TESTS** ➤ Centrifuge Techniques (Reservoir Conditions) ➤ Low and High Pressure Mercury Injection and Withdrawal Technique ➤ Pore Size Distribution (PSD) **RELATIVE PERMEABILITY MEASUREMENTS** ➤ Unsteady State Flooding Technique (Reservoir Conditions) ➤ Centrifuge Technique (Reservoir Conditions) **WETTABILITY TESTS** ➤ Centrifuge USBM Method ➤ Contact angle Measurement (Ambient and Reservoir Conditions) ➤ Interfacial Tension Measurements **PETROGRAPHIC SERVICES** ➤ Sieve Analysis ➤ Particle Size Analysis ➤ Thin section
RESERVOIR FLUID ANALYSIS	➤ Interfacial & Surface tension ➤ Gas and Gas Condensate Viscosity ➤ Refractive index and pH ➤ Contact angle
ADVANCED RESERVOIR ENGINEERING	➤ Water-Oil /Water-Gas Displacement ➤ Gas Flooding and WAG ➤ Chemical Flooding
PETROLEUM RELATED ROCK MECHANICS	➤ Uniaxial, Triaxial, and Hydrostatic Compressive strength ➤ Stress-Strain Behavior ➤ Failure Envelope ➤ Elastic moduli ➤ Bulk and Pore Compressibility ➤ Fracture Toughness

OGRI - KACST - K.S.A - P.O. Box. 6086 Riyadh 11442
Tel. : +966 1 4813307 Fax : +966 1 4813526

EPRASHEED
signature series
2012 – Issue 27
Saudi Arabia oil & gas
www.saudiarabiaoilandgas.com

Contents

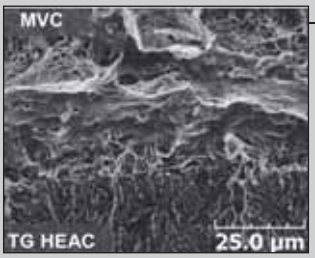

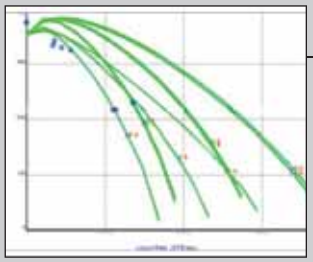

CEO and Founder
EPRasheed
Wajid Rasheed
wajid.rasheed@eprasheed.com

Editors
Majid Rasheed
Mauro Martins

Design
Sue Smith
sue.smith@eprasheed.com

United Kingdom
► Head Office
Tel: (44) 207 193 1602

► Adam Mehar
adam.mehar@saudiarabiaoilandgas.com
Main: (44) 1753 708872
Fax: (44) 1753 725460
Mobile: (44) 777 2096692

Saudi Arabia
► Akram ul Haq
PO BOX 3260, Jeddah 21471
akram.ul.haq@saudiarabiaoilandgas.com
Tel: (966) 557 276 426

► Mohanned AlSagri
mohanned.alsagri@saudiarabiaoilandgas.com

Brazil
► Ana Felix
afelix@braziloilandgas.com
Tel: (55) 21 9714 8690

► Fabio Jones
fabio.jones@braziloilandgas.com
Tel: (55) 21 9392 7821

► Roberto S. Zangrando
rzangrando@braziloilandgas.com
Tel: (55) 22 8818 8507

Change to Fracology℠

Weatherford puts the science in hydraulic fracturing for superior reservoir stimulation.

Fracturing in oil and gas environments requires an ever more sophisticated approach for maximized results.

Fracology **fine-tunes the science of hydraulic fracturing by synchronizing** critical services:

Formation Evaluation reveals candidate viability – identifies gas content, quality and storage capacity of the formation to ensure optimal drilling and fracturing approaches.

Wellsite Analysis of core and mud gas samples pinpoints pay zones **and fluid types – enhances geosteering, well placement and completion** operations.

Execution Monitoring allows fracturing parameters to be adjusted on **the fly for optimal fluid/proppant placement and results.**

Microseismic Verfication Surveys affirm completion quality and provide a 3-D view of the drainage network to ensure optimized treatment is achieved.

Fracology is another example of **Tactical Technology™** that can change the way you think about all of your service needs. Contact your Weatherford representative at **fracology@weatherford.com** or visit us online at **weatherford.com/fracology**. Put science to work in your tight shales.

Drilling
- Drilling Services
  - Fracturing services
  - Rock mechanics
  - Shale rock properties

Evaluation
- Integrated laboratory services
- Surface logging
  - Formation evaluation
- Wireline services
  - Microseismic

Completion
- Pressure pumping services
  - Hydraulic fracturing
  - Fluid systems

Production

Intervention

The *change* will do you good℠

Weatherford
Facility Base, Dhahran Abqaiq Road,
Lot No. 6 & 7 In Plan No 404/1
P.O. Box 79106
Alkhobar 31952, Saudi Arabia
Tel: +966.(3).807.5000

Weatherford®

weatherford.com

Profit from experience.[SM]

Solid experience. Profound results.

Technology works better when it's backed by expertise.

Solid expandable technology offers unprecedented value to the oil and gas industry. This innovative approach to tubulars enables producers to reach total depth and pay zones faster – and with fewer uncertainties – for significant cost savings, increased production and accelerated reserves.

Enventure has been providing SET® solid expandable solutions longer than any other company in the business. With more than 1,200 installations to our credit, we understand the potential problems and know best how to resolve them.

Keep your projects – and bottom line – on target. Contact Enventure's Dubai office at **+971.4.363.7199**, our Saudi Arabia office at **+966.3.812.1399 ext 225**, or visit **www.EnventureGT.com**.

www.EnventureGT.com

Offshore Northern Seas Conference Focuses on Energy

STAVANGER, Norway, 19 September 2012

Saudi Aramco's participation in Offshore Northern Seas (ONS) conference and exhibition Aug. 28-31 in Stavanger, Norway, brought into focus energy-related geopolitical issues.

Thirty influential government and industry leaders met for the first ONS Summit on Aug. 27. Among those attending was Saudi Aramco's senior vice president of Industrial Relations Abdulaziz F. Al-Khayyal.

The key influencers were brought together to make a positive difference in the energy industry.

Participants included Ola Borten Moe, Minister of Oil and Energy for Norway, and Mark Dierikx, Director General of Energy for The Netherlands. Following the

> "... exploiting vast opportunities to enhance energy efficiency; ... using technology in general to minimize the environmental footprint of fossil energy sources..."

“... making greater use of cleaner natural gas in the global energy mix; ... taking advantage of emergent carbon capture and storage technologies; ... gradually deploying renewable and alternatives to complement vast conventional energy sources and their massive worldwide infrastructure.”

summit, the ONS conference was officially opened Aug. 28 by King Harald V of Norway.

“Confronting Energy Paradoxes” was the keynote theme, which was debated on the basis of three global challenges:

1. Prosperity or clean air – or both?
2. Will technology continue to secure energy supply?
3. Why not more natural gas?

Al-Khayyal participated on a panel with other energy experts that also included: Helge Lund, president and CEO of Statoil ASA; Peter Voser, chief executive officer Royal Dutch Shell; Maria Van Der Hoeven, executive director of the International Energy Agency; and Rudi Rubiandini, vice minister of Energy and Mineral Resources, Republic of Indonesia.

Moderated by Zeinab Badawi of the British Broadcasting Service, the debate saw Al-Khayyal raise five strategies that must align in relation to the first challenge: “First, exploiting vast opportunities to enhance energy efficiency; second, using technology in general to minimize the environmental footprint of fossil energy sources; third, making greater use of cleaner natural gas in the global energy mix; fourth, taking advantage of emergent carbon capture and storage technologies; and fifth, gradually deploying renewable and alternatives to complement vast conventional energy sources and their massive worldwide infrastructure.”

The conference was a key feature of the biennial ONS event, which also provided Saudi Aramco with the opportunity to recruit top talent through workshops. More than 50,000 delegates and 1,300 exhibiting companies ensured the event, established in 1974, remains a major international arena for the promotion and advancement of the offshore energy industry.

Company Employees Learn Mangrove Secrets

19 September 2012 – A team of young employees from the Environmental Protection Department (EPD) recently swapped their desks for the mangrove forests of Kenya as they embarked on a mangrove study field trip.

As EPD presses on with its program to plant 1 million mangroves across the Kingdom's East Coast over the next four years, the expedition provided the Saudi Aramco team with valuable insights into mangrove conservation — an important company initiative.

A team of young employees from the Environmental Protection Department (EPD) recently swapped their desks for the mangrove forests of Kenya as they embarked on a mangrove study field trip.

As EPD presses on with its program to plant 1 million mangroves across the Kingdom's East Coast over the next four years, the expedition provided the Saudi Aramco team with valuable insights into mangrove conservation – an important company initiative.

> "... the expedition provided the Saudi Aramco team with valuable insights into mangrove conservation – an important company initiative."

> The expedition reinforced the importance of mangrove ecosystems for human well-being, particularly as a coastline storm protection barrier and their valuable role for the fisheries industry and eco-tourism development.

For 12 days, they joined volunteers from the UK, Mozambique, Tanzania and Kenya as they converged on Gazi Bay, where, just like the Kingdom, mangroves are a crucial element of the local ecosystem.

The trip was organized by UK based Earthwatch, a world renowned environmental charity. Earthwatch receive support from Saudi Aramco through its donation program.

Representing Saudi Aramco and the Kingdom were EPD members Ibrahim Al-Saihati, Muhammad Al-Yousaf and Muaiad Al-Turki.

During the course of the trip, the Saudi Aramco group participated in planting mangroves, conducting field research and collecting scientific data.

The group also received presentations from international mangrove and environmental experts that were often delivered in the field under the shade of mangrove trees.

For the EPD team, the expedition was proof that mangrove conservation is a worldwide concern. Saudi Aramco's mangrove plantation achievements are part of a global effort to preserve mangroves, which are an essential part of the world's ecosystems.

The group also noted that mangrove degradation in Kenya is similar to the problems facing the Kingdom's mangrove habitats.

The expedition reinforced the importance of mangrove ecosystems for human well-being, particularly as a coastline storm protection barrier and their valuable role for the fisheries industry and eco-tourism development.

The EPD group was given the opportunity to present Saudi Aramco's mangrove conservation efforts to the other participants; eliciting positive feedback and suggestions.

Saudi Aramco's own mangrove conservation program is spread across four sites in the Eastern Province. Each site will receive 60,000 mangroves annually. After five years, about 1.2 million mangroves will have been planted.

Also, the company has begun the ground work for the Kingdom's and the region's first mangrove Eco-park in Ras Tanura. The park is scheduled to be established in 2014, will cover an area of 62 square kilometers and will include an elevated boardwalk.

eMap Division Wins ESRI Award

DHAHRAN, 19 September 2012 – Saudi Aramco recently added to its already impressive track record by winning the distinguished Presidential Award for Executive Leadership in the Geographic Information Systems (GIS) field from the world leader in GIS systems, Environmental Systems Research Institute (ESRI).

This carefully selected tribute was awarded to the eMap Division from among a total of only 10 award winners from nominations worldwide. The selection was in recognition of the GIS strategic vision and leadership that has been shown by Saudi Aramco.

"This leading concept includes a world-class innovation, and that it is a source of inspiration for other projects, both within and outside the Middle East," said Dean Angelides, director of international operations for ESRI.

The honoring ceremony took place at the annual ESRI Senior Executive Seminar 2012 in San Diego, California, in the United States. The award was presented by Jack Dangermond, president of ESRI, to eMap Division administrator Khalid A. Al-Arfaj.

"The use of GIS has given us new insights into Saudi Aramco's huge operational area, in hydrocarbon exploration and extraction, safety, emergency management, and to safeguard Saudi Aramco's vast land assets from encroachment," said Computer Applications Department (CAD) manager Adel Doulab.

The award comes on top of previous GIS awards received by eMap in 2007 and 2010 in recognition of its providing robust GIS applications and integrating GIS technologies with corporate solutions such as SAP and PI systems.

MASTERGEAR UK

The **Stainless Steel** Gearbox Range.

Built to withstand the World's most **extreme environments.**

www.mastergearworldwide.com

Address to the 2012 Saudi Aramco Management Development Seminar

By Khalid A. Al-Falih, President and CEO, Saudi Aramco.

"Ladies and gentlemen, we're honored to host such an impressive cross-section of New York's business and civic community, after what I hope was a relaxing Memorial Day weekend. I know you could be unwinding at home after an intense day at work, so we appreciate you taking the time to join us.

For me, it's always a pleasure to be back in New York, a city which has figured prominently in our company's history – particularly as prior to moving to Dhahran in 1952, Aramco's corporate headquarters were at 505 Park Avenue, just two blocks east of where we are tonight.

And while I've visited New York many times, this is the first time I've given a formal speech in the 'Big Apple'. New Yorkers expect a lot from their speakers: from Martin Luther King's 'Beyond Vietnam' speech; to Lou Gehrig's moving farewell at Yankee Stadium, and Abraham Lincoln's 1860 Cooper Union address, which some say propelled him to the White House later that year. Assessing that speech, the New York Tribune said, 'No man ever made such an impression on his first appeal to a New York audience' So let me be clear from the outset that I will not try to outdo Honest Abe tonight!

But for me personally, this evening is made even more memorable by the presence of our former Chairman, President, and CEO, Frank Jungers, and his dear wife Julie. Frank was a genuinely transformative leader of our company, and I am very glad he is now finishing a book chronicling the enormous changes that characterized his era, and which I hope will also capture his personal contributions in making Saudi Aramco what it is today.

Frank's attendance tonight is even more fitting since it was his vision and foresight which led to the establishment of our flagship leadership training program – and the focus of tonight's event – the Saudi Aramco Management Development Seminar.

Back in 1975, Frank recognized that technical proficiency alone would not be enough for our future leaders, even for an engineering-oriented company like Aramco. From his own experience, he understood that so-called 'soft skills' like management prowess, business acumen, effective communications, smart diplomacy, and cross-cultural empathy would be essential for the company's rising leaders. And Frank realized there was no better place to learn those skills than in the epicenter of world economic and political power: the United States of America.

That's why, each year for more than a generation, around twenty of our most capable and promising managers and leaders spend three weeks in Washington and New York, hearing first-hand from distinguished speakers, exploring viewpoints and ideas, learning from their experiences, and drawing on that new-found knowledge to build the world's greatest energy and chemicals company, which is what we aspire to create.

One of those Seminar participants is seated at your table tonight, in part so they can better understand what motivates successful leaders such as yourselves.

“Events over the last four or five years have unfolded at a remarkable pace, revealing an unprecedented level of interdependence among the world’s regions and economic sectors and leading to unforeseen complexities that we all must manage.”

I’m sure each of them knows that effective leaders have finely tuned listening skills, so I will simply remind them of the famously restrained President Calvin Coolidge –known as ‘Silent Cal’ – who once said, ‘No man ever listened himself out of a job.’

One of the insights I hope they will take away from their interactions this evening is that each leader has different motivations, different skills, and different demands upon him or her. Over time, some leadership skills have endured, some have evolved, and yet others are new. But if there is a common requirement for leadership in the 21st century, it’s the ability to adapt not only oneself but also one’s company to an uncertain and fast-changing world.

For example, there was no playbook to turn to when the global financial crisis struck, nor a ready-made game plan for engineering a recovery. Events over the last four or five years have unfolded at a remarkable pace, revealing an unprecedented level of interdependence among the world’s regions and economic sectors and leading to unforeseen complexities that we all must manage. Given that we live in unpredictable times, it would be naive to assume that we have learned all of the lessons needed to steer through the next unexpected bump or twist in the road, or to realize the many opportunities our companies will come upon in the years to come – whatever industry we call our own.

So Saudi Aramco’s future leaders – like the leaders of other global organizations – must be agile enough to adapt to complex and often unexpected short-term challenges, and savvy enough to operate effectively in different business, political and cultural environments. At the same time, they have to focus on our strategic objectives and maximize Saudi Aramco’s contributions to the societies it serves.

Personally I am a firm believer that companies like ours will not stay in the vanguard unless we continue to master emerging economic trends, game-changing technologies, rising competition, shifting markets, uncertain geopolitics, and new priorities on the public agenda. In other words, tomorrow’s leaders will need both short-term dexterity and long-term vision.

That dual imperative has perhaps never been clearer in the world of petroleum than it is today. So, being in New York where markets reign supreme, let me briefly comment on today’s oil environment.

Looking at the short term, the US economy is still not firing on all cylinders, the Eurozone debt crisis remains a ticking bomb, and persistent headwinds continue to slow the global economy. In addition, there are a

> At Saudi Aramco we've raised crude oil production to over 10 million barrels per day – levels not seen in 30 years – which has contributed to global oil supplies exceeding demand by as much as one-and-a-half million barrels a day.

slew of oil market fundamentals and other key factors to consider, though we've argued consistently that petroleum market fundamentals are sound.

At Saudi Aramco we've raised crude oil production to over 10 million barrels per day – levels not seen in 30 years – which has contributed to global oil supplies exceeding demand by as much as one-and-a-half million barrels a day. The net result is that global stockpiles of oil are healthy, and in fact US crude oil inventories are nearing a 22-year high.

Yet geopolitical turbulence, non-oil financial investment flows, and fears of supply interruption as opposed to actual shortfalls fueled market anxiety, complicated the short-term outlook, and sent the price of crude oil up over the past year or so. The market has paid a considerable premium for these uncertainties, and had it not been for our massive investment in our substantial spare capacity, I am convinced that premium would have been much higher.

But as we've seen, with seesawing geopolitical tensions and a more bearish economic outlook, healthy fundamentals have gained the upper hand and oil prices have fallen from recent highs by some 20 dollars per barrel, to their lowest level in many months. Although it may surprise some of you, at Saudi Aramco we actually welcome the price drop, because as a responsible company we look for a stable market with prices that are reasonable for both consumers and producers, because that supports the global economic recovery while also promoting continued investment in growing energy supplies.

Of course, one of the dangers in reacting to short-term gyrations is losing sight of long-term goals, and being blown off course by events.

But just as a skilled sailor adjusts his rudder and sails to steer his way to port, the successful business leader responds to short-term needs without losing sight of strategic objectives, especially in a long-term business like oil. And where the sailor relies upon a compass for navigation, at Saudi Aramco we use our core values as our source of guidance, whether the business environment is fair or foul.

We're not unique in that regard, and we believe that in an era of uncertainty and turbulence, there is a need for all of us in business to step back, look at who we are, and contrast that with how we're perceived in the wider world. When we do, we see a powerful link between adherence to core values and the public perception of our companies and institutions. Indeed, as people's trust in business around the world has eroded, I believe

> “... we spend over 800 million dollars on corporate training and development programs each year, because we genuinely believe that people are our most precious asset and the source of our most distinctive competitive advantage.”

that our response should be to return to the roots of responsibility, which must act as the cornerstone of any company’s value system.

Now, I am not about to argue that oil companies, other industrial enterprises, financial institutions, or indeed any economic sector should ignore the goal of running a profitable business.

Commerciality, shareholder value, and the need to generate a decent rate of return remain at the heart of our respective corporate missions.

But I do believe that in today’s testing environment, we need to step up to the plate, elevate our gaze, and thus aim higher. We must return to the principles and safeguard the values that have made trade and enterprise the greatest forces in history for powering growth, enabling development, and raising living standards around the world for the many, not just the few. In particular, we have to demonstrate to an often-skeptical public that our corporations serve a higher purpose and fulfill their wider responsibilities by pursuing a broader, more balanced, and ultimately values-driven business agenda.

At Saudi Aramco, we strive to do just that.

It doesn’t mean we always meet the expectations of all of our stakeholders — in fact, not even our own high standards — but by focusing on our commitment to people and principles in addition to profits, we send a strong and consistent message about who we are, what we stand for, and what we value.

When it comes to our people, we invest time and treasure in the wellbeing and development of our employees. For example, we spend over 800 million dollars on corporate training and development programs each year, because we genuinely believe that people are our most precious asset and the source of our most distinctive competitive advantage.

But our commitment to people goes well beyond our fence. We are reaching deep into Saudi society to develop educational programs – particularly around the “STEM” disciplines of science, technology, engineering and mathematics – and to cultivate an intellectual environment in which innovation and entrepreneurship can flourish. For example, we have launched a youth enrichment program that will touch two million young Saudis by 2020.

And you heard earlier about our engagement with Joanne DiGenarro’s Center for Excellence in

> “... there are no compromises on environmental standards, and we’ve invested billions of dollars in environmental protection programs, aiming to minimize if not eliminate emissions and discharges of pollutants into the natural ecosystem.”

Education, the King Abdullah University for Science & Technology, and MIT to promote science and math disciplines among top Saudi students. We are also hard at work building the landmark King Abdulaziz Center for World Culture in Dhahran, which will promote cross-cultural understanding, lifelong learning and new knowledge creation.

In terms of safety, once again it’s all about caring for the people. While we have a remarkable on-the-job safety record, we frankly need to do better in extending that safety culture to off-the-job situations, and I see that as a critical challenge for the company. In fact, I frequently tell my colleagues that we should be just as concerned if an employee slips in their home as if they slip in one of our facilities, because the consequences for him or her are the same, regardless of location.

When there is an incident, we investigate, find out what went wrong, and try to prevent it from happening again if we can. That approach makes sound business sense, because lost time is lost cost and forfeited opportunity. But we also benefit from a groundswell of motivation and loyalty when our people see the caliber of the company they work for, and when our local communities realize that health and safety are embedded in our culture – including their own health and safety.

Likewise, if we are to become a widely admired global company, we must act as a principled global citizen, including exercising environmental stewardship – an area particularly crucial for our industry. When we plan our projects there are no compromises on environmental standards, and we’ve invested billions of dollars in environmental protection programs, aiming to minimize if not eliminate emissions and discharges of pollutants into the natural ecosystem.

Here again we are taking our commitment to responsibility outside our fence by establishing wildlife sanctuaries in the desert and fish hatcheries in the Gulf. And over the next five years, we will plant a million mangroves, continuing a two-decade program of protecting Saudi shores against erosion while creating a rich tidal ecosystem.

When it comes to our partners, we have also put principle before profit. When the tragic earthquake and tsunami struck Japan last year, our immediate reaction was one of concern, sadness and sympathy. Then we set about seeing what we could do to help. Tankers laden with crude were already steaming to Japan when we were told that some of our customers’ refineries were damaged and their product distribution systems were disrupted. So we redirected cargos in

transit, and utilized the slack in our system to provide refined products and liquefied petroleum gas.

At the same time, we were also conscious of trying to moderate the market's reaction, which was driving energy prices higher. That mutually supportive combination of partnership, responsibility and values is central to who we are – and it was simply the right thing to do in our friends' darkest hour.

Let me now return to our historic and enduring partnership with the United States, which I believe offers the best example of mutual benefit and collaboration. For decades, Saudi Aramco has been a reliable energy supplier to this nation, and when you flip a switch, step onto a plane or train, or take a cab home tonight, you are touching the tail-end of an immensely complex and technologically sophisticated energy chain which links us all.

We remain committed to the US relationship – not just because this will remain a key oil market for many decades to come, but also because we will continue to look to Yankee ingenuity and innovation, to US educational and research institutions, and to American firms both large and small for many of the goods and services upon which not only our company but the whole industry relies.

Generations of Americans – men like the legendary Max Steineke, who first discovered oil in Saudi Arabia; Tom Barger, who rose from field geologist to CEO, and Frank Jungers, who managed a fundamental transformation of the company – and tens of thousands of Saudis over the years have worked hand in hand to build Saudi Aramco into the reliable and responsible force in the energy markets it is today.

This week, we will open a new chapter in that story of cooperation. I'm delighted to say that on Thursday I will be in Texas to participate in the inauguration of an expansion project that makes our Port Arthur Refinery the largest in the US, and indeed one of the biggest refineries in the world. This expansion more than doubles the refinery's capacity to above 600,000 barrels per day; it's our largest single investment outside of Saudi Arabia, the largest single investment in the history of Texas, and the single biggest expansion of US refining capacity in the last four decades.

We started this project just before the global financial crisis struck, but rather than pull up stakes we persevered, fulfilling our long-term commitment to the American market and American consumers, and investing in American jobs and American energy security. In other words, Port Arthur stands as a ten-billion-dollar vote of confidence in this nation, and in the continued good health of its petroleum sector.

So, ladies and gentlemen, let me conclude by noting that the challenges for 21st century business leaders are as broad as they are deep, and that this is a volatile period for the global economy and the petroleum industry alike. Yet uncertainty brings opportunity, and we can seize this unique moment by taking responsibility, aiming higher, and meeting not only the challenging objectives we have set for ourselves but also the legitimate expectations stakeholders have for us.

If we undertake that mission with a sense of duty and service rather than of obligation and compulsion, and thus live our core values as individual leaders and consequently as companies and organizations, then I have no doubt that we will succeed – regardless of the conditions swirling around us. As Lincoln said at Cooper Union more than a century and a half ago, 'Let us have faith that right makes might, and in that faith, let us, to the end, dare to do our duty as we understand it.'

Thank you very much once again for joining us this evening, and for giving our future leaders and me the opportunity to interact with you tonight."

Water Problems?

It's easier if we all pull together.

Let us partner with you to control water break-through and optimize production.

We help you find the best remedial chemical combination using our Relative Permeability Modifier integrated program of High-tech independent laboratory testing and interpretation.

We also offer a wide range of laboratory services including High-tech Special Core Analysis; NMR Core Analysis and log interpretation; Formation Damage; Reservoir Characterization and PVT.

COREX

Your Partner For Success.

www.corex.co.uk

UK
Howe Moss Drive
Dyce, Aberdeen,
AB21 0GL
United Kingdom
Tel: +44 1224 770434
Fax: +44 1224 771716
E-Mail: sales@corex.co.uk

Egypt
176, Sector No.6,
Industrial Area
Zahraa El Maadi,
Helwan, Egypt
Tel: +202 25218446/7
Fax: +202 25175261
E-Mail: sales@corex.co.uk

Abu Dhabi
Corex AlMansoori
Corniche Road, Mussafah Base
Mussafah Industrial Estate
United Arab Emirates
Tel: +971 2 5559712/5554134
Fax : +971 2 5559713
E-Mail: sales@corex.co.uk

Predicting the Effect of Anodic Chemical Inhibitors on Mitigating Hydrogen Environment Assisted Cracking of Ultra-High Strength Steel

By Dr. Sami M. Al-Ghamdi, Dr. Richard P. Gangloff and Dr. John R. Scully.

Abstract

Low alloy ultra-high strength alloy steel (UHSS) suffers from hydrogen environment assisted cracking (HEAC) limiting their use in marine environments. Minimum HEAC susceptibility is observed at intermediate potentials. Models explain this by a reduction in crack tip diffusible hydrogen concentration ($C_{H,diff}$), enhancing threshold stress intensity (K_{TH}) and reducing stage-II crack growth rate (da/dt_{II}). This research seeks to extend the reduced HEAC susceptibility region by reducing $C_{H,diff}$ using aqueous-phase inhibitors. A multifaceted approach was used to quantitatively study the effect of inhibitors on reducing $C_{H,diff}$. Initial tests were conducted on planar electrodes in molybdate solutions at anodic potentials; however, rescaled crevices of larger dimensions were used to measure local potential and pH as a function of applied potentials and crevice dimensions. H-uptake models were used to predict local CH,diff as a function of local potential, pH and scaling factor in the anodic tests. Micro-mechanical models were used to predict the effects of inhibition on HEAC susceptibility. Results were related to real-size cracks using scaling factors. Last, fracture experiments were undertaken to verify predicted K_{TH} and da/dt_{II} obtained from the integrated investigation approach.

Introduction

The main scientific contribution is to interpret the effects of different inhibitors through the study of $C_{H,diff}$ and provide a protocol to computationally predict the effects of inhibitors on hydrogen environment assisted cracking (HEAC) susceptibility with limited experiments. The engineering contribution is to ultimately identify two inhibitors, one cationic and one anionic, that can be delivered to crack tips from coatings to inhibit HEAC. Traditionally, alloys such as AISI 4340 and 300M have been used as high-strength naval aircraft components, although both exhibit low fracture toughness and poor corrosion resistance. Modern ultra-high strength steel (UHSS) alloys have been engineered to achieve a combined high tensile yield strength (σ_{YS}) and plane strain fracture toughness (K_{IC}). AerMet®100 had been developed with best combined σ_{YS} and K_{IC} at an optimal aging temperature[1]; still, it is not intrinsically immune to corrosion.

UHSS components are usually coated for corrosion protection[2]. In operational service, coated components are seldom free of scratches that expose the bare steel to a galvanic couple potential. Sacrificial coatings cathodically polarize steel at the scratch producing hydrogen that could be absorbed. Low alloy UHSS suffer from HEAC limiting their use in marine environments. HEAC susceptibility is strongly potential dependent[3-5]; applied potential (E_{App}) affects both K_{TH} and da/dt_{II}. Figure 1 shows da/dt_{II} in AerMet 100 as a function of E_{App} in 0.6 M NaCl(1) and the open circuit potential for various coatings in chloride solutions.

(1) $C_{H,diff}$ was back calculated from K_{TH} experimental data for AerMet 100 in uninhibited 0.6 M NaCl solution at neutral pH using a micro- mechanical predictive model[3].

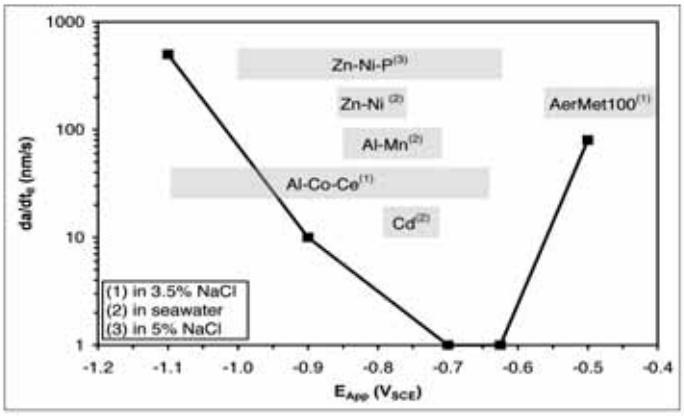

Fig. 1. Stage-II crack growth rate (da/dtII) vs. applied potential (E_{App}) for AerMet® 100 in 0.6 M NaCl (3.5%)[3]. Open circuit potential ranges are shown for various coatings in various chloride solutions[41].

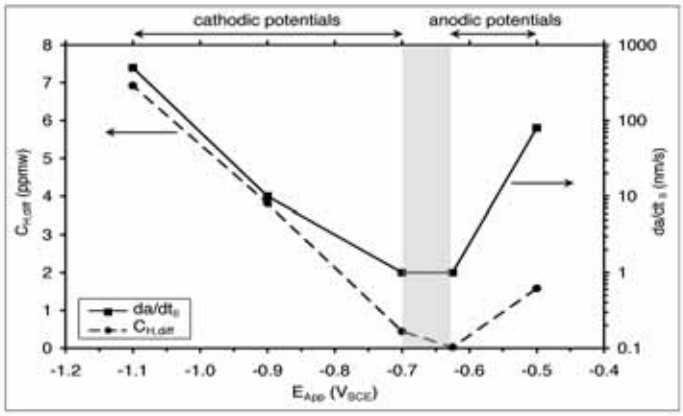

Fig. 2. The dependence of stage-II crack growth rate (da/dt_{II}) and diffusible hydrogen concentration ($C_{H,diff}$) on the applied potential (E_{App}) for AerMet 100 in 0.6 M NaCl[3].

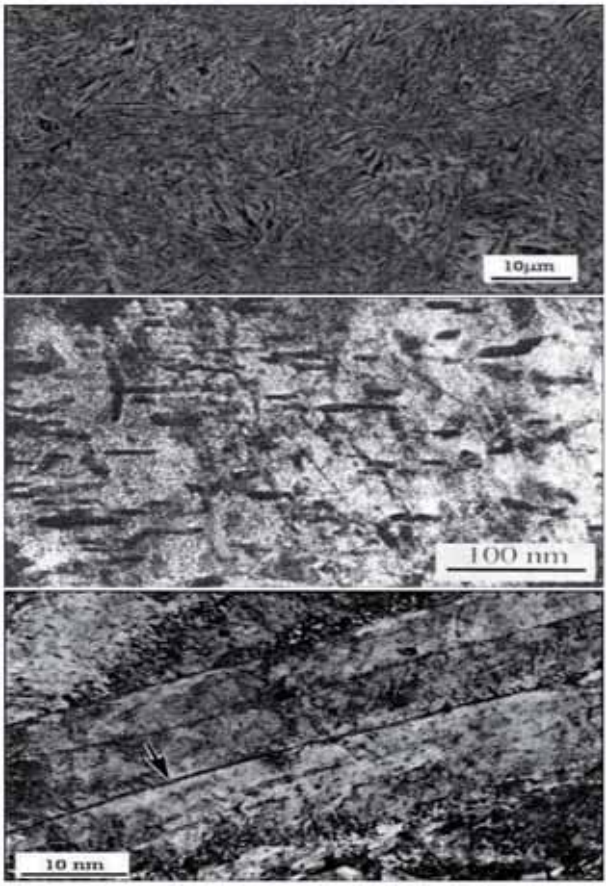

Fig. 3. Microstructural features in AerMet 100: (Top) martensite packets, (Middle) fine dispersed coherent M_2C carbides, and (Bottom) reverted austenite on the martensite lath boundaries[1].

A narrow window of E_{App} is observed around the open circuit potential of AerMet 100 where susceptibility to HEAC is reduced[3]. Prior research on the alloy explains such behavior by the reduction in $C_{H,diff}$, the underlying variable controlling K_{TH} and da/dt_{II}[3,6]. Figure 2 provides the potential dependence of da/dt_{II} and crack tip $C_{H,diff}$ for AerMet 100 in 0.6 M NaCl[(1)]. If the window of reduced HEAC susceptibility can be extended, then AerMet 100, and other UHSS alloys with a similar behavior can be safely used in more cathodic and anodic conditions in marine environments. Chemical inhibitors can be employed to expand this window of reduced HEAC susceptibility more anodically, which is the subject of this article, but first one must understand the dependence of the alloy HEAC susceptibility on important factors, such as the E_{App}, material composition, crack geometry, and crack surface condition.

Material

AerMet 100 is a high purity double-vacuum melted, secondary hardened martensitic steel. The alloy is austenitized at 885°C, air cooled, quenched in liquid nitrogen and aged at 482°C to achieve optimal combined high tensile yield strength and plane strain fracture toughness[1]. Table 1 shows the chemical composition of AerMet 100, where the contaminant elements (Mn, Si, P, and S) were minimized[7].

Fe	Co	Ni	Cr	Mo	C
bal.	12.80	10.89	2.78	1.21	0.23
Mn	Si	Ti	P	S	H (ppmw)
0.019	0.016	0.010	0.001	0.0008	0.35

Table 1. Chemical composition of AerMet 100 (weight percent)[7].

HRC	σ_{UTS} (MPa)	σ_{YS} (MPa)	E (GPa)	K_{IC} (MPa-$m^{1/2}$)
54	1965	1725	194	130

Table 2. Mechanical properties of AerMet 100[8].

The mechanical properties for the optimal aged AerMet 100 are shown in Table 2[8]. The high K_{IC} is mainly attributed to the absence of coarse cementite and the presence of the uniformly dispersed, fine

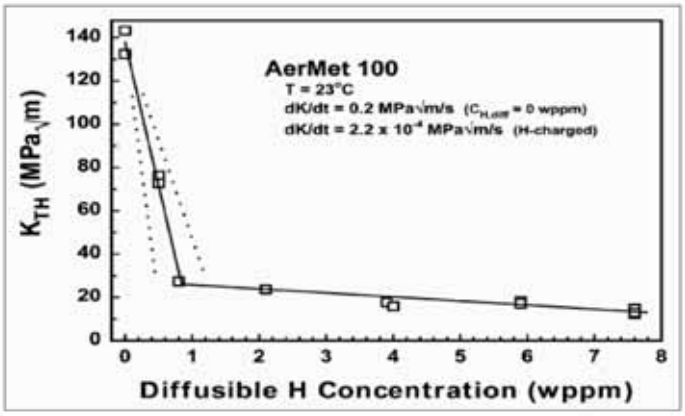

Fig. 4. The degradation of KTH in AerMet 100 with increased diffusible H concentration. Samples were pre-charged with hydrogen and tested in air at room temperature[11].

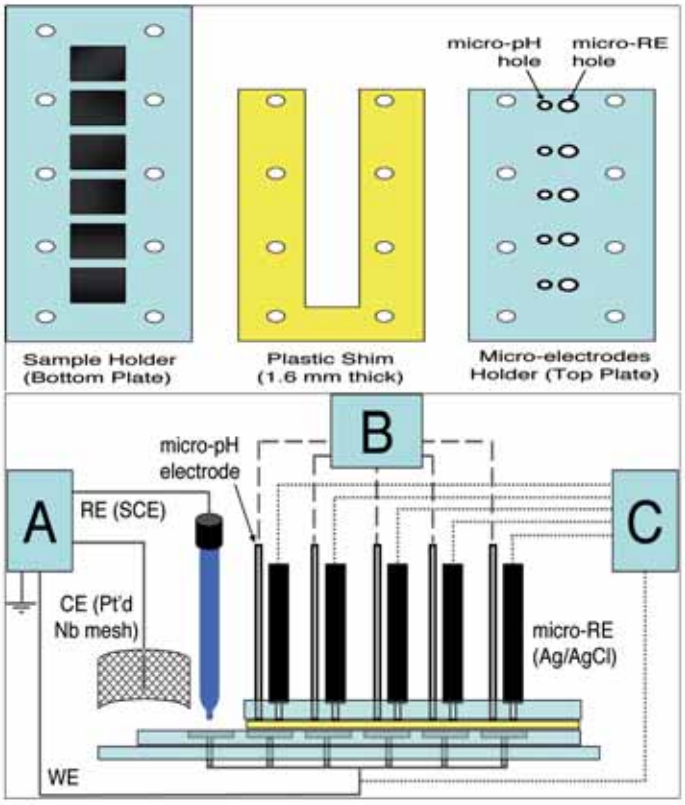

Fig. 5. (Top) The rescaled crevice basic components: bottom plate sample holder, plastic shim, and top plate with micro-electrodes holder, (Bottom) An illustration of the rescaled crevice electrochemical cell components where A is the PAR model 273A Potentiostat, B is the DUO-18 pH data acquisition system and C is the Keithley 2001 multi-meter used to measure E_{local}.

(3 nm), and coherent reverted austenite particles[1]. The secondary strengthening was mainly due to the presence of the fine-cohesive M_2C carbides, where M = Fe, Cr, Mo. Also, high strength was achieved due to the extensive dislocation structure stabilized by the high concentration of Co in AerMet 100. The microstructure of AerMet 100 is rich in hydrogen traps; prior-austenite grain boundaries, martensite laths, high dislocation density, coherent M_2C carbides, and thin film reverted austenite precipitated on lath/plate boundaries, Fig. 3[1]. Each trap site possesses a unique hydrogen binding energy[9].

Minimizing contaminant elements does not eliminate environmental cracking in modern UHSS. They suffer from HEAC along transgranular (TG) sites[6,10].

AerMet 100 suffers an order of magnitude degradation in K_{TH} due to an increase in $C_{H,diff}$, Fig. 4[11]. Such hydrogen concentrations can be achieved at both highly anodic and highly cathodic potentials[6].

In the H-Enhanced Decohesion (HEDE) model, the presence of dissolved H lowers the interatomic bonding forces between metal atoms lowering their cohesion strength and the stress to failure (σ_F). This is further exacerbated by the increased solubility of $C_{H,diff}$ ahead of the crack tip due to the lattice dilation caused by the hydrostatic stress (σ_H)[10]. The high σ_{YS} observed in UHSS results in elevated σH ahead of the crack tip[12]. Hydrogen segregates following the crack tip stress field.

The combined effect of moderate $C_{H,diff}$, or lower σ_F, and high stress fields ahead of the crack tip result in the TG fracture of UHSS along HEAC susceptible sites at $K_{TH} < K_{IC}$. Therefore, ionic inhibitors could be used to lower $C_{H,diff}$ below a critical H concentration (C_c), where no TG fracture is observed.

Experimental Methodology

Rescaled Crevice Method

The rescaled crevice cell was constructed using three main parts: an acrylic bottom plate that holds the specimens, a plastic shim to create the crevice gap and an acrylic top plate, which holds the pH electrodes and micro reference electrodes (REs) for local (electro) chemical measurements. A schematic of the crevice cell parts and a side-view of an assembled crevice cell are shown in Fig. 5. Six AerMet 100 specimens were polished to a 600-grit finish and degreased with ethanol.

The specimens were then mounted in the bottom acrylic plate. For these experiments, the specimens' wires were shorted together to form a continuous working electrode (WE). The plastic shim was used to create a 1.6 mm crevice gap (G). The selected shim thickness was based on crevice scaling factors (x^2/G) relating to real cracks in AerMet 100 fracture tests discussed later. The top plate could then be placed on

top of the plastic shim to create the crevice. The top plate held five pH and five Ag/AgCl micro-REs.

Local pH values were measured using pH indicator paper inserted into the crevice cell and commercially available pH electrodes from Innovative Instruments model AMANI-650 and Thermo Electron Corp. model Orion-910001. Local potential (E_{local}) values were measured using Ag/AgCl micro-Res[13]. The specimens were left at OCP in the non-deaerated cell set-up for an hour before beginning each test. A Princeton Applied Research (PAR) Potentiostat model 273A was employed to potentiostatically apply a potential (E_{App}) for 12 hours, which was determined to be enough for local pH and E_{local} to stabilize. A Keithley 2001 and DUO-18 multi- meters were used for E_{local} and local pH data acquisition, respectively, every 10 seconds throughout the tests.

The rescaled crevice tests of inhibitors were at anodic potentials. The cathodic tests are discussed elsewhere14. The tests in 0.6 M NaCl + 0.01 M Na_2MoO_4 solution at pH = 7.1 and in 0.6 M NaCl + 0.01 M borate buffer solution at pH = 8.0 were conducted at anodic $\eta_{H,bulk}$. These were previously investigated in 0.6 M NaCl[15].

Fracture Testing

Single-edge notch (SEN) specimens were machined from AerMet 100 bulk material aged at 482°C to achieve optimal combined high σ_{YS} and K_{IC}[1]. The specimens had a flat-gauge section 35 mm long (l) x 10.2 mm wide (w) x 2.54 mm thick (b) and had a total length of 46 mm. An edge notch was electrospark-discharge machined in the middle of the gauge section. The specimens were first fatigue pre-cracked in air to the desired initial crack length (a_0)[10].

The fatigue pre-cracked specimens were then loaded in a Plexiglas electrochemical cell, while only exposing the specimen gauge, but not the ends that were threaded into stainless steel grips that were electrically isolated. The grips were connected to the 89 kN INSTRON® machine test frame equipped with a single screw electromechanical actuator with 45 kN capacity. The specimen was grounded through the test frame. A Wenking potentiostat was connected to the specimen (working electrode) to supply external applied potential (E_{App}). The potentiostat was not grounded, but set to floating mode, to avoid a ground loop with the direct current potential difference circuit. A saturated calomel electrode (SCE) was used as reference electrode and a platinized-Nb mesh as the counter electrode. The Plexiglas cell was connected to a MasterFlex® pump circulating non-deaerated test solutions at a rate of 20 mL/min during the experiment from a reservoir at room temperature. Tests were conducted at conditions similar to those in the previous section. Solution pH was measured before and after running the experiments to observe any changes. The samples were polarized potentiostatically before running the experiments. The specimens were preloaded to around 5 MPa-$m^{1/2}$ an hour after specimen polarization.

The direct current potential difference (dcPD) method was used to measure crack length. The dcPD signal increases as the crack grows. The specimens were loaded at a constant-slow actuator displacement rate ($d\delta/dt$). The FTA® software was configured to record the dcPD values in □V, actuator displacement (δ) in mm, applied load (P) in N and time in seconds. The crack length was determined from the dcPD data[16]. The final crack length for each test was corrected from scanning electron microscope (SEM) fractographs. Crack length measurement was truncated once evidence of crack branching or large scale plastic deformation was observed.

The crack mouth opening displacement (CMOD) was calculated[17]. The values for crack length and crack mouth opening displacement will be used later in the analysis to relate the outcome from the HEAC experiments to predicted results from the one-sided rescaled crevice experiments using the scaling factor x^2/G. Analysis of current distribution in the AerMet 100 showed that G for the one-sided crevice was equivalent to ½ CMOD for a real crack (2-sided). Also, using CMOD instead of CTOD allows for the use of x^2/G for trapezoidal cracks with a wide range of K values up to K_{IC} for AerMet 100. Therefore, the scaling factor for real cracks could be expressed as $2a^2/CMOD$[15].

The mode I elastic stress intensity was calculated from the crack length data using Eqn. 1[17].

$$K_I = \sigma\sqrt{\pi a}\left[\sqrt{\frac{\tan(\pi a/2W)}{(\pi a/2W)}}\cdot\frac{0.752+2.02(a/W)+0.37(1-\sin(\pi a/2W))^3}{\cos(\pi a/2W)}\right] \quad \text{Eqn.1}$$

where, K_I = mode I elastic stress intensity in MPa-$m^{1/2}$. The threshold stress intensity (K_{TH}) was previously determined to be the K value at which 0.05% deviation in dcPD signal from the baseline data with displacement (or time) indicating crack growth. An operational K_{TH} was defined as the value of K above which cracking could be detected which was chosen to be at da/dt_{II} = 0.5 nm/s, which was almost double the minimum signal resolution of measuring 1 □m of crack growth in 1 hour or around 0.27 nm/s[3]. Most tests were at

least 12 hours long. A 2nd order polynomial was fitted through the crack growth length profile with time. A crack growth rate could be determined by taking the slope at a midpoint over 51 data point segments in the polynomial. The diffusion-limited crack growth rate (da/dt_{II}) was determined from the K-independent, stage-II subcritical crack growth rate section of the K_I vs. da/dt profile.

Predictive Modeling of HEAC Susceptibility

The susceptibility of UHSS to H environment assisted cracking could be studied by models that predict the dependency of the threshold stress intensity (K_{TH}) and stage-II diffusion-limited crack growth rate (da/dt_{II}) on the stress-enhanced H concentration at the crack tip[18,19]. The predictive models also depend on other parameters related to the metallurgy and surrounding environment.

HER Mechanism-Based H Uptake Predictive Model

The rescaled crevices and cracks are useful in investigating crack tip environments, but results are more informative and useful when combined with crack H uptake correlations. Chemical inhibitors could affect local potentials, pH values, H production rates and H uptake at the crack tip.

An HER mechanism-based H uptake model was developed as a function of η_H complemented with experimental data in chloride-free buffer solutions, where Cl- was found not to affect H uptake[20]. The pH of such solutions ranged from 2 to 10, which was considered to represent crack solution pH values from highly anodic to highly cathodic crack tips[15]. Figure 6 provides a compilation of all H uptake relationships as a function of solution pH for AerMet 100. The figures indicate conditions for H uptake at underpotentials, where $\eta_H \geq 0$ V. The H uptake curves plateau at

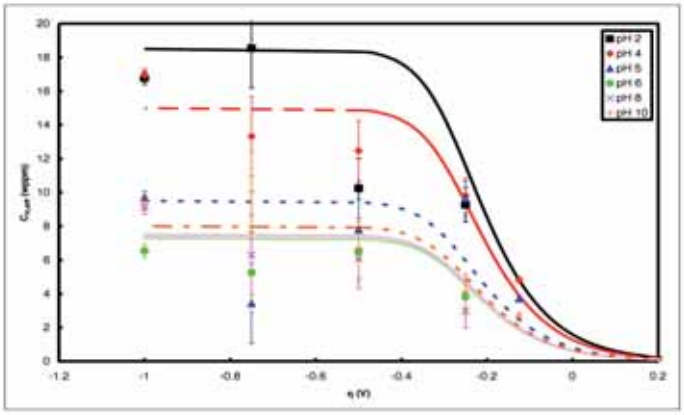

Fig. 6. Barnacle electrode results for AerMet 100 in buffers at pH values of 2, 4, 5, 6, 8, and 10[6].

η_H values more cathodic than -0.4 V regardless of solution pH. That was explained by H surface coverage approaching unity[21].

The model fitted through the data assumed a coupled discharge-recombination HER mechanism. It provides a more accurate relationship between $C_{H,diff}$ and η_H, refer to Eqns. 2a, 2b and 2c. The surface coverage (θ_H) term was obtained assuming a simplified Langmuir isotherm[21].

$$C_{H,diff} = \frac{D_{lattice}}{D_H} \cdot \frac{k_{abs}}{k_{des}} \theta_H \qquad \text{Eqn. 2a}$$

$$C_{H,diff} = \frac{D_{lattice}}{D_H} \cdot \frac{k_{abs}}{k_{des}} \cdot \sqrt{\frac{k_{dis}}{k_r} C_{H^+}} \exp\left[\frac{-\alpha \eta_H F}{2RT}\right] \qquad \text{Eqn. 2b}$$

$$C_{H,diff} = \frac{D_{lattice}}{D_H} \cdot \frac{k_{abs}}{k_{des}} \cdot \sqrt{\frac{k'_{dis}}{k_r}} \exp\left[\frac{-\alpha \eta_H F}{2RT}\right] \qquad \text{Eqn. 2c}$$

where, $D_{lattice}$ = H lattice diffusivity (cm^2/s), D_H = H effective diffusivity (cm^2/s), k_{abs} = absorption rate con- stant (mol/cm^2 s), k_{des} = desorption rate constant (cm/s), θ_H = H surface coverage, k_{dis} = H^+ discharge rate constant (cm/s), k'_{dis} = H_2O discharge rate constant (cm/s), k_r = absorption rate constant (mol/cm^2 s), C_{H+} = proton concentration (mol/cm^3), α = transfer coefficient, F = Faraday's constant (C/mol), R = ideal gas constant (J/K mol), and T = room temperature (K).

Equations 2a, 2b and 2c describes the dependence of $C_{H,diff}$ on η_H in acidic and alkaline solutions, respectively[22-24]. The pre-exponential ratio of the reaction rate constants

$$\frac{k_{dis}}{k_r} C_{H^+} \text{ and } \frac{k'_{dis}}{k_r}$$

were approximated to be $8 \cdot 10^{-3}$ for ease of derivation. As for the H uptake scaling factor

$$\frac{D_{lattice}}{D_H} \cdot \frac{k_{abs}}{k_{des}}$$

values were varied with pH to best fit the experimental data as shown in Table 3[15]. Values show H uptake as a strong function of pH for values less than 6, while becoming almost independent for pH > 6.

pH	2	4	5	6	8	10
$\frac{D_{lattice}}{D_H} \cdot \frac{k_{abs}}{k_{des}}$ (ppmw)	18.5	15	9.5	7.3	7.5	8.0

Table 3. The H uptake mechanism-based model scaling factors as a function of pH[15].

This article will examine the effect of chemical inhibition on local E, pH and η_H measured in rescaled crevice experiments. The HER mechanism-based predictive models will be used to predict the effect of chemical inhibitors on crack tip $C_{H,diff}$ using the measurements of local η_H as functions of crevice scaling factors in anodically polarized AerMet 100 crevices. Crack tip $C_{H,diff}$ will then be related to real size cracks in UHSS alloys that suffer from HEAC using the crevice scaling factors (x^2/G). Care will be taken to discuss and disting- uish between the effects of molybdate on reducing anodic dissolution, hydrolysis and acidification and the effects of borate on chemically buffering solution pH.

KTH H-Enhanced Decohesion Model

The intricate dislocation structures and coherent/incoherent interfaces in UHSS, such as martensite lath boundaries and nano-scale metal carbides[1,25,26], attract absorbed hydrogen atoms acting as H-traps with specific binging energies. In the H-Enhanced Decohesion (HEDE) model, the local accumulation of H at these sites lowers the cohesive strength of metal-metal bonds across the adjacent crack path. Gerberich[18] had shown that KTH could be predicted using a lattice decohesion- based micromechanical model governed by the stress enhanced H concentration at the crack tip ($C_{H\sigma}$), Eqn. 3:

$$K_{TH} = \frac{1}{\beta'}\exp\left[\frac{(k_{IG} - \alpha \cdot C_{H\sigma})^2}{\alpha'' \sigma_{YS}}\right] \qquad \text{Eqn.3}$$

where k_{IG} = critical Griffith stress-intensity factor for cleavage fracture w/o H [MPa-$m^{1/2}$], $C_{H\sigma}$ = stress- enhanced H concentration trapped adjacent to embrittlement site (atom fraction), α = weighing coefficient representing H-induced reduction in cohesive strength relative to kIG [MPa-$m^{1/2}$/atom fraction H], α" = crack-tip stress field constant determined by dislocation modeling [MPa-m], β' = crack-tip stress field constant determined by dislocation modeling [MPa-$m^{1/2}]^{-1}$, and σ_{YS} = yield strength [MPa].

The model predicts K_{TH} relative to K_{IC} in an H-free environment, i.e., $C_{H\sigma}$ = 0 atom fraction, based on H-decohesion brittle cracking in the presence of crack tip plasticity. The term in parentheses in Eqn. 3 could be defined as the Griffith stress-intensity for HEAC (kIH), where $k_{IH} = k_{IG} - \alpha \cdot C_{H\sigma}$. Gerberich[18] used a constant α " = 2·10-4 MPa-$m^{1/2}$ for different types of material, including steel, while β' was chosen to be 0.2 (MPa- $m^{1/2})^{-1}$ for steels. Kehler[15] found that using α = 1.0 MPa- $m^{1/2}$/atom fraction and k_{IG} = 0.72 MPa-$m^{1/2}$ in the micromechanical model corresponded to the lowest crack tip H concentration predicted at K_{TH} = 22.3 MPa- $m^{1/2}$[2,3,10], which was the highest measured threshold value[(2)] for AerMet 100 tested at -0.7 V_{SCE} in 0.6 M NaCl. Finally, the stress-enhanced H concentration at the crack tip was defined by Fermi-Dirac statistics as[18]:

$$C_{H\sigma} = \frac{C_{H,diff}\exp(\sigma_H V_H/RT)}{1 + C_{H,diff}\exp(\sigma_H V_H/RT)} \qquad \text{Eqn.4}$$

where, $C_{H,diff}$ = diffusible H concentration at reversible trap sites (atomic fraction), σ_H = hydrostatic stress causing lattice dilation = $5\sigma_{YS}$ (MPa)[27,28], V_H = H volume fraction (cm^3/mol), R = gas constant = 8.314 J/K·mol, and T = room temperature = 296 K.

It can be seen from Eqn. 4 that the stress-enhanced H concentration is directly proportional to the concentration of H trapped in reversible trap sites or the diffusible H concentration ($C_{H,diff}$). Also, $C_{H\sigma}$ is elevated further in higher tensile yield strength steels, where enhanced hydrostatic stresses (σ_H) ahead of the crack results in further dilation of the lattice. Increased temperatures result in reducing the trapped H atoms ahead of the crack tip.

Diffusion-Limited da/dt_{II} Model

Gangloff[19] summarized a predictive model for stage-II, K-independent, sub-critical crack growth rate based on diffusion-limited HEAC, Eqn. 5. The model assumes that H atoms are readily available on the surface, i.e., no H discharge or adsorption/absorption reaction limitation, and that H diffusion to the fracture process zone (FPZ) is the rate limiting step controlling da/dt_{II}. The model predicts crack propagation once the stress-enhanced H concentration exceeds a critical H concentration (C_c) for crack growth over a critical distance ahead of the crack tip (X_c).

$$\frac{da}{dt_{II}} = \frac{4D_H}{X_c}\left[\text{erf}^{-1}\left(1 - \frac{C_C}{C_{H\sigma}}\right)\right]^2 \qquad \text{Eqn.5}$$

where D_H = effective H diffusivity [cm^2/s], X_c = critical distance ahead of crack tip surface [□m] and C_c = critical H concentration necessary for damage [atom fraction].

The critical distance ahead of the crack tip could be understood as the crack propagation distance when the stress-enhance H concentration exceeds a critical

(2) K_{TH} here was defined as the stress intensity factor at da/dt = 0.5 nm/s, which was twice the dcPD resolution da/dt level[7, 8]. Such method of determining K_{TH} was conservative and resulted in a non-zero H concentration at chosen E_{App} = -0.7 V_{SCE}[6], since $K_{TH} << K_{IC}$.

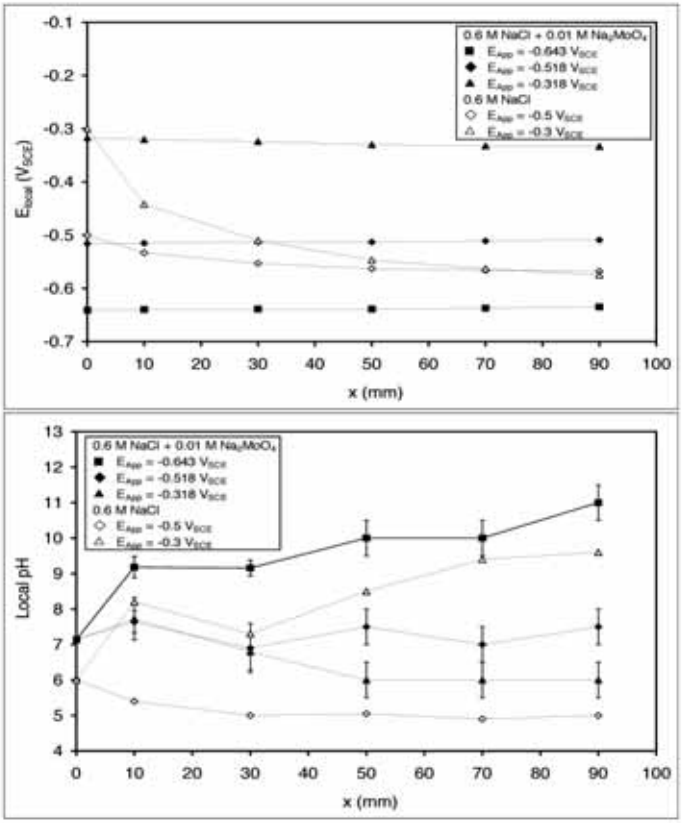

Fig. 7a. (Top) E_{local} and Fig. 7b (Bottom) local pH vs. x for AerMet 100 crevice experiments with G = 1.6 mm after 12 hours of charging. Solid symbols are of tests in non-deaerated 0.6 M NaCl + 0.01 M Na_2MoO_4 solution at pH = 7.1 at E_{App} = - 0.643, -0.518, and -0.318 V_{SCE}. Open symbols are of tests in non-deaerated 0.6 M NaCl solution at pH = 6.8 at E_{App} = -0.5 and -0.3 V_{SCE}[15].

concentration. Gangloff[19] found that X_c was in the range between 5 □m and 5 nm for stage-II HEAC in high strength alloys. Accurate quantification of critical H concentrations might be difficult in actively propagating HEAC in UHSS. For AerMet 100, back-calculation from lowest measured da/dt_{II} in 0.6 M NaCl pH 6.8, at -0.625 V_{SCE}, revealed C_c = 0.157 atom fraction[3]; however, C_c was estimated to be lower around 0.026 atom fraction from rescaled crevice measurements in 0.6 M NaCl pH 6.8 at the least severe E_{App} = -0.7 V_{SCE}[15]. Such estimations depend on the resolution of the test method. Also, back calculated Cc values depend on H diffusivities estimated from planar, non-stressed specimens that do not account for the increased dislocation density ahead of the crack tip decreasing D_H.

The mobility of hydrogen atoms in AerMet 100 is affected by multiple factors; e.g., dislocations, martensite lath boundaries, and metal carbides[9, 29]. In UHSS, the dislocation structures ahead of a propagating HEAC act as H traps reducing H diffusivity; moreover, H trapping can be further complicated by the effect of plastic strain on the rate of dislocation formation ahead of the crack tip. Knowledge of the effect of such factors and others on H mobility helps better measure D_H. For AerMet 100, a correlation between D_H in cm^2/s and $C_{H,diff}$ in ppmw was established based on Thermal Desorption Spectroscopy (TDS) tests on H charged planar samples[29].

The use of the micro-mechanical models has not been previously combined with measurements of crack tip environments in the presence of ionic inhibitors. In this article, measurements of local $C_{H,diff}$ made in crevices with scaling factors similar to real-sized cracks will be used to predict the effect of the chemical inhibitors on increasing K_{TH} and decreasing da/dt_{II}. The models will be used to predict the widening of the potential range of reduced HEAC susceptibility for AerMet 100 to more anodic potentials in sodium chloride solutions.

Results

Inhibition of Local Potential and pH

Figure 7a (top) shows limited change in local potentials measured in molybdate inhibited solutions after 12

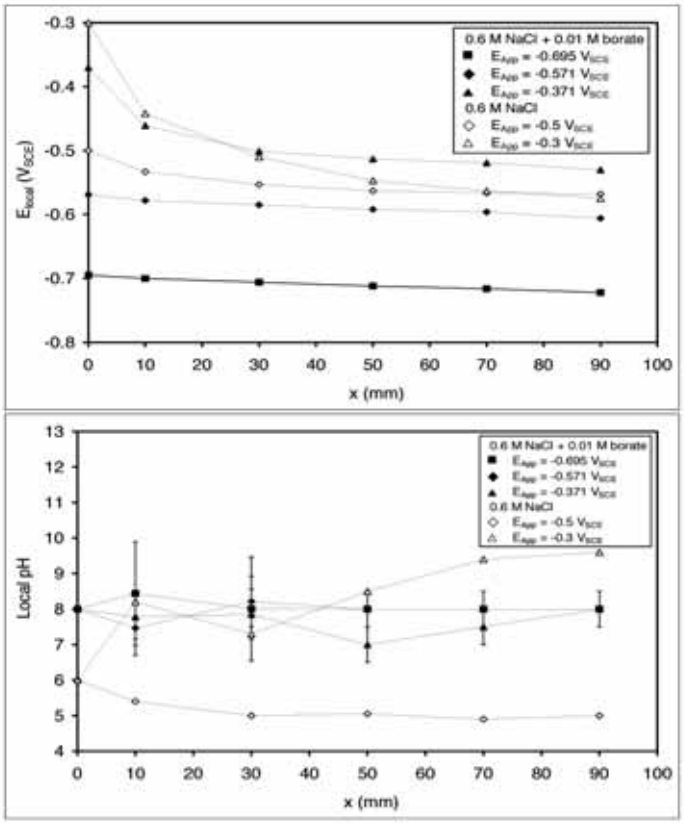

Fig. 8a. (Top) E_{local} and Fig. 8b (Bottom) local pH vs. x for AerMet 100 crevice experiments with G = 1.6 mm after 12 hours of charging. Solid symbols are of tests in non-deaerated 0.6 M NaCl + 0.01 M borate buffer at pH = 8.0 at E_{App} = -0.696, -0.571, and -0.371 V_{SCE}. Open symbols are of tests in non-deaerated 0.6 M NaCl at pH = 6.8 at E_{App} = -0.5 and - 0.3 V_{SCE}[15].

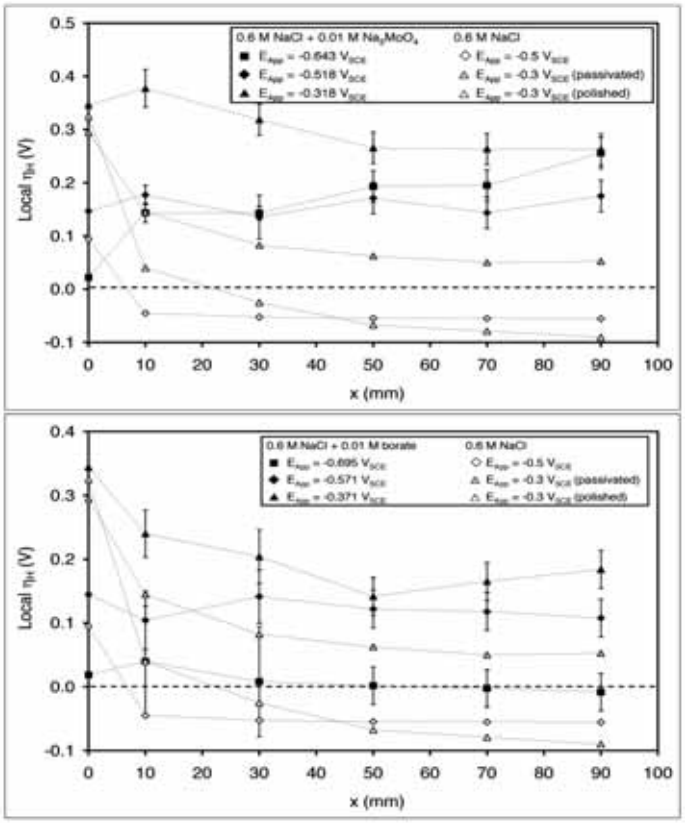

Fig. 9a. (Top) Local η_H vs. x for AerMet 100 crevice experiments with G = 1.6 mm. Solid symbols are of tests in non-deaerated 0.6 M NaCl + 0.01 M Na_2MoO_4 solution at pH = 7.1 at E_{App} = -0.643, -0.518, and -0.318 V_{SCE}, and Fig. 9b (Bottom) 0.6 M NaCl + 0.01 M borate buffer solution at pH = 8.0 at E_{App} = -0.696, -0.571, and -0.371 V_{SCE}.Open symbols are of tests in non-deaerated 0.6 M NaCl solution at pH = 6.8 at E_{App} = -0.5 and -0.3 V_{SCE}[15].

hours compared to the tests ran in uninhibited 0.6 M NaCl solutions at similar $\eta_{H,bulk}$[15]. The maximum potential difference (□E), where □E = E_{local} – E_{App}, measured after 12 hours of charging in 0.6 M NaCl + 0.01 M Na_2MoO_4 solution was +6, +7, -16 mV at E_{App} = -0.643, -0.518 and -0.318 V_{SCE}, or at $\eta_{H,bulk}$ = +0.018, +0.143, and +0.343 V, respectively. Maximum □E in uninhibited 0.6 M NaCl solutions was -68 and -275 mV at η_H = +0.143 and +0.343, respectively. Figure 7b (bottom) provides the local pH profile vs. x at each E_{App} . Local pH became alkaline at E_{App} = -0.643 V_{SCE}, while it was neutral at E_{App} = -0.518 V_{SCE}. At E_{App} = -0.318 V_{SCE}, a slight drop in local pH down to 6 was observed for x ≥ 5 cm. Still, these values are higher than the lowest pH measured in uninhibited 0.6 M NaCl solution at similar $\eta_{H,bulk}$. It must be noted that the increase in local pH at E_{App} = -0.3 V_{SCE} in uninhibited 0.6 M NaCl was an artifact in the rescaled crevice experiment with G = 1.6 mm, most probably due to air leaking into the crevice leading to O_2 reduction increasing local pH. The data does not follow the general decreasing trend observed in with local pH measurements from crevices of different dimensions (x and G) polarized at similar E_{App}[15].

Figure 8a (top) shows the local □E was higher into the borate buffered crevice compared to similar measurements in 0.6 M NaCl + 0.01 M Na_2MoO_4 solution at pH = 7.1 presented previously. Maximum potential drop in the borate buffered crevices were -27, - 37, -160 mV at E_{App} = -0.696, -0.571, and -0.371 V_{SCE}, or $\eta_{H,bulk}$ = +0.018, +0.143, and +0.343 V, respectively. Although the drop in potential was higher in borate compared to molybdate solutions, □E values in the borate buffered solutions were still lower than those measured in uninhibited 0.6 M NaCl. The addition of borate buffer resulted in buffering of pH acidification, Fig. 8b, (bottom) although the overall current density was more anodic than that measured in the molybdate inhibited tests at similar H overpotentials.

Finally, local hydrogen overpotential (η_H) values were calculated from measured E_{local} and local pH measured in 0.6 M NaCl + 0.01 M Na_2MoO_4 solution at pH =

7.1 at E_{App} = -0.318, -0.518 and -0.643 V_{SCE}. Figure 9a (top) shows local η_H as a function of depth in the crevice. The local η_H values in all tested E_{App} in 0.6 M NaCl + 0.01 M Na_2MoO_4 were positive or more anodic than the reversible H potential (EH/H^+). Although these conditions were unfavorable for H production, finite amount of H can still be produced and some is absorbed into the specimens. At E_{App} = -0.316 V_{SCE}, local η_H reached +0.263 V deepest into the crevice. At similar conditions in uninhibited 0.6 M NaCl, local η_H reached -0.090 V for polished samples that are representative of fresh surfaces created by propagating cracks, while specimens with passivated surfaces, local η_H was +0.053 V, which was higher than in polished conditions15, but was not as high as those measured in the molybdate inhibited solution.

Local η_H were calculated in 0.6 M NaCl + 0.01 M borate buffer solution at pH = 8.0 crevice experiments using measured E_{local} and local pH. Figure 9b (bottom) shows local η_H as a function of depth. The local H over-potentials were all positive at E_{App} = -0.371 and -0.571 V_{SCE}, mainly due to borate buffering changes to solution pH. At E_{App} = -0.696 V_{SCE}, local η_H were slightly positive for x ≤ 50 mm and slightly cathodic (negative) reaching - 0.008 V at x = 90 mm. In all cases, local η_H values were more positive (anodic) compared to the crevice tests conducted in unbuffered 0.6 M NaCl solution at pH = 6.8. At most anodic EApp = -0.371 V_{SCE}, local η_H values in the borate buffered solutions were more anodic, less driving force for H production, compared to passivated specimen in unbuffered 0.6 M NaCl solutions, due to mitigation of pH acidification[15].

Reduction of $C_{H,diff}$ in Anodically Polarized Crevices

The local η_H and local pH values were then used to predict local $C_{H,diff}$ using the appropriate HER mechanism based H uptake laws. Although all local η_H values were positive in 0.6 M NaCl + 0.01 M Na_2MoO_4, the H uptake laws show the possibility of H production and absorption at anodic η_H. At these conditions, the total current density (i_{total}), where $i_{total} = i_{an} + i_{ca}$, is anodic because the anodic reaction current density (i_{an}) is much higher than the cathodic reaction current density (i_{ca}), but the cathodic reaction rates is non-zero.

Figure 10a (top) shows the HER mechanism-based H uptake laws plotted on a linear scale showing CH,diff values for underpotentials where η_H > 06. The H uptake relationships collapse together at more anodic η_H, regardless of pH, due to reduced H surface coverage, since it is proportional to exp[-η_H] as seen

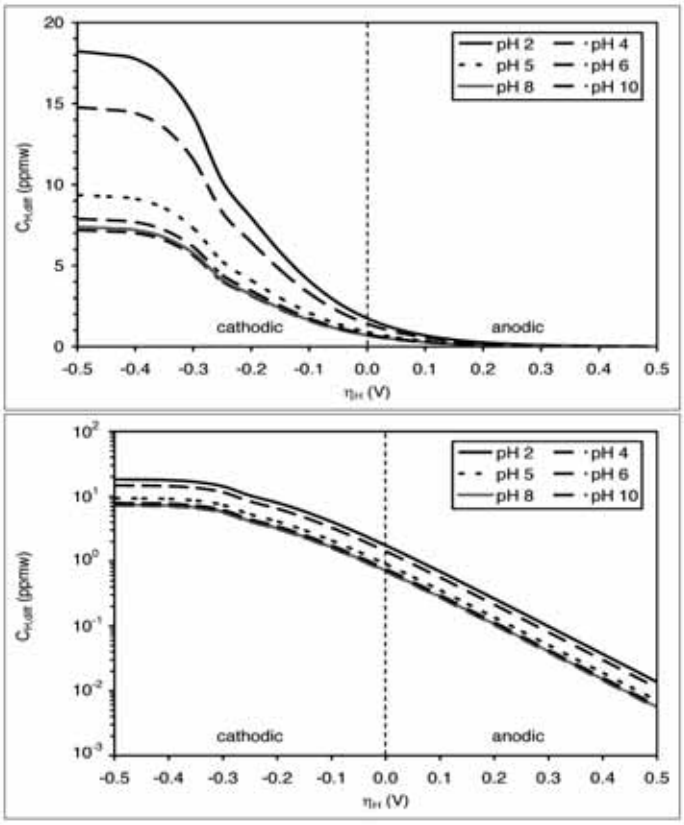

Fig. 10. Mechanism based H uptake laws as a function of H over potentials and solution pH based on barnacle electrode results for AerMet 100 in buffers at pH values of 2, 4, 5, 6, 8, and 10 shown on (Top) linear scale and (Bottom) semi-log scale[6].

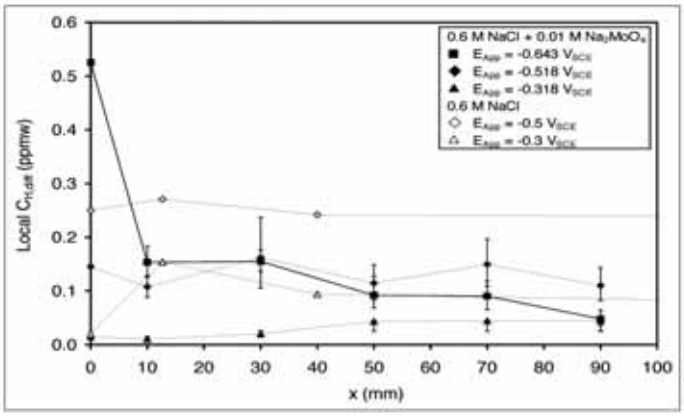

Fig. 11. Local $C_{H,diff}$ vs. x for AerMet 100 crevices with G = 1.6 mm. Solid symbols are tests in non-deaerated 0.6 M NaCl + 0.01 M Na_2MoO_4 solution at pH = 7.1 at E_{App} = -0.643,-0.518, and -0.318 V_{SCE} compared to tests of passivated specimens in non-deaerated 0.6 M NaCl solution at pH = 6.8 at E_{App} = -0.5 and -0.3 V_{SCE}[15].

in Eqns. 2b and 2c. Figure 10b (bottom) shows the H uptake laws on a semi-log scale to show that local $C_{H,diff}$ in pH = 5 to 10 were closely similar, so the reduction in H surface coverage due to the possible presence of an oxide in the molybdate inhibited tests would have little impact on predicted $C_{H,diff}$. That is why the uptake laws developed for uninhibited 0.6 M NaCl were used

to conservatively predict local $C_{H,diff}$ in 0.6 M NaCl + 0.01 M Na_2MoO_4.

Figure 11 shows the predicted local $C_{H,diff}$, calculated using Eqn. 2c, vs. crevice depth for the tests conducted in 0.6 M NaCl + 0.01 M Na_2MoO_4 solution at pH = 7.1. Local $C_{H,diff}$ values in the molybdate inhibited solutions were lower than the results for the passivated specimens in uninhibited 0.6 M NaCl[15]. This was due to the lower increase in local η_H for the passive specimen condition in uninhibited 0.6 M NaCl compared to results in 0.6 M NaCl + 0.01 M Na_2MoO_4 at similar E_{App} and x.

EIS results showed that borate buffer had a negligible effect on reducing dissolution rates[14], $C_{H,diff}$ could then be predicted from the H uptake laws, Fig. 6, for uninhibited sodium chloride solutions at pH 8[15]. Figure 12 shows a major reduction in predicted local $C_{H,diff}$ from buffered test solutions compared to polished specimens in 0.6 M NaCl. Local $C_{H,diff}$ results were comparable, within accuracy of measurements, to those predicted for passivated specimens in 0.6 M NaCl which might be explained by that the passivated condition may have not resulted in reduced dissolution rates but minimized the amount of cations in the crevice enough to minimize hydrolysis and acidification[15].

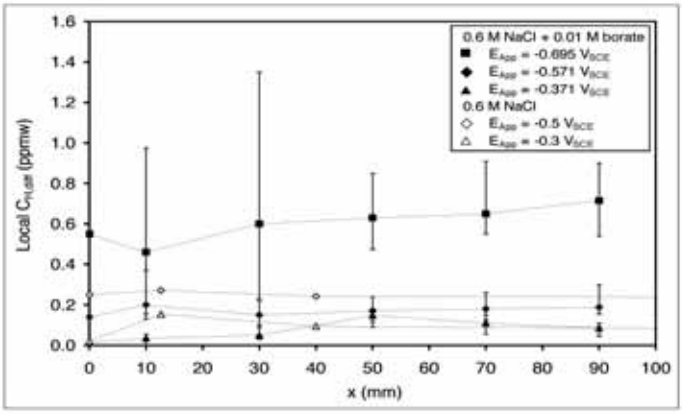

Fig. 12. Local $C_{H,diff}$ vs. x for AerMet 100 crevice experiments with G = 1.6 mm. Solid symbols are of tests in non-deaerated 0.6 M NaCl + 0.01 M borate buffer at pH = 8.0 at E_{App} = -0.695, -0.571, and -0.371 V_{SCE} compared against tests of passivated specimens in non-deaerated 0.6 M NaCl at pH = 6.8 at E_{App} = 0.5 and -0.3 V_{SCE}[15].

The mitigation of local $C_{H,diff}$ was better in molybdate compared to results in borate buffer, although both are considered chemical buffers and local pH was lower in molybdate[14]. This could be explained by the reduction in anodic dissolution in molybdate that may have limited the amount of cations available for hydrolysis limiting acidification. The possible formation of an enhanced surface film might have also limited H absorption. The reduction of H uptake in molybdate could not only be attributed to its ability to chemically buffer changes in pH.

Table 4 summarizes average local $C_{H,diff}$ values predicted from all the anodically inhibited rescaled crevice tests. Results are shown as a function of E_{App} ($\eta_{H,bulk}$) and x^2/G, where 62.5 mm ≤ x^2/G ≤ 1,562.5 mm. The methodology to measure $C_{H,diff}$ in rescaled crevices could be related to real micro-scale cracks, knowing the scaling factor for a real crack as $x^2/G = 2a^2/CMOD$, where x is the distance from the crevice mouth, G is the crevice gap, a is the crack length and CMOD is the crack mouth opening displacement. Note, CMOD was set as 2G, since the potential distribution for the 1-sided rescaled crevice with a gap of G was shown to

	Solution	E_{App} (V_{SCE})	x^2/G (mm)	62.5	562.5	1562.5
			$\eta_{H,bulk}$ (V)	$C_{H,diff}$ (ppmw)		
1.	0.6 M NaCl at pH = 6.8[15]	– 0.300 (polished)	+ 0.343	6.70	6.93	7.49
		– 0.300 (passivated)		0.13	0.12	0.08
		– 0.500 (polished)	+ 0.143	7.20	7.33	7.40
		– 0.500 (passivated)		0.27	0.25	0.25
		– 0.700	– 0.057	0.93	0.88	0.90
		– 0.900	– 0.257	2.85	2.80	2.82
		– 1.100	– 0.457	6.10	5.80	5.65
2.	0.6 M NaCl + 0.01 M borate buffer pH = 8.0	– 0.371	+ 0.343	0.04	0.05	0.15
		– 0.571	+ 0.143	0.20	0.15	0.17
		– 0.696	+ 0.018	0.46	0.60	0.63
3.	0.6 M NaCl + 0.01 M Na_2MoO_4 at pH = 7.1	– 0.318	+ 0.343	0.01	0.02	0.04
		– 0.518	+ 0.143	0.11	0.16	0.12
		– 0.643	+ 0.018	0.15	0.16	0.09

Table 4. Summary of average local $C_{H,diff}$ from the inhibited rescaled crevice tests as a function of E_{App} ($\eta_{H,bulk}$) and x^2/G

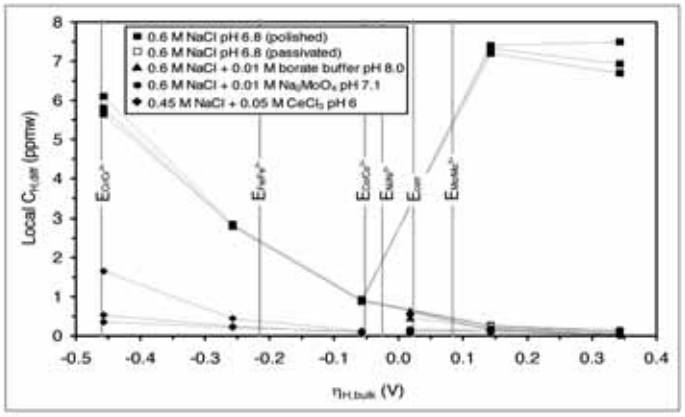

Fig. 13. Average local $C_{H,diff}$ vs. $\eta_{H,bulk}$ for AerMet 100 crevices in 0.6 M NaCl solution at pH 6.8 (polished and passivated)15, 0.6 M NaCl + 0.01 M Na_2MoO_4 solution at pH 7.1, 0.6 M NaCl + 0.01 M borate buffer solution at pH 8.0 and 0.45 M NaCl + 0.05 M $CeCl_3$ solution at pH 6.0 with scaling factors 62.5 mm ( ) , 562.5 mm ( ) and 1562.5 mm ( ). Nernst potentials for Fe, Co, Ni, Cr, and Mo were calculated assuming metal cation concentrations of 10^{-6} M. Also shown is the corrosion potential (E_{corr}) for AerMet 100 determined in 0.6 M NaCl solution at pH = 6.8[3].

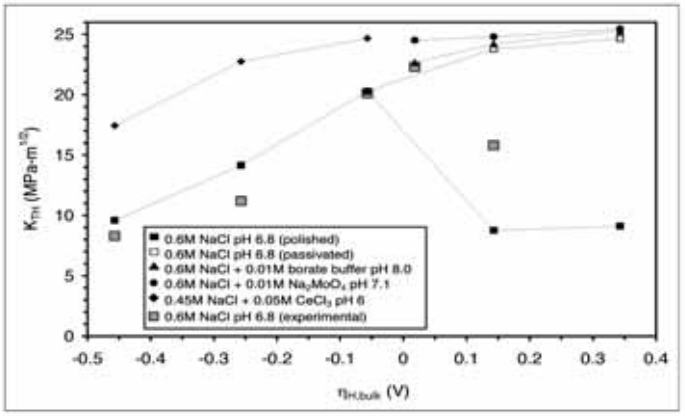

Fig. 14. Predicted K_{TH} as a function of applied bulk η_H (assuming η = 1.0 MPa-$m^{1/2}$/atom fraction and k_{IG} = 0.75 MPa- $m^{1/2}$) for AerMet 100 crevice experiments in 0.6 M NaCl solution at pH 6.8 (polished and passivated conditions)[15], 0.6 M NaCl + 0.01 M Na_2MoO_4 solution at pH 7.1, 0.6 M NaCl + 0.01 M borate buffer solution at pH 8.0 and 0.45 M NaCl + 0.05 M $CeCl_3$ solution at pH 6.0 with scaling factors 62.5 mm. Results are compared against measured K_{TH} values in 0.6 M NaCl[3].

be equivalent to that of a 2-sided crack with a gap of 2G[15].

Figure 13 summarizes the average predicted local $C_{H,diff}$ from the anodic ionic inhibition experiments compared to uninhibited tests[15] as function of $\eta_{H,bulk}$. The $C_{H,diff}$ results were plotted on a logarithmic scale to differentiate amongst the anodic potentials' results in 0.6 M NaCl solution (passivated) compared to 0.6 M NaCl + 0.01 M borate buffer solution, and 0.6 M NaCl + Na_2MoO_4 solution. The results show the effect of x^2/G on local $C_{H,diff}$.anodic potentials, the reduction in H uptake was highest in molybdate solutions, then in borate buffered solutions then for passivated specimen compared to polished specimen in uninhibited sodium chloride solution[15]. The local $C_{H,diff}$ values were reduced in the inhibited solutions with increasing $\eta_{H,bulk}$ since H production driving force was reduced. The figures show that the benefit of molybdate inhibition and borate buffering was reduced with increasing x^2/G. The local $C_{H,diff}$ in borate buffered solutions were similar to results from passivated specimen in uninhibited sodium chloride solutions, within the accuracy of measurements, with x^2/G = 1,562.5 mm.

The local $C_{H,diff}$ values were then predicted as a function of measured E_{local} and local pH using the appropriate empirical H uptake laws. Using the previously discussed predictive models, K_{TH} and da/dt_{II} could then be predicted in the presence of the ionic inhibitors using $C_{H,diff}$, the main variable controlling both HEAC parameters. The effect of the inhibitors on the predicted K_{TH} and da/dt_{II} could be studied as a function of E_{App}, or $\eta_{H,bulk}$ to account for the bulk pH of the inhibitive solutions, and x^2/G to account for the crack geometry.

Model Prediction of KTH

The values for $C_{H\sigma}$ were used in the H-decohesion model shown in Eqn. 4[8] to predict K_{TH} vs. $\eta_{H,bulk}$ in the anodically, Fig. 14. Results for cathodically inhibited solutions are discussed elsewhere[14]. The Griffith stress-intensity factor (k_{IG}) was assumed to be 0.75 MPa-$m^{1/2}$, while the weighing coefficient representing reduction in the cohesive strength (α) was assumed to be 1.0 MPa- $m^{1/2}$/atom fraction. As previously discussed, these assumptions were made to best fit the predictive model to highest measured K_{TH} = 22.3 MPa-$m^{1/2}$ in 0.6 M NaCl, assuming no H uptake in the reduced HEAC susceptibility region[3,10].

In anodic bulk H over potentials, predicted K_{TH} in 0.6 M NaCl + 0.01 M Na_2MoO_4 and 0.6 M NaCl + 0.01 M borate buffer were higher than values predicted from polished specimens in 0.6 M NaCl and similar to passivated specimens in 0.6 M NaCl[15], especially at most anodic over potentials; still, values in molybdate were slightly higher, especially at +0.018 V. Unlike the polished condition in 0.6 M NaCl, predicted values slightly increased in more anodic (positive) H over potentials. There was no effect of scaling factor on predicted K_{TH} within the experimental determination

of H uptake from the rescaled crevices. Finally, experimentally determined K_{TH} in 0.6 M NaCl[3] were plotted to compare against model predictions from inhibited solutions.

Model Prediction of da/dt_{II}

Similar to previous section, the values for $C_{H\sigma}$ were used in the diffusion-limited da/dt_{II} model, Eqn. 5, to predict the dependence of da/dt_{II} on $\eta_{H,bulk}$ in the inhibited solutions. The critical distance was chosen to be 1.0 μm, which was within the range of X_c in high strength alloys for fastest measured HEAC da/dt_{II} in aqueous chloride solutions[19]. The effective diffusivities were calculated using $C_{H,diff}$ values measured in the inhibited rescaled crevice experiment[29].

The critical H concentration was initially chosen to be 0.002 atomic fraction, the lowest predicted $C_{H\sigma}$ from the molybdate inhibited rescaled crevice. Equation 5 shows that $C_c/C_{H\sigma} \leq 1$ results in $da/dt_{II} \geq 0$; therefore, no HEAC is predicted for $C_{H\sigma} < C_c = 0.002$ atom faction.

This low C_c value results in dampening the potential effect on predicted da/dt_{II}. Alternatively, a higher C_c = 0.05 atom fraction was assumed which was the lowest $C_{H\sigma}$ predicted in uninhibited 0.6 M NaCl crevice experiment at $\eta_{H,bulk}$ = 0.018 V (or E_{App} = -0.625 V_{SCE}). The H diffusivities were reduced by a factor of 8 for the predicted da/dt_{II} value to model the experimental measurement of da/dt_{II} in uninhibited 0.6 M NaCl at $\eta_{H,bulk}$ k = -0.457 V (or E = -1.1 V). This is the most cathodic App SCE condition where the driving force for H production is highest, so H atoms are most confidently assumed to be readily available at the crack tip surface and H diffusion to the FPZ is the rate determining step of da/dt_{II}. The additional reduction in DH by a factor of 8 is supported by the higher density of dislocations predicted ahead of the crack tip governed by strain gradient plasticity (SGP)[30]. Assuming the above C_c and D_H values, the prediction captures the trend of da/dt_{II} experimental data in 0.6 M NaCl (polished). At -0.457 V, da/dt_{II} slightly decreased with increasing x^2/G, while at 0.343V, da/dt_{II} slightly increased with increasing x^2/G. The trend shows high sub-critical crack growth rates at extreme anodic potentials with a minimum at$\eta_{H,bulk}$ = -0.057 V.

The selection of a higher C_c = 0.05 atom fraction predicts no HEAC from the local E and pH measured in the crevice experiments for passivated specimens tested in uninhibited 0.6 M NaCl at anodic E_{App}, for tests in molybdate and borate solutions at anodic E_{App}. Such an outcome is predicted because in these conditions the values for $C_{H\sigma} < C_c$ necessary for da/dt_{II}, Eqn. 5. Although the prediction of no HEAC in the inhibited tests is an acceptable outcome, it does not allow for the analysis of the effect of chemical inhibition on reducing HEAC susceptibility at the anodic E_{App}. Also, the verification of chemical inhibition conducted in HEAC fracture tests, to be discussed in next section, showed resolvable measurements of da/dt_{II} in all chemically inhibited solutions.

The low crack tip $C_{H,diff}$ values < 0.88 ppmw for the passivated surface condition and when using chemical inhibitors, may not be high enough after stress enhancement to exceed $C_{c,1}$ = 0.05 atom fracture necessary to nucleate a crack at $X_{c,2}$ = 1 μm ahead of the crack tip[10]. The stress-enhanced concentrations might nucleate a crack by exceeding $C_{c,2}$ = 0.002 atom fraction at a different highly incoherent interface further away from the crack tip assumed at $X_{c,2}$ = 5 μm[19]. Therefore, in this study $C_{c,1}$ and $X_{c,1}$ were used to predict da/dt_{II} from polished specimen data with local $C_{H,diff}$ > 30 ppmw, while $D_{H,1} = f(C_{H,diff})/8$ to predict the highest measured da/dt_{II} = 500 nm/s at most cathodic $\eta_{H,bulk}$ = -0.457 V or E_{App} = -1.1 V_{SCE}. $C_{c,2}$ and $X_{c,2}$ were used to investigate the effect of the passivated surface condition and chemical inhibition on reducing da/dt_{II}, while $D_{H,2} = f(C_{H,diff})/1.6$ to predict the lowest measured da/dt_{II} = 1 nm/s at $\eta_{H,bulk}$ = 0.018 and -0.057 V or E_{App} = -0.625 and -0.7 V_{SCE}, respectively; Fig. 15.

HEAC Testing at Anodic Potentials

Initially, HEAC experiments were conducted in 0.6 M NaCl + 0.01 M Na_2MoO_4 solution at pH = 7.1. Figure 16 shows the subcritical crack growth rate vs. stress intensity in molybdate inhibited sodium chloride solutions at E_{App} = -0.55 and -0.50 V_{SCE} or anodic H over potentials ($\eta_{H,bulk}$) = 0.11 and 0.16 V. Changes in crack growth rates for $K < K_{TH}$ were most probably artifacts due to crack opening, limited crack tip plasticity or low variation in the dcPD signal causing such rates. Slow loading of the fatigue pre-cracked SEN specimens showed inhibition of the threshold stress

(4) For tests with initial loading rates (dK/dt_i) ≤ $7 \cdot 10^{-4}$ MPa-$m^{1/2}$/s, the operational definition of K_{TH} was defined in section 7.3. For tests with 3-times higher loading rates, K_{TH} was defined as the K value that produces da/dt = 1.5 nm/s, since the resolution limit was proportional to the loading rate.
(5) This was the average of two K_{TH} measurements of 18.1 and 19.9 MPa-$m^{1/2}$ with initial dK/dt values $7 \cdot 10^{-4}$ and $2 \cdot 10^{-3}$ MPa-$m^{1/2}$/s, respectively, at $\eta_{H,bulk}$ = 0.16 V.
(6) This was the average of two da/dt_{II} measurements of 1.3 and 1.7 nm/s with initial crack lengths (a_0) 0.213 and 0.998 mm, respectively.
(7) Fe-0.3C-1.1Cr-0.9Mn-0.3Mo-0.2Si-0.04S-0.035P.
(8)This is a further reduction in D_H by 10, so $D_{H,1} = f(C_{H,diff})/80$ and $D_{H,2} = f(C_{H,diff})/16$.

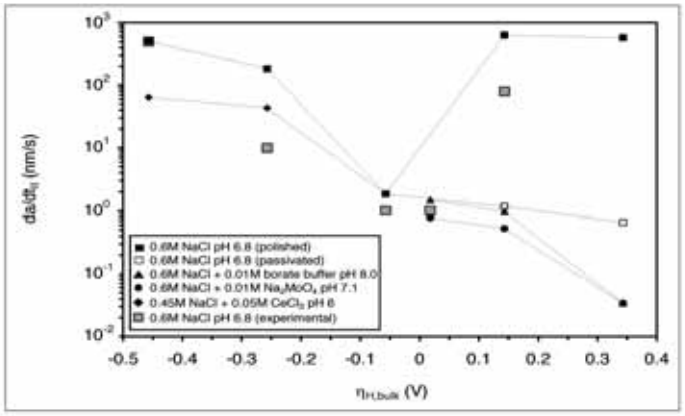

Fig. 15. Predicted da/dt_{II} as a function of applied bulkη_H (assuming $X_{c,1}$ = 1 □m, $X_{c,2}$ = 5 □m, $C_{c,1}$ = 0.05 atom fraction, $C_{c,2}$ = 0.002 atom fraction, $D_{H,1}$ = f($C_{H,diff}$)/8 and $D_{H,2}$ = f($C_{H,diff}$)/1.6) for AerMet 100 crevice experiments in 0.6 M NaCl solution at pH 6.8 (polished and passivated conditions)[15], 0.6 M NaCl + 0.01 M Na_2MoO_4 solution at pH 7.1, 0.6 M NaCl + 0.01 M borate buffer solution at pH 8.0 and 0.45 M NaCl + 0.05 M $CeCl_3$ solution at pH 6.0 with scaling factor 62.5 mm. Results are compared against measured da/dtII values in 0.6 M NaCl[3].

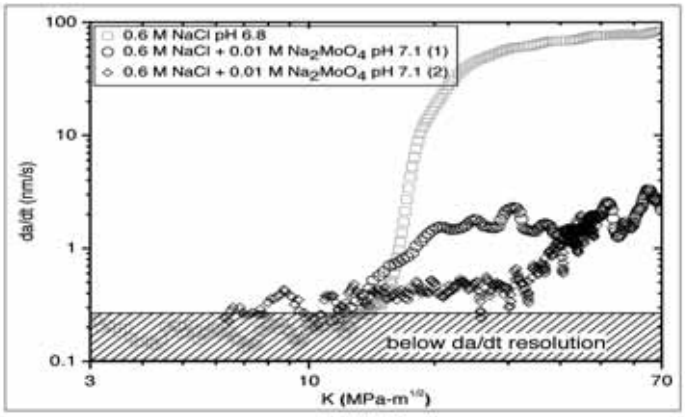

Fig. 16. Subcritical crack growth rate (da/dt) vs. stress intensity (K) for AerMet 100 tested in 0.6 M NaCl solution at pH = 6.83 and 0.6 M NaCl + 0.01 M Na_2MoO_4 solution at pH = 7.1 at $\eta_{H,bulk}$ = 0.16 V (E_{App} = -0.50 V_{SCE}).

intensity (K_{TH})[4] and stage-II subcritical crack growth rate (da/dtII) in 0.6 M NaCl + 0.01 M Na_2MoO_4 at pH = 7.1 compared to results in 0.6 M NaCl at pH = 6.8 at similar $\eta_{H,bulk}$[3]. Results show K_{TH} was enhanced from 12.6 to 14.8 MPa- $m^{1/2}$ at $\eta_{H,bulk}$ = 0.11 V (E_{App}= -0.55 V_{SCE}) and from 15.8 to 19.0 MPa-$m^{1/2}$ at $\eta_{H,bulk}$ = 0.16 V (E_{App} = -0.50 V_{SCE})[5]. More significantly, average da/dt_{II} dropped from 51 to 1.2 nm/s at $\eta_{H,bulk}$ = 0.11 V (-0.55 V_{SCE}) and from 80 to 1.5 nm/s[6] at $\eta_{H,bulk}$ = 0.16 V (-0.50 V_{SCE}). Later, in the experiment at $\eta_{H,bulk}$ = 0.11 V, increasing the over potential more anodically to 0.21 V (-0.45 V_{SCE}) during dynamic loading in stage-II regime had minimal effect on average da/dt_{II} after a two-hour incubation time, where crack growth rate slowed down below da/dt resolution. In

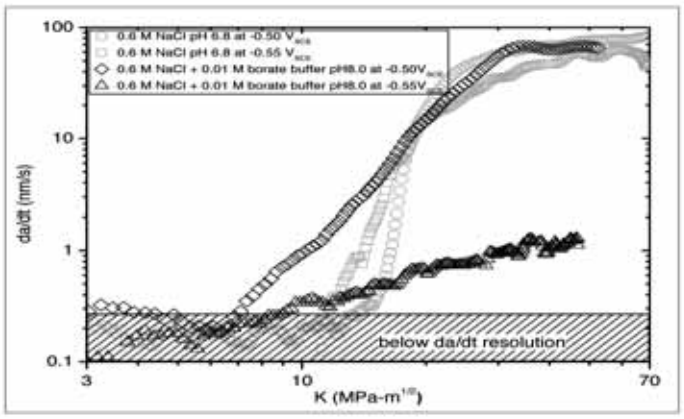

Fig. 17. da/dt vs. K for AerMet 100 in 0.6 M NaCl solution at pH = 6.8[3] and 0.6 M NaCl + 0.01 M borate buffer solution at pH = 8.0 at $\eta_{H,bulk}$ = 0.16 and 0.21 V, E_{App} = -0.55 and -0.50 V_{SCE}, respectively.

the molybdate experiments, the actuator displacement was held towards the end of the tests; crack growth rate decreased during static loading, dropping below the instrumentation detection limit. Finally, testing at $\eta_{H,bulk}$ = 0.16 V (E_{App} = -0.5 V_{SCE}) with higher loading rates, where dK/dt_i = 6.8·10-2 MPa-$m^{1/2}$/s, showed no resolvable HEAC propagation in the SEM fractographs, although dcPD data show elevated potential difference signal through the specimen usually indicative of crack propagation, but was more likely due to crack mouth opening or due to plastic deformation.

HEAC fracture testing was then conducted in 0.6 M NaCl + 0.01 M borate buffer solution at pH = 8.0. As mentioned before, the idea was to use the results in borate buffer to separate the effect of molybdate on indirectly minimizing crack acidification by reducing crack tip dissolution resulting in the reduction of metal ion hydrolysis from molybdate chemically buffering changes to solution pH alone. Figure 17 shows the sub-critical crack growth rate vs. stress intensity in borate buffered sodium chloride solutions at $\eta_{H,bulk}$ = 0.16 and 0.21 V or E_{App} = -0.55 and -0.50 V_{SCE}, respectively.

Table 5 shows, at similar $\eta_{H,bulk}$, an improvement in K_{TH} from 15.8 MPa-m1/2 in 0.6 M NaCl[3] at 0.14 V to 18.8 MPa-$m^{1/2}$ in 0.6 M NaCl + 0.01 M borate buffer at 0.16 V and a reduction in da/dt_{II} from 80 nm/s in 0.6 M NaCl[3] to 1.1 nm/s in 0.6 M NaCl + 0.01 M borate buffer. Such an enhancement in the resistance to HEAC susceptibility was degraded at more anodic $\eta_{H,bulk}$ = 0.21 V, where da/dt_{II} increased to 66.4 nm/s compared to 1.2 nm/s in 0.6 M NaCl + 0.01 M Na_2MoO_4.

Solution		0.6 M NaCl at pH = 6.8		0.6 M NaCl + 0.01 M Na_2MoO_4 at pH = 7.1			
E_{App}	(V_{SCE})	-0.55	-0.50[3]	-0.55	-0.50		-0.45
$\eta_{H,bulk}$	(V)	0.09	0.14	0.11	0.16		0.21
a_0	(mm)	0.943	0.250	0.964	0.213	0.998	–
Δa	(mm)	0.693	~ 2	0.075	0.049	0.186	0.027
test termination		branched	branched	switched to -0.45V_{SCE}	fractured	branched	stopped
dK/dt_i	(MPa-$m^{1/2}$/s)	$4.8 \cdot 10^{-4}$	$6.8 \cdot 10^{-4}$	$4.5 \cdot 10^{-4}$	$7.0 \cdot 10^{-4}$	$2.0 \cdot 10^{-3}$	–
K_{TH}	(MPa-$m^{1/2}$)	12.6	15.8	14.8	18.1	19.9[5]	–
da/dt_{II}	(nm/s)	51.9	80.0	1.2	1.3	1.7	1.2
CMOD	(mm)	$5.8 \cdot 10^{-3}$	$3.4 \cdot 10^{-3}$	$6.9 \cdot 10^{-3}$	$4.0 \cdot 10^{-3}$	$9.4 \cdot 10^{-3}$	–
$2a^2$/CMOD	(mm) (a)[6]	306	37	270	23	212	–
	(b)[7]	208	21	107	13	109	65

Table 5. Summary of test parameters and results from anodic HEAC tests in 0.6 M NaCl solution at pH = 6.8 compared to 0.6 M NaCl + 0.01 M Na_2MoO_4 at pH = 7.1

Figure 18 shows SEM fractographs of the fracture surfaces for specimens tested in uninhibited 0.6 M NaCl solution at pH = 6.8 and 0.6 M NaCl + 0.01 M Na_2MoO_4 solution at pH = 7.1. Testing in 0.6 M NaCl at 0.09 V, part (a), showed widespread HEAC beyond the fatigue pre-crack leading to crack branching after around 0.7 mm crack growth at K = 42 MPa-$m^{1/2}$. Evidence of crack tip corrosion was shown, even after specimen cleaning, at higher magnification examination of the HEAC region as shown in part (b). The HEAC test in 0.6 M NaCl + 0.01 M Na_2MoO_4 at 0.11 V, part (c), showed limited HEAC growth between 20 μm and 100 μm, shown more closely in part (d) with no visible corrosion product on the fracture surface. Finally, the HEAC testing in 0.6 M NaCl + 0.01 M Na_2MoO_4 at more anodic $\eta_{H,bulk}$ = 0.16 V, part (e), also showed limited crack growth up to 50 μm. The surfaces of the HEAC affected regions in the molybdate tests contained finer micro-structural features compared to uninhibited tests, possibly TG cracking along the martensite lath boundaries, which made it difficult to calibrate data results to initial crack lengths. Only when the specimen catastrophically failed in 0.6 M NaCl + 0.01 M Na_2MoO_4 at $\eta_{H,bulk}$ = 0.16 V, part (f), was there prominent dimpled features evident of ductile microvoid cracking (MVC).

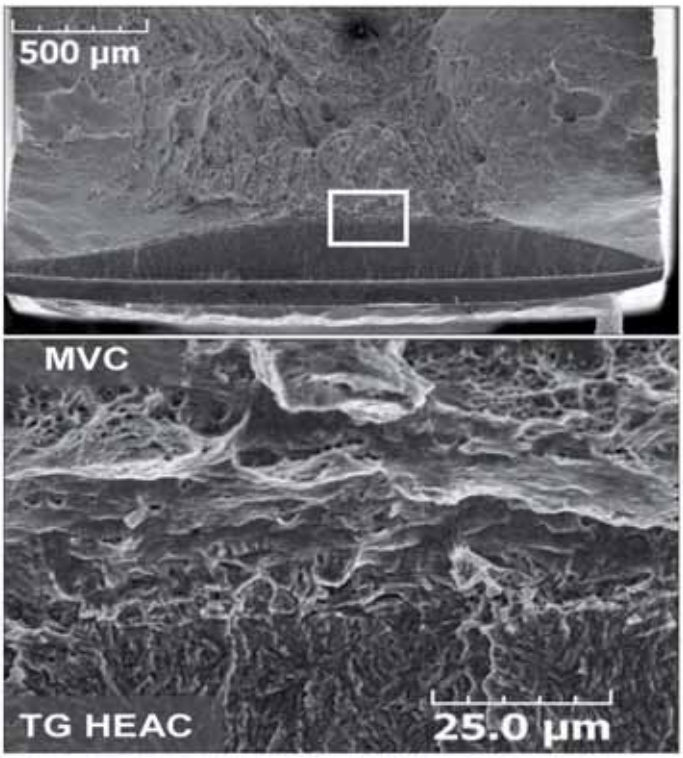

Fig. 18. (Top) SEM fractographs of AerMet 100 tested in 0.6 M NaCl + 0.01 M Na_2MoO_4 at pH = 7.1 at $\eta_{H,bulk}$ = 0.16 V (E_{App} = -0.50 V_{SCE}) and (bottom) a_0 = 0.213 mm in a higher magnification, surface features expanded from the box indicating TG HEAC and MVC ahead of the crack front. All crack growth occurred from bottom to top [acceleration voltage = 20 kV, WD = 39 mm].

Figures 19a and 19b shows SEM micrographs of the surface of the specimens tested in 0.6 M NaCl + 0.01 M borate buffer solution at pH = 8.0. At less anodic conditions, part (a), crack growth was limited to slightly above 20 μm, further shown in (b) as a band of growth beyond the fatigue pre-crack. At more anodic conditions, widespread TG HEAC was observed leading to branching after around 0.7 mm crack growth at a K level of 52 MPa-$m^{1/2}$. Unlike the previous specimens, the fracture surface was covered by extensive corrosion product that could not be removed by post-test cleaning in methanol and acetone.

There was no evidence of bulk charging in any of the anodic tests as there is no driving force for H production on the bulk surfaces. Finally, the unevenness

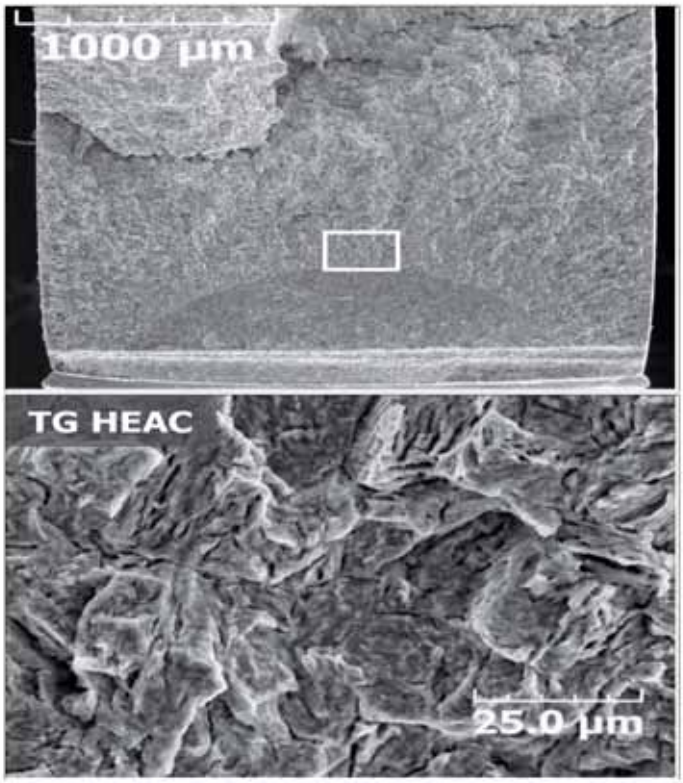

Fig. 19. (Top) SEM fractographs of AerMet 100 tested in 0.6 M NaCl + 0.01 M borate buffer at pH = 8.0 at $\eta_{H,bulk}$ = 0.21 V (E_{App} = -0.50 V_{SCE}) and (Bottom) a_0 = 0.503 mm, with widespread HEAC growth. All crack growth occurred from bottom to top [acceleration voltage = 20 kV, WD = 39 mm].

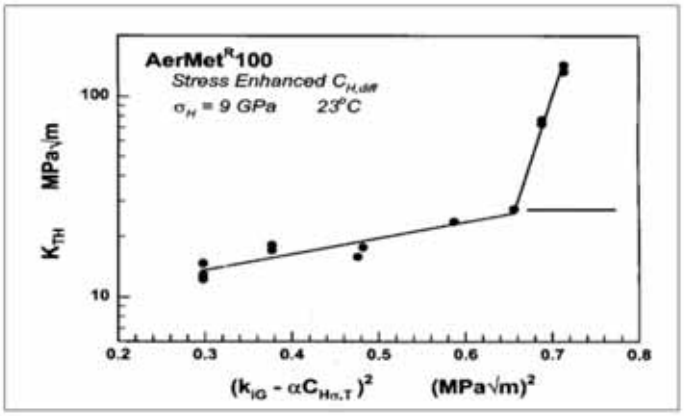

Fig. 20. The measured and Gerberich model predicted effect of stress enhanced H concentration on K_{TH} for AerMet 100. (σ_H = 9 GPa, α = 0.5 MPa-m$^{1/2}$/atom fraction, and k_{IG} = 0.85 MPa- m$^{1/2}$)[11].

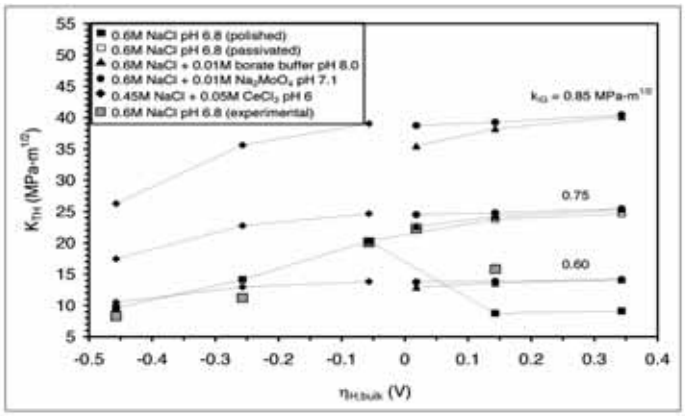

Fig. 21. Predicted K_{TH} as a function of applied bulk η_H (assuming α = 1.0 MPa-m$^{1/2}$/atom fraction and varying k_{IG} = 0.6, 0.75, and 0.85 MPa-m$^{1/2}$) for AerMet 100 crevice experiments in 0.6 M NaCl solution at pH 6.8 (polished and passivated conditions)15, 0.6 M NaCl + 0.01 M Na_2MoO_4 solution at pH 7.1, 0.6 M NaCl + 0.01 M borate buffer solution at pH 8.0 and 0.45 M NaCl + 0.05 M $CeCl_3$ solution at pH 6.0 with a scaling factors x_2/G = 62.5 mm. Results are compared against measured K_{TH} values in 0.6 M NaCl[3].

of the fatigue pre-cracks could not be eliminated, especially for small a_0 specimens; the dcPD method, used during fatigue pre-cracking, averages the potential difference over the length of the sample notch leading to the correct average pre-crack length, but not insuring its straightness. Also, the issue of SEN specimens' curv- ature and more specific manufacturing matters in some specimen, such as the double notch in the borate specimen shown (top), played a role in not attaining straight fatigue pre-cracks.

Discussion

The comparison between predicted and measured KTH and da/dtII values in 0.6 M NaCl + 0.01 M Na_2MoO_4 at pH = 7.1, 0.6 M NaCl + 0.01 M borate buffer at pH = 8.0 and 0.45 M NaCl + 0.05 M $CeCl_3$ at pH = 6.0 will be presented in 6.2 as part of the verification of HEAC mitigation for AerMet 100 in sodium chloride solutions.

Effect of Key Parameters on the H-Enhanced Decohesion Threshold Stress Intensity Model

In the H-enhanced decohesion model, trapped H lowers the cohesive strength of the metal atom bonds along interconnected trap site interfaces. The micromechanical model predicts K_{TH} relative to crack tip Griffith toughness (k_{IG}) in a hydrogen free environment, based on H- decohesion brittle cracking in the presence of crack tip plasticity. The reduction in cohesive strength is proportional to the product of the weighing constant (α) and the stress enhanced H concentration ($C_{H\sigma}$) at the crack tip FPZ. For similar $C_{H\sigma}$, the reduction in K_{TH} could be higher in higher α alloys, based on their microstructure and the distribution of the H-traps.

Figure 20 shows the predicted effect of the Griffith stress-intensity for HEAC (k_{IH}) on K_{TH}, where $k_{IH} = k_{IG} - \alpha \cdot C_{H\sigma}$. The model had closely predicted the trend of the AerMet 100 K_{TH} experimental results. The change in the slope of the K_{TH} vs. k_{IH}^2 correlation at K_{TH} >

30 MPa-m$^{1/2}$ was attributed to mixed mode cracking, involving microvoid coalescence and H-induced TG cracking, while TG cracking was observed at lower K_{TH}[11]. Although the K_{TH} model was initially developed for cleavage fracture, its application to intergranular/TG HEAC of UHSS was possible with differences in key model parameters, e.g., k_{IG} and k_{IH}, were minimal[18]. Gerberich had previously used k_{IG} = 0.85 MPa-m$^{1/2}$ to model threshold stress intensities for AISI 4130[(7)] steel at two different strength levels in 77 kPa H_2 environment.

As for AerMet 100 in NaCl solutions, k_{IG} was selected to be 0.75 MPa-m$^{1/2}$ (α = 1.0 MPa-m$^{1/2}$/atom fraction) to best fit K_{TH} experimental data in uninhibited 0.6 M NaCl solution at pH = 6.8, refer to Fig. 14. Choosing k_{IG} values that are lower than 0.75 MPa-m$^{1/2}$, or having a lower applied strain energy to grow the crack, would dampen the predicted effect of applied potentials and the benefit of ionic chemical inhibition on K_{TH}, while higher k_{IG} values would amplify it as shown in Fig. 21.

Thomas, et al., had previously shown the close correlation between $C_{H,diff}$ in AerMet 100 and K_{TH}, refer to Fig. 4[11]; the increase in $C_{H,diff}$ to 1 ppmw resulted in a 5-fold reduction in K_{TH}, which explained the window of reduced HEAC susceptibility in AerMet 100 around the reversible H potential, where minimal H atoms were produced. Therefore, through measurement of crack tip $C_{H,diff}$ as a function of applied potential and scaling factor the model provides a means of predicting the effects of chemical inhibition on HEAC susceptibility. The model could also be used to study the surmised effect of changing CH,diff with inhibition concentration on the resulting KTH. For example, reducing the crack tip $C_{H,diff}$ by 1⁄2 results in increasing predicted K_{TH} and widening of the enhanced K_{TH} window, while doubling $C_{H,diff}$ results in reducing K_{TH} to values approaching those predicted in uninhibited 0.6 M NaCl solutions, Fig. 22.

Use and Limitation of the Diffusion Limited Stage-II Crack Growth Rate Models

The diffusion limited stage-II crack growth rate model predicts crack propagation rate once $C_{H\sigma}$ exceeds C_c for propagation over X_c ahead of the crack tip, Eqn. 5. The rate of crack growth was assumed to be controlled by hydrogen diffusion from the crack tip surface to the FPZ[19]. The rate of H discharge, adsorption, and absorption reactions at the crack tip were assumed to be fast compared to H diffusion, so the surface reactions are not considered to limit the crack growth kinetics.

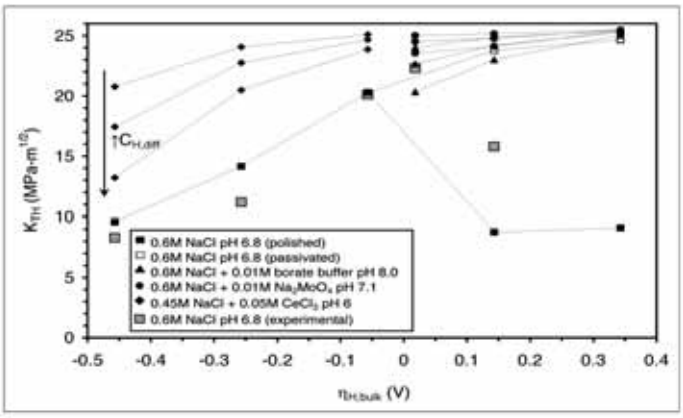

Fig. 22. Predicted K_{TH} as a function of applied bulk η_H (assuming α = 1.0 MPa-m$^{1/2}$/atom fraction and varying k_{IG} = 0.75 MPa-m$^{1/2}$), while $C_{H,diff}$ = 2$C_{H,diff}$ ( ), $C_{H,diff}$ ( ), and ½ CH,diff ( ) from AerMet 100 crevice experiments in 0.6 M NaCl solution at pH 6.8 (polished and passivated conditions)[15], 0.6 M NaCl + 0.01 M Na_2MoO_4 solution at pH 7.1, 0.6 M NaCl + 0.01 M borate buffer solution at pH 8.0 and 0.45 M NaCl + 0.05 M $CeCl_3$ solution at pH 6.0 with a scaling factors x_2/G = 62.5 mm. Results are compared against measured K_{TH} values in 0.6 M NaCl[3].

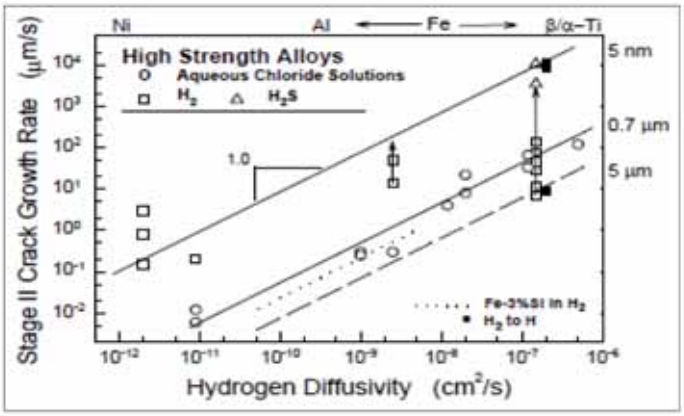

Fig. 23. The dependence of the fastest-measured da/dt_{II} on D_H measured from permeation experiments for a wide variety of high strength alloys that exhibit HEAC in aqueous chloride, H_2 and H_2S environments at 25ÀC[19].

The critical distance was defined by many researchers as the distance to the point of the highest hydrostatic tensile stress ahead of the crack tip[31]. Figure 23 shows that the correlation between fastest da/dt_{II} and D_H in high strength alloys in different environments, including aqueous chloride solutions, suggests that X_c ranges from 5 nm to 5 □m[19]. For the prediction of da/dt_{II} in AerMet 100 using polished specimens tested in uninhibited NaCl solutions, $X_{c,1}$ was assumed to be 1 □m, which is approximately the width of a martensite lath, while $X_{c,2}$ was assumed to be 5 □m[15], which could approximate the width of the martensite packet. As previously mentioned, $C_{c,1}$ was assumed to be 0.05 atom fraction to predict da/dt_{II} for polished specimens tested in uninhibited 0.6 M NaCl with crack tip $C_{H,diff}$

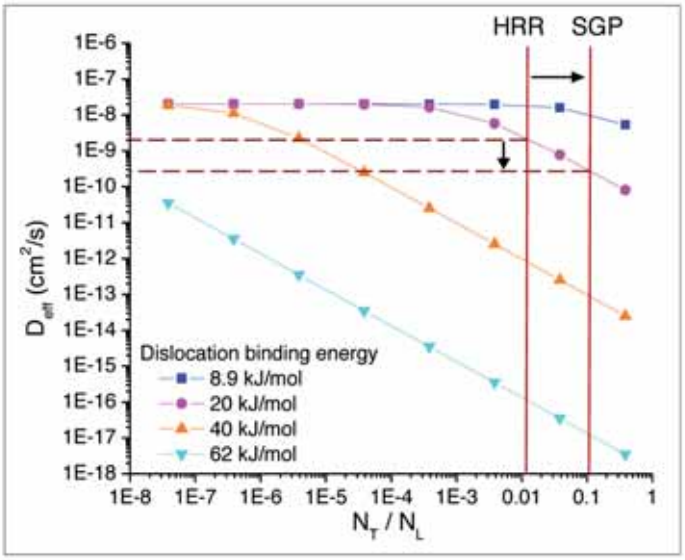

Fig. 24. Model predicted effect of geometrically necessary dislocation density on H-trap sensitive diffusivity (D_{eff} or D_H) in AerMet 100[30].

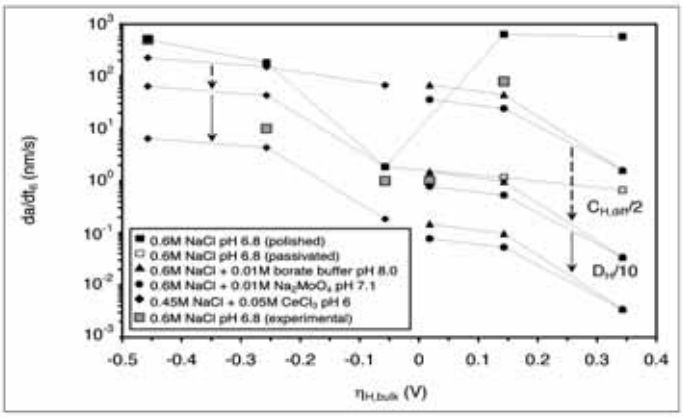

Fig. 25. Effect of reduction in $C_{H,diff}$ and D_H[(8)] on the prediction of da/dt_{II} correlation with $\eta_{H,bulk}$ for AerMet 100 in 0.6 M NaCl solution at pH = 6.8 (polished and passivated conditions)[15], 0.6 M NaCl + 0.01 M Na_2MoO_4 solution at pH = 7.1, 0.6 M NaCl + 0.01 M borate buffer solution at pH = 8.0 and 0.45 M NaCl + 0.05 M $CeCl_3$ solution at pH = 6.0 at lowest scaling factor (x_2/G) = 62.5 mm, $C_{c,1}$ = 0.05 atomic fraction, $C_{c,2}$ = 0.002 atom fraction, $X_{c,1}$ = 1 □m and $X_{c,2}$ = 5 □m. Results are compared against measured da/dtII values in 0.6 M NaCl[3].

	Material	D_H (cm^2/s)	x Range (cm)	$[x/D_H]_c$ (cm/s)$^{-1}$
(a)	AISI 4340	$4.5 \cdot 10^{-7}$	0.07	$1.6 \cdot 10^{5}$
			0.20	$4.4 \cdot 10^{5}$
(b)	99.5% Fe	$6.0 \cdot 10^{-8}$	0.03	$4.2 \cdot 10^{5}$
		$1.6 \cdot 10^{-8}$	0.01	$5.6 \cdot 10^{5}$

Table 6. Ratio of the critical distance to effective H diffusivity from permeation results in AISI 4340[33] and 99.5%[34] in alkaline solutions below which H absorption was considered the rate determining step

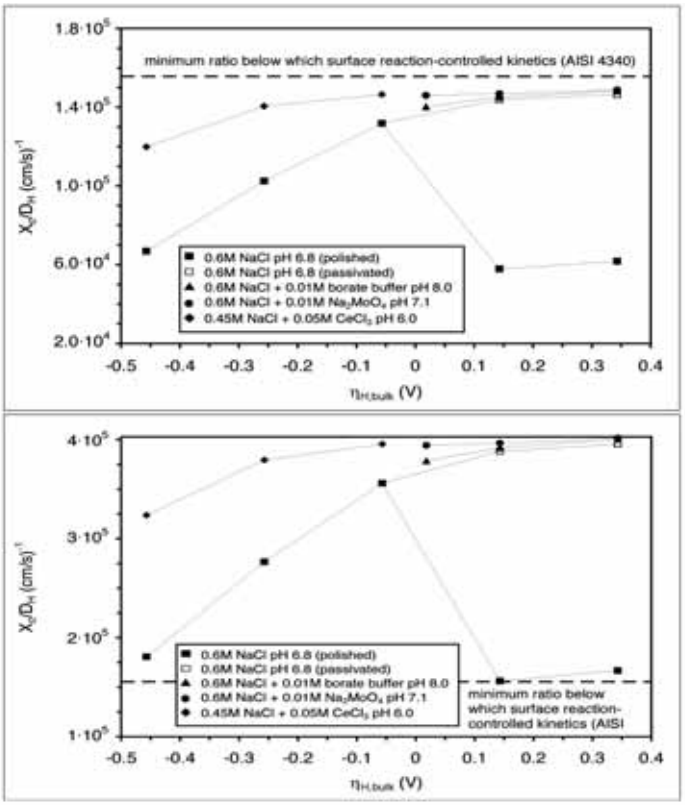

Fig. 26. The dependence of the ratio of critical distance to the effective H diffusivity on the bulk H over potential for AerMet 100 in 0.6 M NaCl pH 6.8 (polished and passivated conditions)[15], 0.6 M NaCl + 0.01 M Na_2MoO_4 pH 7.1, 0.6 M NaCl + 0.01 M borate buffer and 0.45 M NaCl + 0.05 M $CeCl_3$ pH 6.0 at x_2/G = 62.5 mm, $C_{c,1}$ = 0.05 atomic fraction, $C_{c,2}$ = 0.002 atomic fraction, $X_{c,1}$ = 1 □m and $X^{c,2}$ = 5 □m. Results are compared to the minimum $[x/D_H]_c$ below which da/dt_{II} kinetics was surface-controlled in AISI 4340[33] for (Top) $D_{H,1} = f(C_{H,diff})/8$ and $D_{H,2} = f(C_{H,diff})/1.6$, and (Bottom) $D_{H,1} = f(C_{H,diff})/20$ and $D_{H,2} = f(C_{H,diff})/4$.

≥ 0.844 ppmw. $C_{c,2}$ was assumed to be 0.002 atom fraction for passivated specimen and for results in inhibited 0.6 M NaCl solutions with crack tip $C_{H,diff}$ < 0.844 ppmw. The crack tip $C_{H,diff}$ has an effect on the critical H concentration and critical distance ahead of the crack tip at which crack nucleates.

Lee[10] had previously hypothesized that with lower crack tip $C_{H,diff}$ further micro-structural features that require lower C_c in AerMet 100 may nucleate TG H- induced crack damage, while with higher crack tip $C_{H,diff}$ features that require higher C_c can nucleate cracks at closer X_c. Therefore, as H diffuses from the crack tip surface following the stress field, it may not reach the higher C martensite lath interface at closer $X_{c,1}$, but it may reach $C_{c,2}$ causing decohesion and TG cracking along the dislocation-rich martensite packet boundaries at further $X_{c,2}$. The nucleation of a crack at the lower $C_{c,2}$ might be due to the higher packet

boundary strength in the presence of high dislocation density[32]. This is activated with lower crack tip $C_{H,diff}$ values at longer critical distance from the crack tip surface as previously seen in Fig. 13. The argument here is that C_c is function of the incoherent interface and the crack tip $C_{H,diff}$ necessary to cause decohesion and TG cracking, which adds further variability in predicting da/dt_{II}.

By reducing $C_{H,diff}$, inhibitors can also reduce D_H leading to further reduction in da/dt_{II}[29]. The relationship was used as first estimate for D_H at the crack tip, but H diffusivity in steels also depends on the plastic strain and dislocation structure forming ahead of a stationary or propagating crack. As previously discussed, the dislocation structures are H trap sites that lower H mobility in the alloy. The trap-sensitive H diffusivities were initially calculated from local $C_{H,diff}$ values then $D_{H,1}$ values were reduced by a factor of 8 to model measured da/dt_{II} in 0.6 M NaCl solution at E_{App} = -1.1 V_{SCE} or $\eta_{H,bulk}$ = -0.457 V. Such a reduction in DH in the crack tip process zone is supported by a new model of stresses and strains about sharp crack tips governed by material hardening due to strain gradient plasticity (SGP)[30]. The notion is that the very large strain gradient ahead of the crack tip causes a significant density of dislocations. Figure 24 shows the predicted effect of the ratio of H-trap sites (N_T) to interstitial lattice sites (N_L) on D_H in AerMet 100[30]. The vertical lines indicate two assumptions for crack tip dislocation densities based on the classic Hutchinson-Rice-Rosengren (HRR) prediction for a blunted crack tip and the new SGP model for a sharp crack tip. For the case of the dislocation structure having a binding energy around 20 kJ/mol, the effective H diffusivity is reduced by a factor of 7 to 8, which is in agreement with the reduction factor used to predict D_H and da/dt_{II}, Fig. 15.

The critical concentration and critical distance were varied to leverage the use of crack tip $C_{H,diff}$. As previously mentioned, $C_{H,diff}$ is the most important parameter controlling diffusion-limited da/dt_{II}. In theory, reducing $C_{H,diff}$ (and D_H) with chemical inhibitors will bring about a reduction in da/dt_{II}, widening the window of reduced HEAC susceptibility, Fig. 25.

The assumption of a diffusion limited da/dt_{II} model might not be applicable at potential conditions close to minimum HEAC susceptibility. Crack-surface reactions control HEAC propagation kinetics, if the rate of H^+ (H_2O) reduction, H adsorption or absorption occurring on the surface is slower that H diffusion to the FPZ. Prior work on AISI 4340 revealed that H absorption was the rate limiting for sharp cracks in alkaline 0.6 NaCl solutions[33]. The H diffusivity was around $4.5{\cdot}10^{-7}$ cm^2/s, while the permeation foil thickness (x) was of the order between 0.07 and 0.20 cm, below which H absorption was rate limiting. Analysis showed that surface reaction-controlled da/dt_{II} was possible when the ratio of x to D_H was below a critical limit $[x/D_H]_c$ of 1.6 10^5 to 4.4 10^5 $(cm/s)^{-1}$[33]. Similarly, analysis of 99.5% Fe shows that H absorption was rate limiting in alkaline environments for x/D_H below $4.2{\cdot}10^5$ to $5.6{\cdot}10^5$ $(cm/s)^{-1}$, Table 6[34].

Although the permeation critical distances do not signify the distance of crack nucleation ahead of the crack, the estimates of $[x/D_H]_c$ were comparable for these materials, so they could be utilized to examine the rate limiting steps, diffusion vs. surface reactions, in the H uptake kinetics. Subsequently, the crack growth rates in AerMet 100, which was not previously attempted in studying the prediction of da/dt_{II} and HEAC susceptibility.

Figure 26a (top) shows the ratio of the critical distance to H diffusivity (X_c/D_H) in AerMet 100 as a function of H over potentials. It was observed that maximum X /D was around 1.3·105 $(cm/s)^{-1}$ for AerMet 100 in 0.6 M NaCl at $\eta_{H,bulk}$ = -0.057 V. This ratio and all others calculated in the inhibited 0.6 M NaCl solutions were lower than the $[x/D_H]_c$ limit determined in AISI 4340. Figure 26b (bottom) shows the dependence of X_c/D_H on η_H in AerMet 100, but with D_H reduced by a factor of 20 instead of 8 to account for SGP. The higher reduction factor is quite justifiable with slightly higher (2x) trap density or N_T/N_L, Fig. 24. The further decrease in DH results in higher X_c/D_H values for AerMet 100 above the critical limit for AISI 4340 indicating H diffusion limited kinetics.

The view of a constant $[x/D_H]_c$ limit over a wide range of potentials is simplistic. The limit could vary with different crack environments, strain rates, alloy compositions, and in the presence of a surface oxide at the crack tip. In uninhibited solutions, highly anodic and highly cathodic applied potential will result in a higher driving force for H production and uptake. In these cases, the effective diffusivities may be higher possibly leading to lower X_c/D_H values, while crack tip $C_{H,diff}$ and D_H are lower in the potential range of reduced HEAC leading to a higher X_c/D_H values for diffusion control. At anodic applied potentials, the formation of a surface film in the presence of molybdate could

Solution	$\eta_{H,bulk}$ (V)	dK/dt_i (MPa-$m^{1/2}$/s)	K_{TH} (MPa-$m^{1/2}$) (a)	(b)	dcPD baseline (μV)	diff. (%)
Anodic HEAC Testing						
0.6 M NaCl pH = 6.8	0.09	$4.8 \cdot 10^{-4}$	12.6	12.3	156	-2.8
0.6 M NaCl + 0.01 M Na_2MoO_4 pH = 7.1	0.11	$4.5 \cdot 10^{-4}$	14.8	12.7	190	-14.6
0.6 M NaCl + 0.01 M Na_2MoO_4 pH = 7.1	0.16	$7.0 \cdot 10^{-4}$	18.1	12.5	81	-30.8
0.6 M NaCl + 0.01 M Na_2MoO_4 pH = 7.1	0.16	$2.0 \cdot 10^{-3}$	19.9	16.0	183	-19.3
0.6 M NaCl + 0.01 M borate buffer pH = 8.0	0.16	$5.7 \cdot 10^{-4}$	18.8	17.1	69	-9.2
0.6 M NaCl + 0.01 M borate buffer pH = 8.0	0.21	$6.2 \cdot 10^{-4}$	8.2	9.0	119	10.0

Table 7. Summary of K_{TH} determined (a) at da/dt = 0.5 nm/s for initial dK/dt_i [a] 7Û10^{-4} MPa-$m^{1/2}$/s and 1.5 nm/s for dK/dt_i ‘ 2Û10-3 MPa- $m^{1/2}$/s and (b) using a 0.05% offset in dcPD baseline. The % difference is shown for the use of the dcPD offset method vs. the determination at certain da/dt values

Solution	0.6 M NaCl at pH = 6.8		0.6 M NaCl + 0.01 M borate buffer at pH = 8.0	
E_{App} (V_{SCE})	-0.55	-0.50[3]	-0.55	-0.50
$\eta_{H,bulk}$ (V)	0.09	0.14	0.16	0.21
a_0 (mm)	0.943	0.250	0.270	0.503
Δa (mm)	0.693	~ 2	0.024	0.694
test termination	branched	branched	stopped	branched
dK/dt_i (MPa-$m^{1/2}$/s)	$4.8 \cdot 10^{-4}$	$6.8 \cdot 10^{-4}$	$5.7 \cdot 10^{-4}$	$6.2 \cdot 10^{-4}$
K_{TH} (MPa-$m^{1/2}$)	12.6	15.8	18.8	8.2
da/dt_{II} (nm/s)	51.9	80.0	1.1	63.1
CMOD (mm)	$5.8 \cdot 10^{-3}$	$3.4 \cdot 10^{-3}$	$4.6 \cdot 10^{-3}$	$2.8 \cdot 10^{-3}$
$2a^2$/CMOD (mm) (a)	306	37	31	183
(b)	208	21	17	101

Table 8. Summary of test parameters and results from anodic HEAC tests in 0.6 M NaCl solution at pH = 6.8 compared to 0.6 M NaCl + 0.01 M borate buffer at pH = 8.0

act as a barrier for H diffusion leading to higher $[x/D_H]_c$ limits similar to those observed for the reduced HEAC potential range in uninhibited 0.6 M NaCl. Strain rates leading to film rupture rates higher than oxide repassivation rates can expose fresh surfaces and increase D_H leading to lower $[x/D_H]_c$ limits where H diffusion control would still prevail.

In summary, the limitation separating conditions for diffusion- vs. surface-controlled crack growth rates is complex. It cannot be said that conditions are always surface-controlled, and it is reasonable to conclude that diffusion controlled kinetics may prevail under many conditions.

Comparing KTH to da/dt_{II} as Measures for Mitigating HEAC Susceptibility Using Chemical Inhibitors

As previously mentioned, the operational definition of K_{TH} was given as the K level that produced a crack growth rate that was double the resolution limit[3]. This method was utilized because crack growth rates were evident in all experiments and were physically confirmed using SEM fractography. This was a more objective method to consistently estimate threshold stress intensity regardless of crack growth rates and the different inhibitive environments. The K_{TH} might have been overestimated, in some cases, which meant that crack growth might have initiated at lower K levels. Haynes previously used a method where the onset of crack initiation was determined using a deviation or an offset in measured dcPD data vs. actuator displacement, since the potential difference across the crack increases as it grows. The baseline potential was of the order of 500 □V and the deviation used was between 0.025% to 0.05%, or 0.125 □V to 0.25 □V35. Table 7 provides the threshold stress intensity for the anodic HEAC tests attempted using a 0.05% deviation in dcPD baseline compared to the values determined using the operational definition.

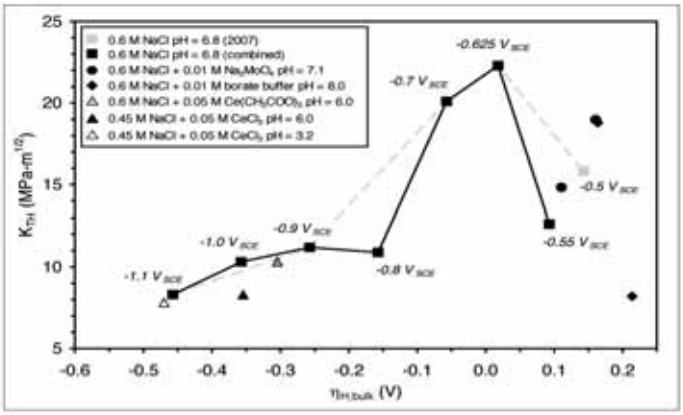

Fig. 27. K_{TH} as a function of $\eta_{H,bulk}$ for AerMet 100 tested in 0.6 M NaCl at pH = 6.8 (combined) compared to 0.6 M NaCl + 0.01 M Na_2MoO_4 at pH = 7.1 and 0.6 M NaCl + 0.01 M borate buffer at pH = 8.0 (anodically)[9].

The dcPD offset method was not used because of the difficulty in repeatedly and reliably applying it due to the subjectivity in determining the potential baseline and the baseline-to-crack growth transition. This was more evident in the chemically inhibited HEAC tests where very low da/dt values were observed. This was evident from the difference % between the latter methods compared to K_{TH} values, Table 8. This and other factors that led to the uncertainty in determining the threshold stress intensity made it difficult to use KTH as a measure for mitigating HEAC susceptibility in AerMet 100 compared to da/dt_{II}. The latter is a more rigorous parameter since it is averaged over a range of K values compared to K_{TH} which depends on assigning a deflection point in the data baseline or a subjective da/dt level at which crack growth was resolvable.

Figure 27 shows that K_{TH} for AerMet 100 tested in 0.6 M NaCl solution was a strong function of E_{App} or $\eta_{H,bulk}$[3]. The potential window of enhanced K_{TH} was attributed to the reduced H overpotentials minimizing the driving force for H production and uptake resulting in HEAC. The highest threshold stress intensity of 22.3 MPa-$m^{1/2}$ occurred at the least cathodic $\eta_{H,bulk}$ of 0.02 V (E_{App} = -0.625 V_{SCE}). Also, the K_{TH} values in 0.6 M NaCl were compared to results obtained in 0.6 M NaCl + 0.01 M borate buffer and 0.6 M NaCl + 0.01 M Na_2MoO_4 at anodic potentials.

The uninhibited data shown in Fig. 27 were complemented with additional results at E_{App} = -0.55, -0.8, and -1.0 V_{SCE}, or $\eta_{H,bulk}$ = 0.09, -0.16, and -0.36 V, respectively. The additional data define a narrower enhanced K_{TH} potential range. The lower threshold stress intensity of 12.6 MPa-$m^{1/2}$ occurred at $\eta_{H,bulk}$ = 0.09 V and a scaling factor of 306 mm compared to 15.8 MPa-$m^{1/2}$ at a more anodic overpotentials 0.14 V and lower scaling factor of 37 mm. The analysis from the rescaled crevices tests in 0.6 M NaCl did not predict a large enough difference in local $C_{H,diff}$ (< 0.3 ppmw) in the above range of x^2/G that could explain the above difference in K_{TH}. This might have been a result of such measurements not being able to capture the exact local environment of a propagating crack at anodic potentials. The addition of molybdate enhanced K_{TH} from 14.8 to 19.0 MPa-$m^{1/2}$ as $\eta_{H,bulk}$ increased more anodically from 0.11 to 0.16 V. The enhanced mitigation might have been due to the formation of a surface film more resistant to crack tip dissolution at more anodic poten- tials in addition to the molybdate chemical buffering of changes in crack electrolyte pH. The addition of borate buffer initially increased K_{TH} to 18.8 MPa-$m^{1/2}$ at $\eta_{H,bulk}$ = 0.16 V, but K_{TH} dropped to 8.2 MPa-$m^{1/2}$ at more anodic $\eta_{H,bul}$ = 0.21 V. This reduction in buffering capacity might have been due to increased metal ion concen- tration in the crack leading to hydrolysis and production of H^+ overwhelming the buffering capacity of borate. The titration tests in 0.6 M NaCl + 0.01 M borate buffer revealed that the loss of the buffering capacity occurred in $[H^+] \geq 5.9$ mM, which corresponds to $[Cr^{3+}] \geq 13.0$ mM in the crack, assuming the hydrolysis reaction in the AerMet 100 was dominated by chromium(III)[14]. This was not predicted from the rescaled crevice experiments in 0.6 M NaCl + 0.01 M borate buffer, even at more anodic E_{App}. The increased K_{TH} resemble results in unbuffered, uninhibited 0.6 M NaCl solution from polished specimens that may approximate the crack tip condition of a propagating crack.

Figure 28 shows that da/dt_{II}, similar to K_{TH}, for AerMet 100 tested in uninhibited 0.6 M NaCl was a strong function of applied potential[3]. The lowest measured da/dt_{II} of 1 nm/s was observed at $\eta_{H,bulk}$ of 0.02 and -0.06 V, or at E_{App} of -0.625 and -0.7 V_{SCE}. Again, the low da/dt_{II} and reduced HEAC susceptibility was attributed to the reduced driving force for H production and uptake, and the da/dt_{II} values in 0.6 M NaCl at pH = 6.8 were complemented with additional tests at $\eta_{H,bulk}$ = 0.09, -0.16, and -0.36 V. These data fit the previous da/dt_{II} vs. $\eta_{H,bulk}$ trend better than the threshold values fit the K_{TH} vs. $\eta_{H,bulk}$ trend, Fig. 27; the new da/dt_{II} data better defined and reinforced the previously established window of reduced HEAC susceptibility for AerMet 100

(9)The italicized numbers next to the 0.6 M NaCl pH 6.8 data points were the applied potentials (E_{App}) at which the tests were performed. Results were plotted against $\eta_{H,bulk}$ rather thanE_{App} to account for the different inhibited solutions' bulk pH values.

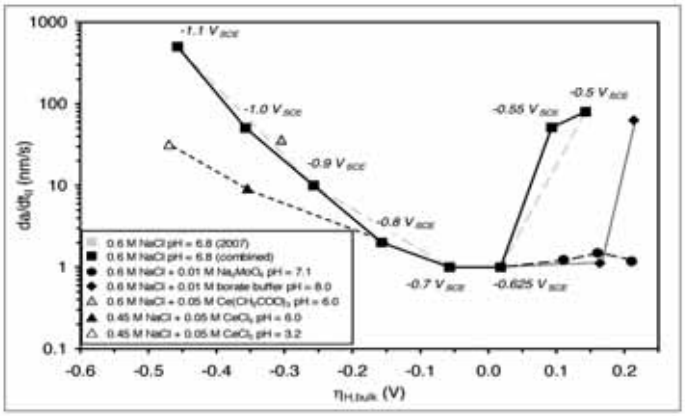

Fig. 28. da/dt_{II} as a function of $\eta_{H,bulk}$ for AerMet 100 tested in 0.6 M NaCl at pH = 6.8 (combined) compared to 0.6 M NaCl + 0.01 M Na_2MoO_4 at pH = 7.1 and 0.6 M NaCl + 0.01 M borate buffer at pH = 8.0 (anodic) and 0.6 M NaCl + 0.05 M $Ce(CH_3COO)_3$.

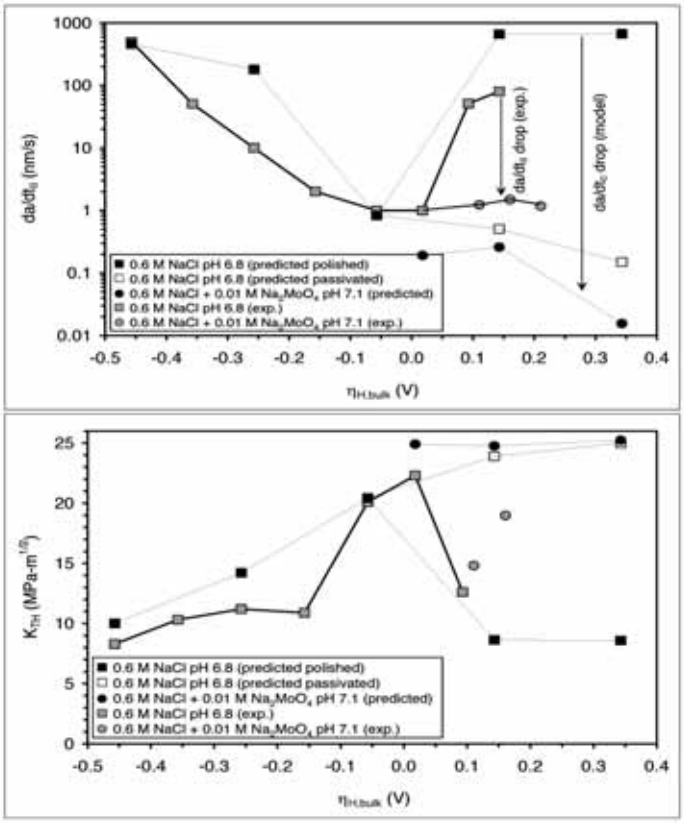

Fig. 29. Model predicted and experimentally determined (top) da/dt_{II} and (bottom) K_{TH} vs. $\eta_{H,bulk}$ for AerMet 100 in 0.6 M NaCl pH 6.8[3,6] compared to 0.6 M NaCl + 0.01 M Na_2MoO_4 pH 7.1.[x_2/G = 562.5 mm, x_2/G = 562.5 $mm^{1/2}$/atom fraction and k_{IG} = 0.75 MPa-$m^{1/2}$, X_c = 1 □m, = 1 C_c = 0.05 atom fraction and $D_H = f(C_{H,diff})/8$].

in 0.6 M NaCl, unlike the new K_{TH} data that restricted the window of reduced HEAC susceptibility. Also, Fig. 28 illustrates the mitigation benefits of molybdate and buffering of borate at anodic potentials in reducing da/dt_{II}. The effects on the stage-II crack growth rate were more pronounced compared to results from the K_{TH} analysis from the same inhibited tests. Again, the fact that da/dt_{II} is averaged over a range of K makes it a more precise parameter compared to K_{TH} that is difficult to determine and require some subjectivity in determining the onset of crack growth, especially in the low crack growth tests in ionic inhibitors.

In the next section, the HEAC mitigation mechanisms of each chemical inhibitor, molybdate and borate buffer will be discussed in light of findings from the re-scaled crevice tests in similar electrochemical environ- ments. The crevice scaling factor x^2/G, or $2a^2/CMOD$, will be used to explain the HEAC test results and probe the local environments in real-sized cracks in AerMet 100.

Correlating Local Electrochemistry Measurements to HEAC Susceptibility in Real-Sized Cracks at Anodic Potentials

The experimentally determined da/dt_{II} and K_{TH} results in molybdate inhibited and borate buffered sodium chloride solutions are compared to the model predictions over the range of tested bulk H over potentials. The stage-II crack growth model is used to back-calculate, using the model parameters, the crack tip $C_{H,diff}$ in the single edge notch specimens used in the HEAC tests. The crack growth model was chosen over the threshold model since the da/dt_{II} data showed mitigation of HEAC susceptibility consistently with chemical inhibitors. Knowledge of local environments helps explain the overall dependency of AerMet 100 HEAC susceptibility on $\eta_{H,bulk}$ (or E_{App}) and the presence of ionic chemical inhibitors.

Figure 29 shows the experimental da/dt_{II} and K_{TH} values determined in 0.6 M NaCl solution at pH = 6.8, including prior work[3] and 0.6 M NaCl + 0.01 M Na_2MoO_4 solution at pH = 7.1 compared to predicted values from rescaled crevices in 0.6 M NaCl solution at pH = 6.815 and 0.6 M NaCl + 0.01 M Na_2MoO_4 at pH = 7.1. Molybdate can inhibit HEAC by reducing crack tip dissolution, resisting chloride effects, forming a permeation barrier, or by chemically buffering changes in crack solution pH[14].

The diffusion limited da/dt_{II} model captured the trend of decreasing crack growth rates observed from the HEAC tests in molybdate inhibited sodium chloride solutions. Figure 29a (top) shows that the model predicts slightly higher da/dt_{II} in 0.6 M NaCl solution and lower da/dt_{II} in 0.6 M NaCl + 0.01 M Na_2MoO_4 solution compared to experimental results. The da/dt_{II} model predicted a reduction in da/dt_{II} at more anodic

conditions in 0.6 M NaCl + 0.01 M Na_2MoO_4 due to the reduction in local $C_{H,diff}$ at more anodic η_H in the continued presence of a protective surface film. The η_H had no effect on experimental results; such trend was not observed most probably due to continued crack propagation and the formation of fresh surfaces during slow strain rate HEAC testing. The exposed surfaces, before repassivation, could present an increased opportunity for H^+ discharge, H adsorption and adsorption increasing local $C_{H,diff}$ responsible for HEAC.

The discrepancy between experimental and predicted K_{TH} values could be linked to the challenge in experimentally determining threshold, but might have been a result of the difficulty in modeling crack nucleation using the steady state measurements of local potential and pH from the rescaled crevice assembly. The K_{TH} model was shown to be useful in predicting HEAC in AerMet 100 in uninhibited, unbuffered 0.6 M NaCl solutions, based on measurements of local $C_{H,diff}$ [15], Fig. 29b (bottom), while other model parameters were optimized in previous studies[11].

Repassivation in 0.6 M NaCl + 0.01 M Na_2MoO_4 was shown to be quick and was achieved within 1 second from the manual scratch, which resembles film rupture during crack growth, at E_{App} = -0.55 V_{SCE} or η_H = 0.11 V. During this repassivation time, H could diffuse up to x = 0.52□m < X_c, assuming $x = (\pi \cdot t \cdot D_H)^{1/2}$ and D_H = 7·10-10 cm^2/s. The H uptake law predicts a crack tip $C_{H,diff}$ of around 0.2 ppmw at η_H = 0.11 V and pH = 6. Assuming that at some stage x = X_c, through slower repassivation due to possible chloride accumulation in the crack[36], the stress-enhanced H concentration still does not initially exceed C_c. Nevertheless, the fact is that stage-II H environment assisted cracking does grow in molybdate, albeit at slower rates, which indicates that the effect of strain rate on the crack tip environment was more complex to simply model compared to using inputs from the rescaled crevice experiments.

During actuator displacement (δ) hold at K = 40 MPa-$m^{1/2}$ on crack growth rates in 0.6 M NaCl + 0.01 M Na_2MoO_4 at pH = 7.1 and E_{App} = -0.5 V_{SCE} (η_H = 0.16 V) crack growth rates instantaneously dropped below the detection limit during static loading. This behavior was observed in prior AerMet 100 HEAC tests in uninhibited sodium chloride, but the reduction in da/dt was not as quick and not as low as in the presence of molybdate[10,14]. This drop in da/dt may have been due to the decrease in crack tip strain rates below what is needed to rupture the surface film resulting in decreased crack tip H uptake below C_c at X_c ahead of the crack tip necessary to propagate HEAC[37,38]. Scully and Moran showed that the presence of an oxide formed on the surface of AISI 4340 in alkaline sodium chloride and in absence of plastic strain inhibited H permeation[33, 39].

It was proposed[36] that molybdate inhibits metal dissolution by reacting with initially oxidized Fe^{2+} forming a non-soluble, protective $FeMoO_4$ on the surface, Fig. 30[36]. The crack solution acidification could then be minimized by the reduction in metal cation concentration that would have otherwise reacted with water molecules (hydrolysis) releasing H^+, decreasing pH = -log[H^+], leading to a local cathodic η_H favorable for higher rate for H production and uptake in absence of an anodic inhibitor.

$$Fe^{2+} + MoO_4^{2-} \rightarrow FeMoO_4 \qquad \text{Eqn. 6}$$

The presence of a surface film formed in 0.6 M NaCl + 0.01 M Na_2MoO_4 solution at pH = 7.1 could also act as a barrier reducing H diffusion through the oxide-substrate interface, thereby reducing H uptake further. It has been shown[33] that the presence of prior corrosion product formed in alkaline sodium chloride on the surface of AISI 4340 reduced H permeation at cathodic current densities in galvanostatically-controlled experiments. Figure 31 shows the effect of the corrosion film on AISI 4340 specimen in reducing the permeation steady state current density compared to the instantaneous cathodic polarization case at similar H charging current density. The permeation

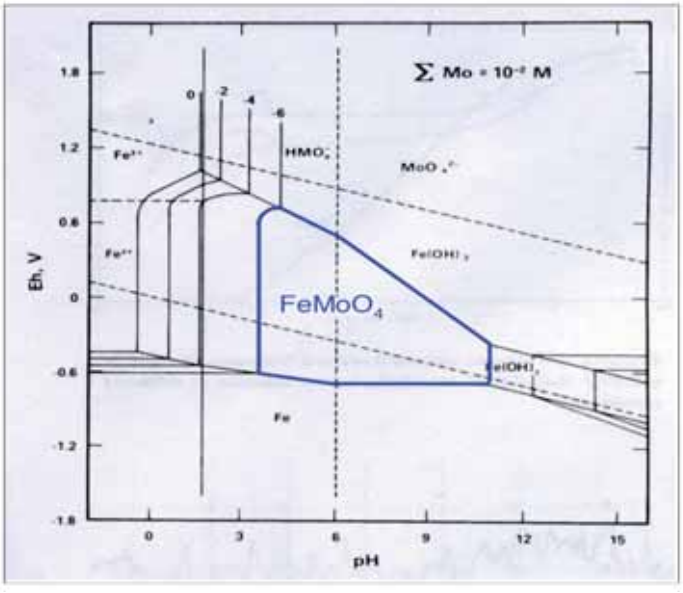

Fig. 30. Fe predominance diagram in 0.01 M Na_2MoO_4 showing the E-pH region of $FeMoO_4$ stability at 298 K[36].

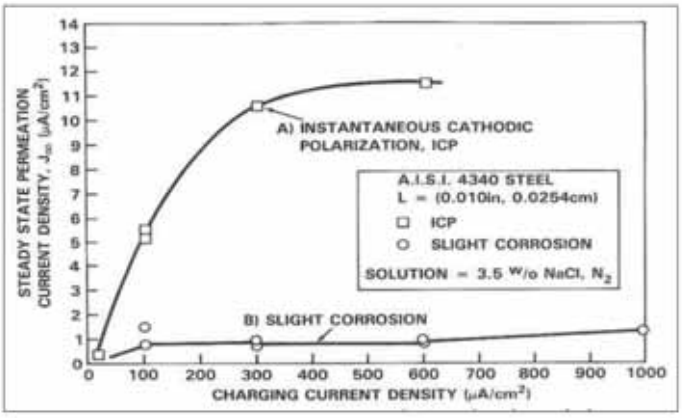

Fig. 31. Relationship between galvanostatic cathodic current density and steady-state hydrogen permeation rate for AISI 4340 steel under slightly corroded conditions and after instantaneous cathodic polarization in alkaline sodium chloride solution[33].

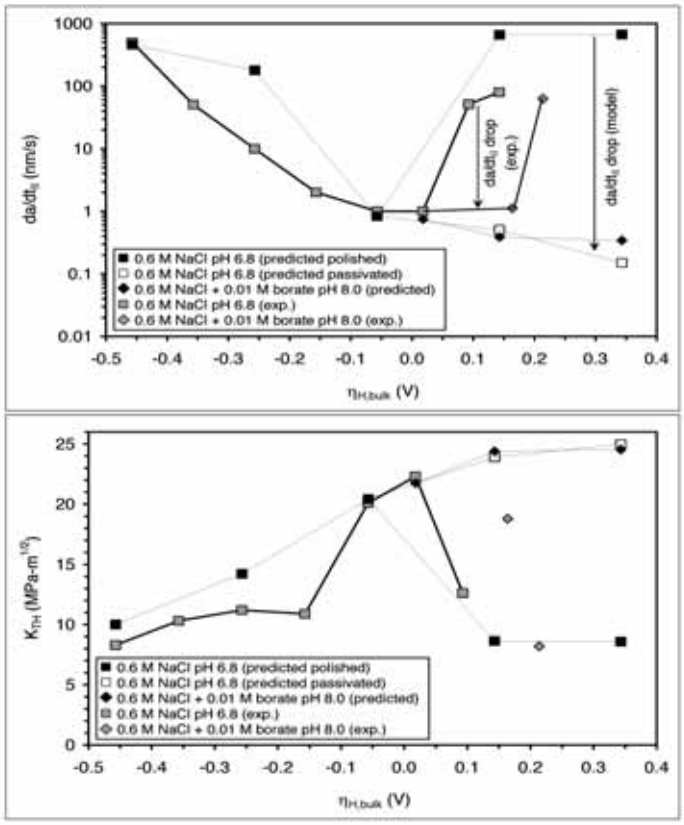

Fig. 32. Model predicted and experimentally determined (a) da/dt$_{II}$ and (b) K_{TH} vs. $\eta_{H,bulk}$ for AerMet 100 in 0.6 M NaCl pH 6.8[3,6] compared to 0.6 M NaCl + 0.01 M borate buffer pH 8.0.[x_2/G = 562.5 mm, α = 1.0 MPa-m$^{1/2}$/atom fraction and k_{IG} = 0.75 MPa-m$^{1/2}$, X_c = 1 □m, C_c = 0.05 atom fraction and D_H = f($C_{H,diff}$)/8].

results showed that the presence of an oxide film in alkaline sodium chloride solutions reduced H surface coverage and, consequently, H absorption.

Molybdate can also operate as a chemical buffer preventing hydrolytic acidification in anodically polarized crack tips. The equilibrium between the two species - making up the solution at pH = 7.1, weak acid ($HMoO_4^-$) and conjugate base (MoO_4^{2-}), results in the mitigation of acidification by the consumption of H^+, Eqn. 7[40]. The maximum molybdate buffering capacity was observed when pH = pK_a = 6. This happened to be the lowest pH value measured from the AerMet 100 rescaled crevice experiments indicating the possibility of chemical buffering playing a role in minimizing change to solution pH[14].

$$HMoO_4^- \underset{K_{-a}}{\overset{K_a}{\Leftrightarrow}} MoO_4^{2-} + H^+ \ (\text{at } pK_a = 6.0) \qquad \text{Eqn. 7}$$

To examine the difference between the effect of indirectly mitigating acidification by inhibiting crack tip dissolution in the presence of a surface oxide and buffering crack solution acidification on H uptake and HEAC, fracture tests were conducted in borate buffered sodium chloride solutions. Borate buffers solution pH by maintaining equilibrium between its weak acid (H_3BO_3) and conjugate base ($H_2BO_3^-$). The borate buffer concentration and pH were selected to minimize any effect on the surface oxide and to still retain buffering capacity, respectively[14].

Figure 32 shows the experimental da/dt$_{II}$ and K_{TH} values in 0.6 M NaCl solution at pH = 6.8 and in 0.6 M NaCl + 0.01 M borate buffer solution at pH = 8.0 compared to predicted values from rescaled crevices in similar solutions. The addition of borate buffer initially reduced da/dt$_{II}$ extending the window of reduced HEAC susceptibility to $\eta_{H,bulk}$ = 0.16 V, but such benefit was not observed at higher $\eta_{H,bulk}$ = 0.21 V when da/dt$_{II}$ increased to 63 nm/s. The latter crack growth rate was as high as values expected between $\eta_{H,bulk}$ = 0.09 and 0.14 V in unbuffered 0.6 M NaCl solution at pH = 6.8. The in- crease in da/dt$_{II}$ at more anodic potentials in 0.6 M NaCl + 0.01 M borate buffer indicates the possibility of the increase in metal cation concentration leading to hydrolysis and acidification that might have overwhelmed the solution buffering capacity.

By comparing Fig. 29 and Fig. 32, it was apparent that the molybdate mitigation of da/dt$_{II}$ extending the window of reduced HEAC susceptibility more anodic from $\eta_{H,bulk}$ = 0.06 to 0.21 V was not the result of chemical buffering of pH change in the crack electrolyte alone, since borate buffer, a chemical buffer, was not able to maintain reduced da/dtII up to 0.21 V.

Conclusions

1. The comprehensive method of using the rescaled crevices, hydrogen uptake laws and the micro-mechanical predictive models was able to capture the

trend of AerMet 100 HEAC susceptibility as a function of E_{App} ($\eta_{H,bulk}$), x_2/G, and tested ionic inhibitors. The method explains the widening of the potential range of reduced susceptibility as a result of the reduction in $C_{H,diff}$ with ionic inhibition.

2. The effect of the ionic inhibitors on reducing experimental da/dt_{II} was a better measure of reducing HEAC susceptibility compared to K_{TH}. The latter parameter was a more subjective parameter due to the difficulty on deciding what K level HEAC initiated, while da/dt_{II} was a more rigorous parameter averaged over a wide range of K level.

3. Molybdate reduced da/dt_{II} at all tested anodic E_{App} expanding the potential window of reduced HEAC susceptibility observed in uninhibited solutions to more anodic potentials. The enhanced mitigation might have been due to the formation of a surface film more resistant to crack tip dissolution at more anodic potentials in addition to the molybdate chemical buffering of changes in crack electrolyte pH both leading to lower crack tip $C_{H,diff}$.

4. The addition of borate buffer initially reduced da/dt_{II}, but da/dt_{II} increased at the most anodic E_{App}. The increase could be attributed to the loss of buffering capacity in the presence of increased metal ion concentration in the crack leading to hydrolysis and production of H^+. This was not predicted from the rescaled crevice experiments in borate buffer.

5. The discrepancies between the predicted and experimentally determined da/dt_{II} could be attributed to the dynamic strain rate acting at the crack tip. Enhanced strain rates could act to rupture the film on the crack tip surface in molybdate inhibited solutions, respectively, exposing the bare surface and enhancing $C_{H,diff}$ and crack propagation in both cases. The complex effect of the crack tip strain rate could not be modeled in the rescaled crevices, although approximations were made in the predictive models to account for it. During static loading, da/dt_{II} dropped immediately indicating the importance of dynamic straining on propagating HEAC.

6. The assumption of diffusion limited crack growth kinetics was reasonable, even for low H uptake conditions, allowing for the use of the diffusion limited da/dt_{II} model. The SGP model justifies further reduction in D_H increasing X^c/D_H above the critical limit $[x/D_H]_c$ indicating the applicability of H diffusion limited kinetics.

References

1. Ayer, R. and Machmeier, P.M.: "Transmission Electron-Microscopy Examination of Hardening and Toughening Phenomena in AerMet 100," Metallurgical Transactions A, Vol. 24, No. 9, September 1993, pp. 1,943-1,955.

2. Agarwala, V.S., Berman, D.A. and Kohlhaas, G.: "Causes and Prevention of Structural Materials Failures in Naval Environments," Material Performance, Vol. 24, No. 6, June 1, 1985, pp. 9-16.

3. Lee, Y. and Ganloff, R.P.: "Measurement and Modeling of Hydrogen Environment-Assisted Cracking of Ultra-High Strength Steel," Metallurgical and Materials Transactions A, Vol. 38, No. 13, 2007, p. 2,174.

4. Dautovich, D.P. and Floreen, S.: "The Stress Corrosion and Hydrogen Embrittlement Behavior of Maraging Steels," in: Staehle, R.W., editor, International Corrosion Conference - Stress Corrosion Cracking Hydrogen Embrittlement Iron Base Alloys, Houston, Texas, 1977, pp. 798-815.

5. Brown, B.F.: "Stress Corrosion Cracking of High Strength Steels," in: Scully, J.C., editor, The Theory of Stress Corrosion Cracking in Alloys, Brussels: North Atlantic Treaty Organization, Scientific Affairs Division, 1971, p.186.

6. Kehler, B.A. and Scully, J.R.: "Predicting the Effect of Applied Potential on Crack Tip Hydrogen Concentration in Low Alloy Martensitic Steels," paper 07RTS4, presented at CORROSION 2007, Nashville, Tennessee, March 11-15, 2007.

7. AerMet®100 Chemical Analysis. Waukesha, WI: Quant Corporation, 2005.

8. AerMet®100 Data Sheet. Reading, PA: Carpenter Technology Corporation, 1992.

9. Li, D., Gangloff, R.P. and Scully, J.R.: "Hydrogen Trap States in Ultrahigh Strength AERMET 100 Steel," Metallurgical and Materials Transactions A, Vol. 35A, No. 3, 2004, pp. 849-864.

10. Lee, Y. and Gangloff, R.P.: "Measurement and Modeling of Hydrogen Environment Assisted Cracking of Ultra-High Strength Steel," Metallurgical and Materials Transactions A, Vol. 38, No. 13, 2007.

11. Thomas, R.L.S., Scully, J.R. and Gangloff, R.P.: "Internal Hydrogen Embrittlement of Ultra-High Strength AERMET 100 Steel," Metallurgical and Materials Transactions A, Vol. 34, No. 2, 2003, pp. 327-344.

12. Rice, J.R. and Thomson, R.: "Ductile vs. Brittle Behavior of Crystals," Philosophical Magazine, Vol. 29, No. 1, 1974, pp. 73-97.

13. Hassel, A.W., Fushimi, K. and Seo, M.: "An Agar-based Silver-Silver Chloride Reference Electrode for use in Micro-Electrochemistry," Electrochemistry Communications, Vol. 1, No. 5, May 1, 1999, pp. 180-183.

14. Al-Ghamdi, S.M.: The Effect of Aqueous Phase Inhibitors on Mitigating Potential-Dependent Hydrogen Environment Assisted Cracking of an Ultra-High Strength Steel, ProQuest, UMI Dissertation Publishing, October 1, 2011, p. 388.

15. Kehler, B.A.: "Modeling and Experiments to Explain the Potential Dependency of an UHSS to Hydrogen Environment Assisted Cracking," ProQuest, UMI Dissertation Publishing, May 2008, p. 296.

16. Johnson, H.H.: "Calibrating the Electric Potential Method for Studying Slow Crack Growth," Materials Research and Standards, Vol. 5, 1965, p. 442.

17. Tada, H., Paris, P.C. and Irwin, G.R.: "The Single Edge Notch Test Specimen," The Stress Analysis of Cracks Handbook, St. Louis, Missouri: Paris Production Inc., 1985, p. 210.

18. Gerberich, W.W., Marsh, P.G. and Hoehn, J.W.: "Hydrogen Induced Cracking Mechanisms - are there Critical Experiments?" in: A.W. Thompson, N.R. Moody, editors. Hydrogen Effects in Materials, 5th Proceedings of the International Conference on the Effect of Hydrogen on the Behavior of Materials. Moran, WY: The Minerals, Metals & Materials Society, September 11-14, 1994, p. 539.

19. Gangloff, R.P.: "Diffusion Control of Hydrogen Environment Embrittlement in High Strength Alloys," in: N.R. Moody, A.W. Thompson, R.E. Ricker, G.W. Was, R.H. Jones, editors. Hydrogen Effects on Material Behavior and Corrosion Deformation Interactions. Warrendale, PA: The Minerals, Metals & Materials Society, 2003.

20. Lillard, R.S. and Scully, J.R.: "Hydrogen Absorption in Iron Exposed to Simulated Concrete Pore Solutions," Corrosion, Vol. 52, No. 2, February 1996.

21. Gileadi, E.: "Electrode Kinetics for Chemistry, Chemical Engineering and Material Science," Charlottesville, VA: University of Virginia (reprint), March 1993, p. 616.

22. Subramanyan, P.K.: "Electrochemical Aspects of Hydrogen in Metals," in Comprehensive Treatise of Electrochemistry, Vol. 4: Electrochemical Materials Science, New York, NY: Plenum Press, 1981. p. 411.

23. Brokris, J.O.M. and Subramanyan, P.K.: "The Equivalent Pressure of Molecular Hydrogen in Cavities within Metals in Terms of the Overpotential Developed during the Evolution of Hydrogen," Electrochimica Acta, Vol. 16, No. 12, December 1971, pp. 2,169-2,179.

24. Conway, B.E. and Salomon, M.: "Electrochemical Reaction Orders: Applications to the Hydrogen- and Oxygen-Evolution Reactions," Electrochimica Acta, Vol. 9, No. 12, December 1964, pp. 1,599- 1,615.

25. Ayer, R. and Machmeier, P.M.: "Microstructural Basis for the Effect of Chromium on the Strength and Toughness of AF1410-based High Performance Steels," Metallurgical and Materials Transactions A, Vol. 27, No. 9, 1996, pp. 2,510- 2,517.

26. Ayer, R. and Machmeier, P.: "On the Characteristics of M2C Carbides in the Peak Hardening Regime of AerMet 100 Steel," Metallurgical and Materials Transactions A, Vol. 29, No. 3, March 1998, pp. 903-905.

27. Akhurst, K.N. and Baker, T.J.: "The Threshold Stress Intensity for Hydrogen-Induced Crack Growth," Metallurgical Transactions A, Vol. 12, No. 6, 1981, pp. 1,059-1,070.

28. Anderson, T.L.: Fracture Mechanics: Fundamentals and Applications, Boca Raton, FL: CRC Press, 1995.

29. Thomas, R.L.S., Li, D., Gangloff, R.P. and Scully, J.R.: "Trap-governed Hydrogen Diffusivity and Uptake Capacity in Ultra-high Strength AERMET 100 Steel," Metallurgical and Materials Transactions A, Vol. 33, No. 7, 2002, pp. 1,991- 2,004.

30. Scully, J.R. and Gangloff, R.P.: "Mechanism- based Modeling of Hydrogen Assisted Cracking in High Strength Alloys for Marine Applications," University of Virginia, 2008.

31. Yamakowa, K., Yonezawa, S. and Yoshizawa, S.: "Hydrogen Embrittlement of High Strength Steel. International Congress on Metallic Corrosion, 2. Toronto, Canada: National Research Council, 1984, p. 254.

32. Wang, M.Q., Akiyama, E. and Tsuzaki, K.: "Determination of the Critical Hydrogen Concentration for Delayed Fracture of High Strength Steel by Constant Load Test and Numerical Calculation," Corrosion Science, Vol. 48, January 2006, pp. 2,189-2,202.

33. Scully, J.R. and Moran, P.J.: "The Influence of Strain

on Hydrogen Entry and Transport in a High Strength Steel in Sodium Chloride Solution," Journal of the Electrochemical Society, Vol. 135, No. 6, June 1988, pp. 1,337-1,348.

34. Lillard, R.S., Enos, D.G. and Scully, J.R.: "Calcium Hydroxide as a Promoter of Hydrogen Absorption in 99.5% Fe and a Fully Pearlitic 0.8% C Steel during Electrochemical Reduction of Water," Corrosion, Vol. 56, No. 11, November 2000.

35. Haynes, M.J.: "Elevated Temperature Fracture of Advanced Aluminum Alloys," Ph.D. Thesis in Materials Science & Engineering, Charlottesville, VA: University of Virginia, 1997.

36. Kodama, T. and Ambrose, J.R.: "Effect of Molybdate Ion on the Repassivation Kinetics of Fe in Solutions Containing Chloride Ions," Corrosion, Vol. 33, No. 5, May 1, 1977, pp. 155-161.

37. Somerday, B.P., Young, L.M. and Gangloff, R.P.: "Crack Tip Mechanics Effects on Environment Assisted Cracking of Beta-titanium Alloys in Aqueous NaCl," Fatigue & Fracture of Engineering Materials & Structures, Vol. 23, No. 1, January 2000, pp. 39-58.

38. Toribio, J. and Elices, M.: "The Role of Local Strain Rate in the Hydrogen Embrittlement of Round-Notched Samples," Corrosion Science, Vol. 33, No. 9, September 1992, pp. 1,287-1,395.

39. Scully, J.R. and Moran, P.J.: "Influence of Strain on the Environmental Hydrogen-Assisted Cracking of a High-Strength Steel in Sodium Chloride Solutions," Corrosion, Vol. 44, No. 3, March 1988, pp. 176-185.

40. Pourbaix, M.: Atlas of Electrochemical Equilibria in Aqueous Solutions, Houston, TX: NACE International, 1974.

41. Scully, J.R., Kehler, B.A., Lee, Y. and Gangloff, R.P.: "Strategies for Mitigation of Hydrogen Environment Assisted Cracking of High Strength Steels," Tri-Service Corrosion Conference, NACE, Houston, Texas, 2005.

Biographies

Dr. Sami M. Al-Ghamdi is the Downstream Corrosion Technology Team Leader in the Consulting Services Department of Saudi Aramco. He joined Saudi Aramco in 1999. Sami is a member of the Corporate Corrosion Management Program Team and the Materials and Corrosion Standards' Committee.

He received his B.S. degree in Chemical Engineering from Tulsa University, Tulsa, OK, and both his M.S. and Ph.D. degrees in Materials Science and Engineering from the University of Virginia, Charlottesville, VA.

Sami has been a member of NACE International since 2003 and ASM International since 2009.

Dr. Richard P. Gangloff is the Ferman W. Perry Professor of Materials Science and Engineering in the University of Virginia in Charlottesville, VA. He has been with the university since 1986, prior to which he worked for Exxon Research and Engineering and General Electric Company.

Richard is also a Fellow of ASM International and ASTM International. He received his B.S., M.S. and Ph.D. degrees in Metallurgy and Materials Science from Lehigh University, Bethlehem, PA.

Richard has published widely; he is the author or coauthor of more than 300 technical papers and more than 70 reports, the editor of five books, and the developer of five university courses.

Dr. John R. Scully is the Charles Henderson Professor of Materials Science and Engineering and Co- Director of the Center for Electrochemical Science and Engineering in the University of Virginia, Charlottesville, VA. He has been with the university since 1990, prior to which he worked for Sandia National Laboratories, AT&T Bell Laboratories, and the Naval Ship Research and Development Center. John is also a Fellow of ASM International, the Electrochemical Society, National Association of Engineers, and NACE International.

He received his B.E.S., M.S. and Ph.D. degrees in Materials Science and Engineering from John Hopkins University, Baltimore, MD.

John has published widely; he is the author or coauthor of more than 250 technical papers and more than 50 reports, the coauthor of 10 books, and the co- editor of eight books. He was recently appointed as the Technical Editor of the Corrosion Journal, NACE International.

Saudi Arabia oil & gas

Saudi Arabia Oil & Gas (Print) ISSN 2045-6670
www.saudiarabiaoilandgas.com
Saudi Arabia Oil & Gas (Online) ISSN 2045-6689

For advertising, contact:

UNITED KINGDOM
Adam Mehar
268 Bath Road, Slough, Berkshire,
United Kingdom
Main 44 1753 708872
Fax 44 1753 725460
Mobile 44 777 2096692
adam.mehar@saudiarabiaoilandgas.com

UNITED ARAB EMIRATES
Abdul Hameed
abdul.hameed@eprasheed.com
Tel: (971) 5056 8515

SAUDI ARABIA
Akram ul Haq
PO Box 3260, Jeddah 21471
akram.ul.haq@saudiarabiaoilandgas.com
Tel: (966) 557 276 426

EPRASHEED
signature series

Purchase Now

The Hydrocarbon Highway

"I found the book excellent because it provides a balanced and realistic view of the oil industry and oil as an important source of energy for the world"

Dr AbdulAziz Al Majed, Chairman, Department of Petroleum Engineering, King Fahd University of Petroleum & Minerals.

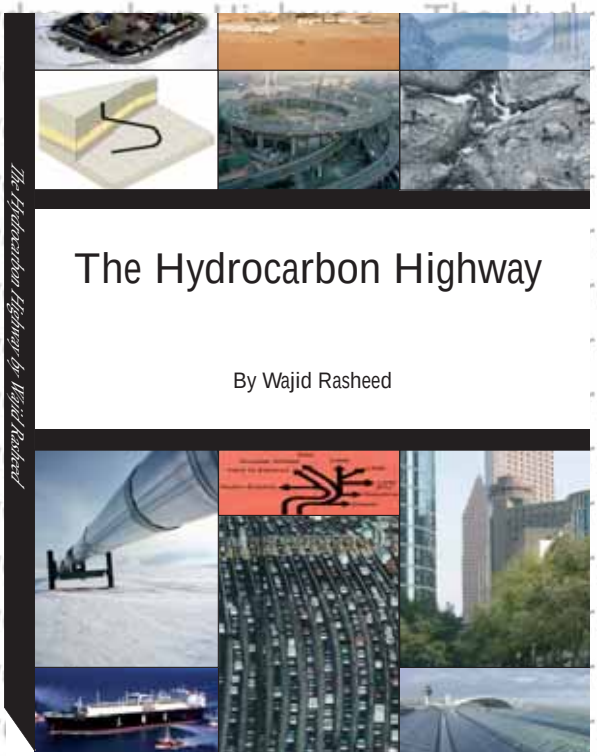

Please send me ☐ copies of The Hydrocarbon Highway

Name: .....

Title: .....

Company: .....

Mailing Address .....

.....

.....

Phone: Fax: .....

Please debit my credit card:

Visa/Mastercard Number .....

Name on Card..... Expiry.....

☐ I enclose a cheque or banker's order in US Dollars, payable to EPRasheed Ltd

Charges Per Book:
The Hydrocarbon Highway: $39.95
Standard Delivery: $10.00 ☐ Express Delivery $30.00 ☐

Signature .....

Mail all Orders to:
11 Murray St, Camden, NW1 3RE, London, England

Testing Methodology for Smart Wells Completion Toward Attaining Optimal Production Rate Setting for Maximum Hydrocarbon Recovery

By Samih M. Alsyed and Karam S. Al-Yateem.

Reprinted with kind permission from the Saudi Aramco Journal of Technology.

Every oil company strives to produce its fields smartly, effectively and efficiently to ensure maximum recovery and minimize any unrecovered reserves. In its position as the largest integrated oil company with the most reserves, Saudi Aramco has placed itself at the forefront of such efforts by utilizing real time data and controls, also referred to in our industry as smart or intelligent wells and controls. Some of these efforts are evident from the recent development of the Haradh III increment (2006), part of Ghawar field, which is considered to be the world's first fully intelligent field[1]. Prior to that, the company launched individual intelligent field ventures in many fields, including Safaniya, the world's largest offshore oil field. Safaniya holds a wide range of intelligent field equipment and is expected to be fully automated in the near future. Completing wells with smart completion jewelry is one step toward automation. With an increasing number of smart well completions in Safaniya, the need now is to ensure that the maximum benefit is gained from them and that the completion design is optimized early on.

This article addresses the procedure adopted to conduct the first tests on smart well completions in one of Saudi Arabia's offshore fields. The article details the processes and practices of testing smart well completions for the inflow performance and capacity of all laterals, and the operation of the downhole valves. To evaluate the various completion practices and configurations in horizontal multilateral wells, the test was conducted on two different wells with two different completion configurations. This practice helped optimize the completion design (tubing size, number of multilaterals) of dual lateral wells with inflow control valves (ICVs) to maximize production.

Introduction

A smart well is a well that contains downhole instrumentation coupled with a surface controlled actuation system. Some of the downhole sensors and controls include a permanent downhole monitoring system (PDHMS): gauges and hydraulically operated inflow control valves (ICVs). Traditionally, these components are installed at the end of the production tubing and run with control lines strapped to the outside of the tubing. More recently, the components have been run separately: they are installed and hung first, using a separate packer, and then the production tubing is run with the control lines. The mating of the two is done through a snap latch connection.

These smart wells allow for continuous monitoring of fluid flow rates and pressures, and the subsequent adjustment of downhole valves from the surface[2] without the need for any well intervention. The first intelligent completion was installed in August 1997 at Saga's Snorre Tension Leg Platform in the North Sea[3], and since then the technology application has increased exponentially. Saudi Aramco is at the forefront with the Haradh III increment (2006), part of Ghawar

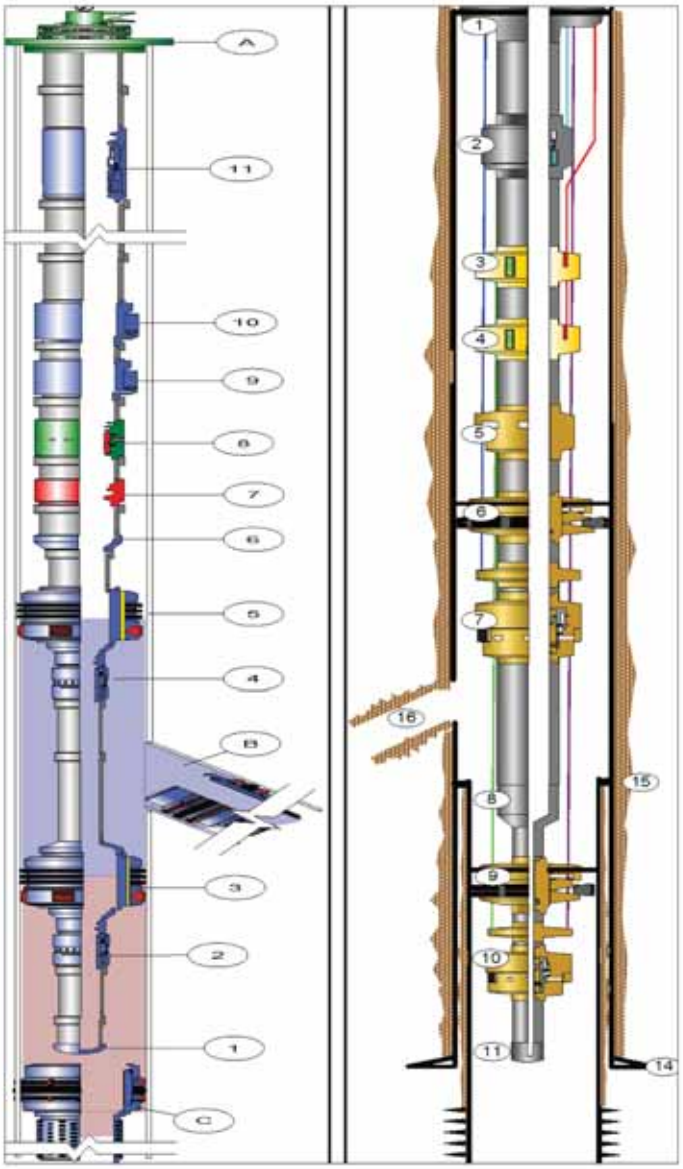

Left: (A) 4½" Tubing Hanger, (11) SSSV, (10) Upper Gauge Mandrel, (9) Lower Gauge Gandrel, (8) Sleeve, (7) X-nipple, (6) X-over, (5) Mechanical Packer, (4) Lateral ICV, (3) Mechanical Packer, (2) Motherbore ICV and (1) Bull Plug.

Right: (1) Tubing Hanger, (2) SSSV, (3) Upper Gauge Mandrel, (4) Lower Gauge Mandrel, (5) X-nipple, (6) Mechanical Packer, (7) Lateral ICV, (8) X-over, (9) Mechanical Packer, (10) Motherbore ICV, (11) Bull Plug and (16) Lateral Window.

Fig. 1. Typical Safaniya smart well completions configuration.

field, which is considered to be the world's first fully intelligent field[1]. The advantage of such technology is the anticipated increase in hydrocarbon recovery by delaying water breakthrough, especially in horizontal wells with multiple laterals. This delay is achieved by continuously monitoring downhole pressures and adjusting the downhole chokes and ICVs accordingly.

To maximize the benefits of this or any new technology, optimization is important. It is also essential to identify any improvements and/or changes early on in the technology application so lessons learned are applied swiftly. This article is one such effort to ensure that the recently installed smart completions in the world's largest offshore oil field, Safaniya, are optimized to their maximum capability, and that any changes in completion design and/or size are applied as early as possible to benefit the ongoing rapid deployment of this technology in the field.

Reservoir Properties and Well Completions

Safaniya is a sandstone reservoir with high permeability, > 1 Darcy, and moderate porosity, > 20%. It produces relatively heavy sweet oil, API ~ 28°. The reservoir pressure is maintained by a natural water drive mechanism, and the gas-oil ratio is low, < 250 scf/bbl, in the produced fluid.

Although horizontal wells have been drilled in Safaniya since the early 1990s, the first dual lateral well was drilled and completed only in 2007. Even though this well was completed with a PDHMS and therefore could be monitored continuously, there was no means of controlling the flow from the laterals. The first smart completion in a dual lateral well with a PDHMS and the means to control production from each lateral was completed in late 2008 and put on production early in the following year. Since drilling the first dual lateral well, the lateral completion configuration in the field has evolved from cemented and selectively perforated laterals to sand screens and passive inflow control devices (ICDs) set in open hole laterals. ICDs are designed to control the flow from different compartments and zones in the lateral at a preset restriction rate. The compartmentalization of each lateral is accomplished by setting open hole packers for isolating different zones. The preset restriction is determined by looking at the rock quality during drilling of the open hole. All this is done to ensure uniform oil production throughout the lateral.

The current smart completions in Safaniya are dual laterals, and most of them were completed with sand screens and ICDs, with individual lateral production controlled by an ICV installed at the end of the production tubing. Figure 1 shows a typical smart well completion for a Safaniya well.

The main reasons for the ICD and ICV completion practice are:

• ICDs help delay water breakthrough by controlling or choking back production from prolific reservoir sections and allowing more flow from poorer quality

reservoir sections. This is done inside the individual lateral.

• ICVs are helpful in choking back or closing one lateral in case of water production.

• The downhole monitoring system is helpful in measuring the contribution from an individual lateral.

• Continuous downhole pressure monitoring is also beneficial in reservoir management and helps in keeping an eye on reservoir depletion.

The old and new completion practices, as described above, were employed in the two subject wells. Well-A was completed under the new thinking of compartmentalization, i.e., with ICDs in both laterals, while Well-B was completed with the old completion technique of cemented laterals with selective perforations. As in all smart completions, the valves controlling the flow from each lateral have certain setting positions, some from 1 to 5 and some from 1 to 10. A setting of 1 is the smallest valve opening, while the largest number (5 or 10) is the fully open position. Both Well-A and Well-B were completed with 10 position ICVs.

As for the upper completion, both wells were completed with 4½" tubing, a downhole packer and a subsurface safety valve (SSSV).

Basic Correlations

To determine the performance of any conventional oil or gas well, inflow performance relationship (IPR) and outflow or tubing performance relationship (TPR) curves are used. Figure 2 shows typical IPR curves for a conventional Safaniya well, while Fig. 3 shows typical TPR curves for a Safaniya well. When plotted together, the resultant curve, Fig. 4, gives the flow from different completions and a way to choose the optimum completion size and type. There has been a lot of work done on these curves on simple wells, with results published in petroleum engineering books. Similar IPR and TPR curves were generated to evaluate our subject smart well completions' performance.

Testing Procedure for Smart Wells

Given that the first smart well in Safaniya was put on production only in 2009, there was a need to expedite the evaluation and optimization of the initial smart well's performance so engineers could implement any necessary changes to the completion design in future wells. Flow rate and pressure tests were carried out with the systematic actuation of the ICVs. It is worth mentioning that before this performance evaluation and optimization commenced, both subject wells had been producing with both lateral valves fully open. Also, at the time of the test, the surface control panels had not been installed, so a portable panel was utilized to temporarily actuate and test the controls, and optimize the wells.

The following is the step-by-step test procedure applied to both wells:

1. Both motherbore and lateral valves were closed, and the wellhead pressure (WHP) at the surface was depleted to ensure that the ICVs were holding at a fully closed position.

2. The motherbore ICV was left fully closed and the lateral ICV was set to a fully open position. The surface choke was adjusted to record WHP and downhole pressure, and their corresponding surface rates were recorded using the multi-phase flow meter (MPFM) installed on the platform.

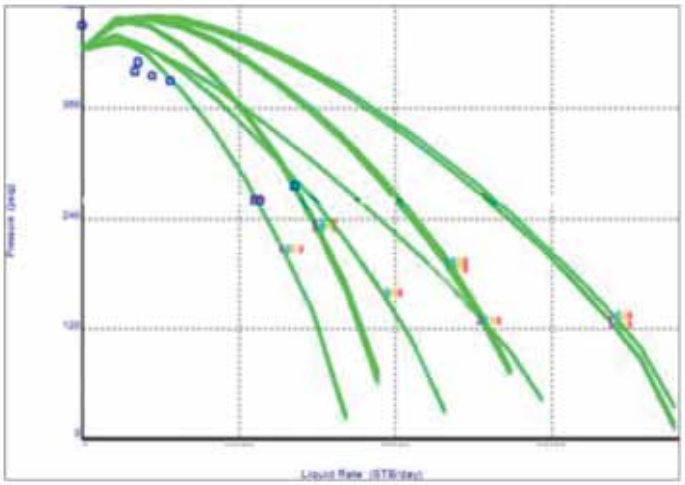

Fig. 2. A set of typical IPR curves.

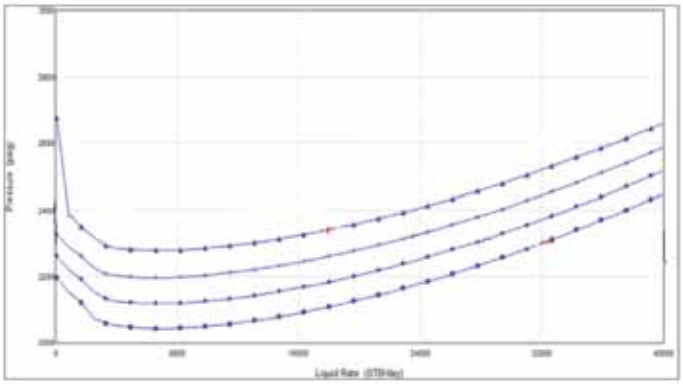

Fig. 3. A set of typical TPR curves.

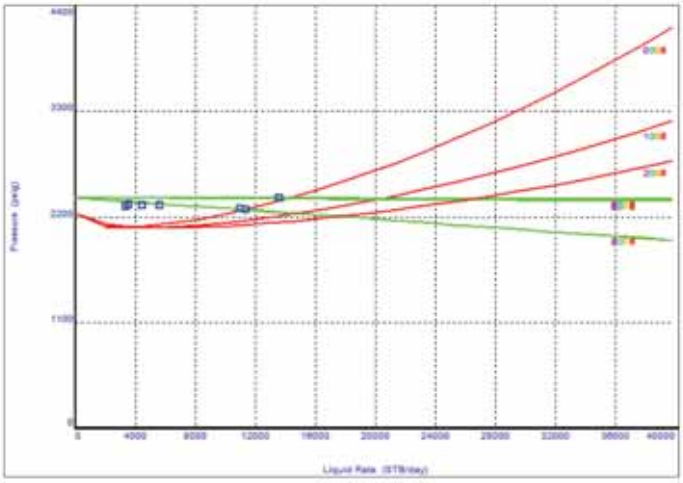

Fig. 4. Sensitivity analysis through plotting various IPR and TPR curves together.

3. The lateral ICV was set to the fully closed position and the motherbore ICV was set to the fully open position. The surface choke was adjusted to record WHP and downhole pressure, and their corresponding surface rates were recorded using the MPFM. Four different pressure and rate points were acquired.

4. With the lateral ICV closed and the setting of the surface choke fixed, the motherbore ICV was manipulated from position 2 to 9 while the surface and downhole pressures were recorded, in addition to surface production rate.

5. The previous step (Step 4) was than repeated for the lateral, leaving the motherbore ICV fully closed.

6. Both ICVs were set at position 5, and the surface and downhole pressures were recorded, in addition to the production rate.

7. With the motherbore ICV set to position 10 (fully open) and the lateral ICV set to position 5 (50% open), the surface and downhole pressures were recorded, in addition to the production rate.

8. The previous step (Step 7) was repeated with the lateral ICV at position 10 and the motherbore ICV at position 5.

9. Finally, the well was flowed with both the motherbore and lateral ICVs set at position 10 (fully open).

The above procedure was accomplished in 28 steps in the first well, but was optimized for the second well to be completed in 21 steps.

Testing and Simulation Runs

All the acquired data, i.e., production rate from the MPFM vs. downhole pressure, and production rate from the MPFM vs. WHP, was plotted to give the base IPR and TPR curves. The matched data can be seen in Figs. 5 and 6. These were then used as a base case to simulate performances for different completions to evaluate the completion design could be optimized for future dual lateral smart wells in the field. This optimization was mainly done by changing the size of the tubular and trying the different ICV positions available to control the flow from each lateral.

Discussions

By using the base case and simulating for the optimum tubing size, it was clearly observed that the 4½" tubing was restricting the flow when both laterals were put on full open production. In fact, the contribution from one lateral was almost negligible because of the extra pressure that the flow had to overcome due to the smaller tubing. Figure 7 shows a drop in friction and WHP as the size of the tubing is increased while keeping the same flow parameters. Figure 8 shows the IPR vs. TPR curve, which indicates that the production rate could be main- tained at a stable rate even if the well tubular is increased to 5½" or even 7" sizes.

To ensure that the bigger tubing size will not be detrimental in the later life of the well, a similar curve was simulated for up to 40% water cut, and the result was promising. A stable flow could still be maintained at 40% water cut in a 5½" tubular, Fig. 9.

It was also observed that the production rates from the two differently completed wells, one where both laterals were completed with screens and ICDs, and the other where both laterals were completed with cemented perforated liners, were the same. It is anticipated that in the long run, through the life of the well, the perforated laterals may start to cut water earlier than laterals in the ICD completed wells, because with ICDs the oil sweep should be controlled, thereby delaying water breakthrough. This is yet to be seen, as these wells are still in their early stages of production.

Conclusions

The following conclusions were drawn from the optimization study conducted on newly completed smart wells in this offshore sandstone field.

1. A simple method of IPR and TPR curves was used to optimize the design of the newly implemented smart well completions in the field. This could form

the basis for optimizing future completions in the same reservoir.

2. The initially installed tubing size is restricting the flow from the well and needs to be increased to maximize production; the simulated well performance indicates that the bigger tubing size is suitable for early as well as later stages of the well life.

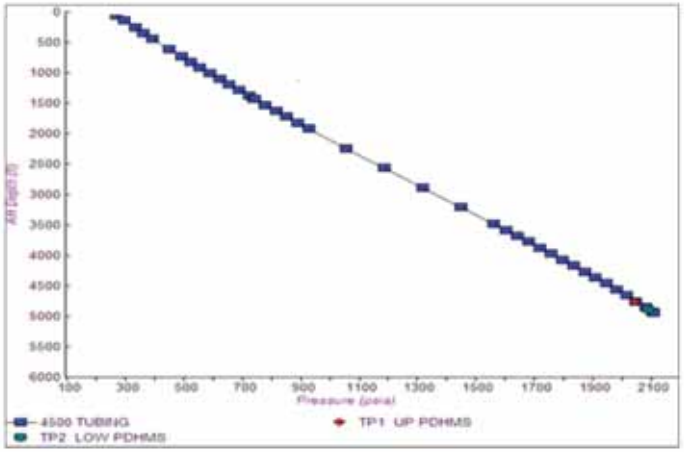

Fig. 5. Matched simulation with actual field data from downhole pressure tests.

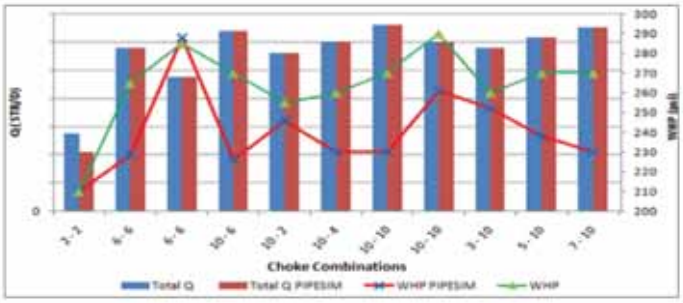

Fig. 6. Matched simulation with actual field data from WHP tests.

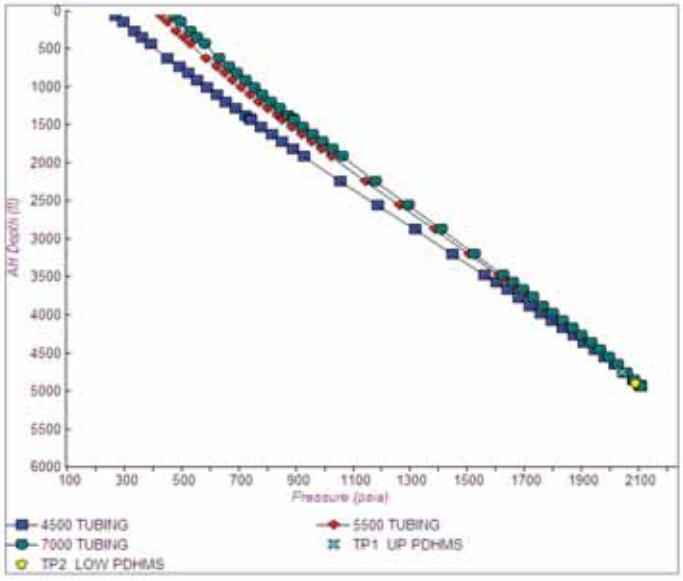

Fig. 7. Simulation results for friction pressures with different sizes of tubing.

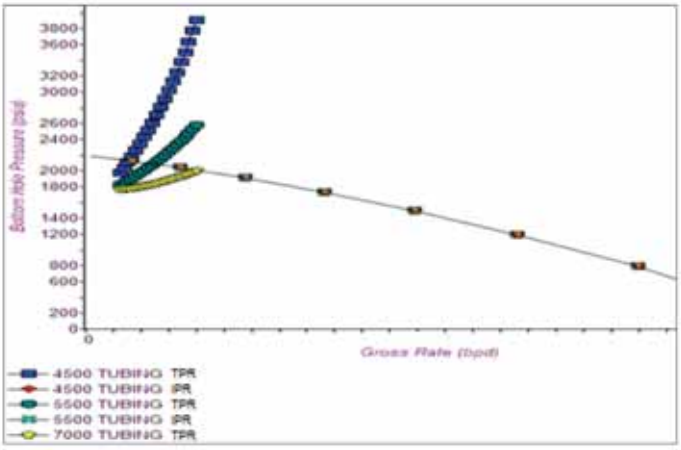

Fig. 8. IPR and TPR curve for different sizes of tubing.

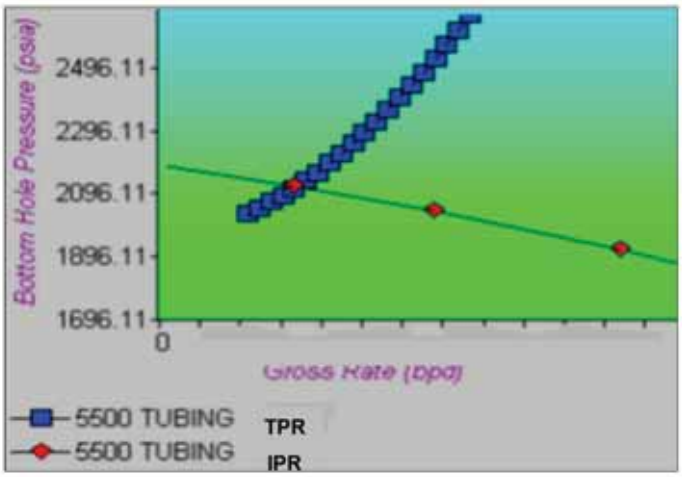

Fig. 9. IPR and TPR curves for simulated late life production.

3. Initial production rates were similar in both the open hole ICD screen completion well and the cemented, selectively perforated liner completion well.

Acknowledgements

The authors would like to thank Saudi Aramco management for their permission to present and publish this article. Special thanks go to Faisal N. Al-Nughaimish for his insightful feedback and support, and to the technical review committee of the Northern Area Production Engineering & Well Services Department (NAPE&WSD).

This article was presented at the SPE Intelligent Energy International Conference and Exhibition, Utrecht, The Netherlands, March 27-29, 2012.

References

1. Al-Arnaout, I.H., Al-Driweesh, S.M., Al-Zahrani, R.M. and Jacob, S.: "Intelligent Wells to Intelligent Fields: Remotely Operated Smart Well Completions

in Haradh- III," SPE paper 112226, presented at the Intelligent Energy Conference and Exhibition, Amsterdam, The Netherlands, February 25-27, 2008.

2. Yeten, B., Durlofsky, L.J. and Aziz, K.: "Optimization of Smart Well Control," SPE paper 79031, presented at the SPE International Thermal Operations and Heavy Oil Symposium and International Horizontal Well Technology Conference, Calgary, Alberta, Canada, November 4-7, 2002.

3. Gao, C., Rajeswaran, T. and Nakagawa, E.: "A Literature Review of Smart Well Technology," SPE paper 106011, presented at the Production and Operations Symposium, Oklahoma City, Oklahoma, March 31 - April 3, 2007.

Biographies

Samih M. Alsyed is a Senior Production Engineer with Saudi Aramco in the Safaniya Production Engineering Division. He joined Saudi Aramco in 2008 and is currently working as Lead Engineer for the Safaniya oil field. Samih was also involved in the successful startup of Karan, Saudi Aramco's first offshore nonassociated gas field, in 2011, where he played an integral role on the Northern Area Gas Production Engineering team. Prior to joining Saudi Aramco, Samih worked for Schlumberger for 12 years in its Coiled Tubing and Fracturing Services. His work experience spans the U.S. (Gulf of Mexico, Texas, Louisiana and California), Canada (Red Deer) and Algeria (Hassi Messaoud).

Samih received his M.S. degree in Geophysics from Quaid-e-Azam University, Islamabad, Pakistan, and another M.S. degree in Petroleum Engineering from Montana Tech of the University of Montana, Butte, MT.

He has been a member of the Society of Petroleum Engineers (SPE) since 1996. Samih is a patent holder in fracturing fluids technology and has coauthored several SPE papers.

Karam S. Al-Yateem started his professional career with Saudi Aramco immediately after graduation. Since then, he has completed several assignments in various onshore and offshore field locations. Karam has worked as a Reservoir Engineer, Field Engineer, Testing Engineer and Production Engineer. He worked with the Computational Modeling Technology team as a summer student trainee. Karam later worked on the 3D Well Planning and Analysis System Project and was a mentor to many newly hired young professionals.

He has authored and coauthored several technical papers. Karam has represented Saudi Aramco in various international forums and conferences, and he chaired the first Society of Petroleum Engineers (SPE) Young Professionals Technical Symposium (YPTS) in 2007. He is the recipient of the 2008 Young Member Outstanding Service Award. Karam is an active SPE member and currently serves as a member of the Young Professionals task force of Production & Operation, as an executive board member of the Saudi Arabia Section of SPE and as a board member of the Saudi Oil and Gas and Brazil Oil and Gas magazines. Karam is also an executive board member of the University of Southern California (USC) Alumni Club of Arabia. He is a member of the Arabian Society for Human Resource Management (ASHRM), Society of Exploration Geophysicists (SEG) and Saudi Council of Engineers.

In 2005, Karam received his B.S. degree in Petroleum Engineering from King Fahd University of Petroleum and Minerals (KFUPM), Dhahran, Saudi Arabia. In 2010, he received his M.S. degree from the University of Southern California (USC), Los Angeles, CA, in Petroleum Engineering, specializing in Smart Oil Field Technologies and Management.

Maximizing the Value of the Intelligent Field: Experience and Prospective

By Dr. Ahmed H. Al-Hutheli, Dr. Fahad A. Al-Ajmi, Sultan S. Al-Shamrani and Abdel Nasser Abitrabi B.

Reprinted with kind permission from the Saudi Aramco Journal of Technology.

Abstract

In recent years, most of our industry has embarked on implementing the intelligent field initiative, which is a clear indication of the general surge to adapt to the new methods, processes and workflows being used to manage existing and new fields. The extent to which this technology has been implemented worldwide is a sign of a strong buy-in from the industry, which clearly believes that this technology will deliver on its promises in terms of maximizing hydrocarbon production, recovery and profits, as well as improving health, safety and environmental compliance.

Saudi Aramco is considered a leader in deploying and utilizing the intelligent field technology to maximize the value of its hydrocarbon reservoirs. This article discusses the implementation of the intelligent field initiative in Saudi Arabian fields, particularly in the world's largest intelligent field, the Khurais complex. It highlights the huge infrastructure needed to measure and transmit data and to manage and control production in this field. As a result of the lessons learned from Saudi Aramco's experience, classical reservoir management concepts are undergoing a major transformation as they adapt to the fundamental change in data acquisition and production controls. Moreover, engineers are confronting a new challenge in the reservoir monitoring process and overall field optimization, which requires a paradigm shift in analysis, interpretation and decision making to maximize the value of the intelligent field. So far, the industry's efforts to utilize intelligent field technology have been mainly focused at the well level to optimize production rate and ensure target rate compliance. Saudi Aramco's efforts, however, are going beyond the well level to optimize reservoir performance and enhance oil recovery. This article illustrates some of those efforts, which have resulted in a better understanding of well deliverability and reservoir connectivity.

In addition, this article highlights the major challenges facing operating companies managing those fields. It provides methods and workflows to mitigate these challenges, maximize the value of intelligent fields, and fully utilize the existing in- frastructure and capabilities.

Introduction: Real Time Reservoir Management

The first section of this article deals with the definition of real time reservoir management, which is essential to set the stage for discussing the value of intelligent fields. The benefits realized from intelligent field technology are highly correlated to the operator's success at implementing real time reservoir management. This section starts with a general definition of reservoir management, and then discusses the evolution of the reservoir management process and the introduction of real time reservoir management. Finally, it highlights Saudi Aramco's efforts to build four major layers to ensure successful implementation of real time reservoir management.

Reservoir management is an integrated process that develops a hydrocarbon field with goals to maximize profit while achieving higher recovery. As illustrated in

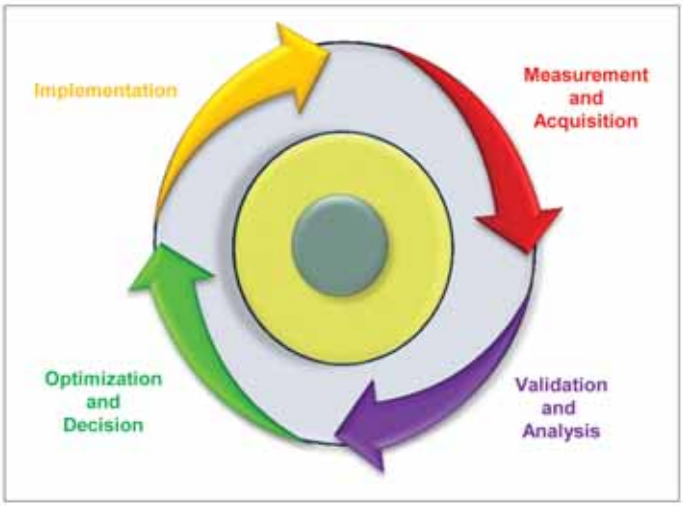

Fig. 1. Reservoir management cycle[1].

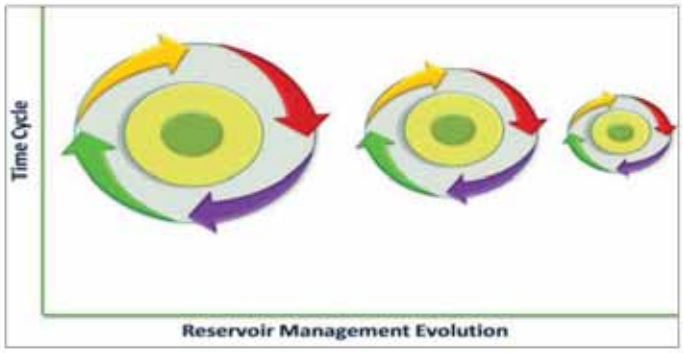

Fig. 2. Reservoir management evolution.

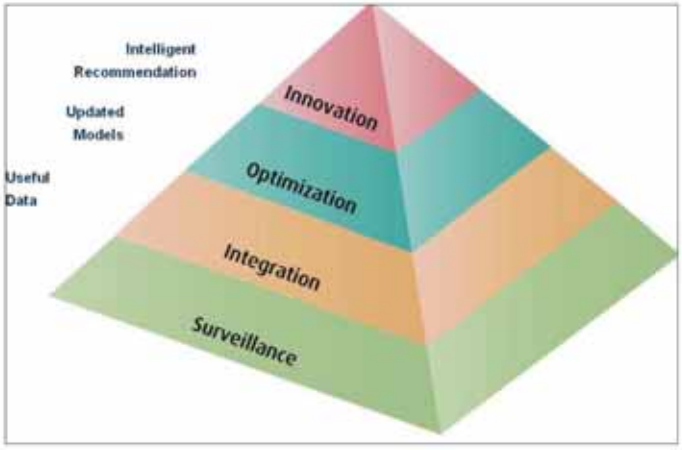

Fig. 3. Intelligent field infrastructure layers[3].

Fig. 1, it consists of four major stages[1]. The first stage is the process of measuring and acquiring data related to a reservoir and its wells and surface facilities. Prior to any further utilization, the data has to be validated to identify any anomaly that might lead to erroneous analysis. This occurs in the analysis stage, which is also where tools and workflows are introduced to manage and integrate the data. At this stage, engineers strive to achieve an understanding of the field's performance using either simple analytical tools, such as material balance, or more sophisticated tools, such as numerical simulation. Once the analysis is completed and proper understanding of the field performance has been captured, the process enters the third stage, that of optimization and decision making. Normally, this stage involves taking a multidisciplinary approach, guided by optimization workflows and tools, to make informed decisions. The fourth and last stage is the implementation of these decisions in the field. Operational engineers and operators are responsible for adequately implementing these decisions. This four-stage process is repeated periodically throughout the entire life of the field.

The time cycle required to complete this process depends on the technology and workflows adopted at each stage. It also depends on the collaborative environments and integration processes in place. Traditionally, a time cycle might last for months, considering the difficulties that might arise, particularly during the data measurement and acquisition and the implementation stages. A crew of people is sent to the field many times to collect the required data, such as static reservoir pressure and wellhead measurements. Although it sounds trivial, this data collection requires a lot of coordination among various field organizations, which might take more than three months, depending on the number of wells and the size of the field. The implementation of decisions made to improve the reservoir performance also requires deploying another crew of people, which entails more coordination and time.

The recent advances in intelligent field technology provide the means for engineers to intervene with the well's operations remotely, rather than sending out a crew. It also facilitates the transmitting of real time high frequency data streams to remote offices, thereby providing immediate feedback on the outcome of the decisions made and actions taken. Real time reservoir management became a reality once technology succeeded in significantly curtailing the time between data acquisition and action implementation, Fig. 2. Therefore, the degree of our success in implementing real time reservoir management determines the ultimate benefit of the intelligent field and its value.

Saudi Aramco's efforts to build the infrastructure required for intelligent fields to successfully implement

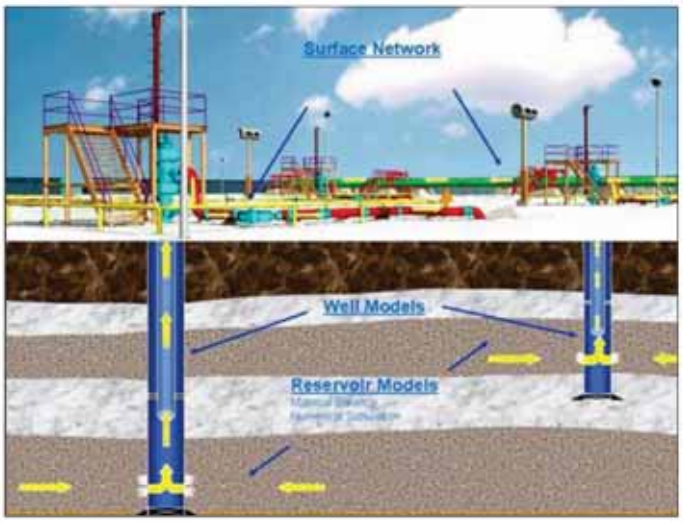

Fig. 4. Production system components.

the concept of real time reservoir management has been discussed in other literature[2]. The implementation architecture consists of four major layers, Fig. 3[3]. The surveillance layer, which is the key enabler for intelligent fields, involves installing real time measurement devices, such as the permanent downhole monitoring system (PDHMS), and control devices, such as inflow control valves (ICVs). It also provides continuous maintenance and monitoring of these devices, and ensures their full functionality. Moreover, it involves building the required infrastructure for real time data acquisition, communication, data management and validation, visualization and an alert system. This layer supports the first and last stages of reservoir management outlined in Fig. 1.

The integration layer involves building the required tools and workflows to constantly monitor reservoir performance and report anomalies, such as rate violations, unexpected high water or pressure decline. It facilitates the integration of various reservoir parameters to study reservoir behaviors, such as injection efficiency and inter-reservoir communications. In addition, it provides the basis for integrating data used by various disciplines, such as geology or reservoir engineering, and the facility to build analytical or numerical simulation models. This layer supports the second stage of the reservoir management cycle and provides actionable information for the optimization layer that follows.

The optimization layer provides a comprehensive optimization system that covers the entire production system with its various processes, assets and recourses, Fig. 4. Providing an environment that integrates all applications and models is a key component to ensuring a successful optimization process. In addition, the needed post-simulation and optimization tools are developed in this layer.

The last layer is the innovation layer, where maximum advantage of the intelligent field can be taken through efficient transformation of data to knowledge and informed decisions. It provides the proper environment to capture experience, to motivate cross-functional dialogue and thinking, to introduce innovative solutions and to maximize the value of the intelligent field technology. The optimization and innovation layers support the third stage of the reservoir management cycle.

The above mentioned layers represent Saudi Aramco's outline for what it takes to fully realize the benefits of the intelligent field and ensure successful implementation of real time reservoir management. The next section of this article presents examples from the Khurais complex, illustrating the implementation of these layers.

Field Experience: Khurais Complex

Field Geology

The Khurais complex consists of three main oil fields discovered in the early 1970s, Fig. 5. The production from the complex was limited during the late 1980s and early 1990s until a comprehensive development plan was put into place. It is geographically located around 100 miles (160 kilometers) east of the capital city of Riyadh[4].

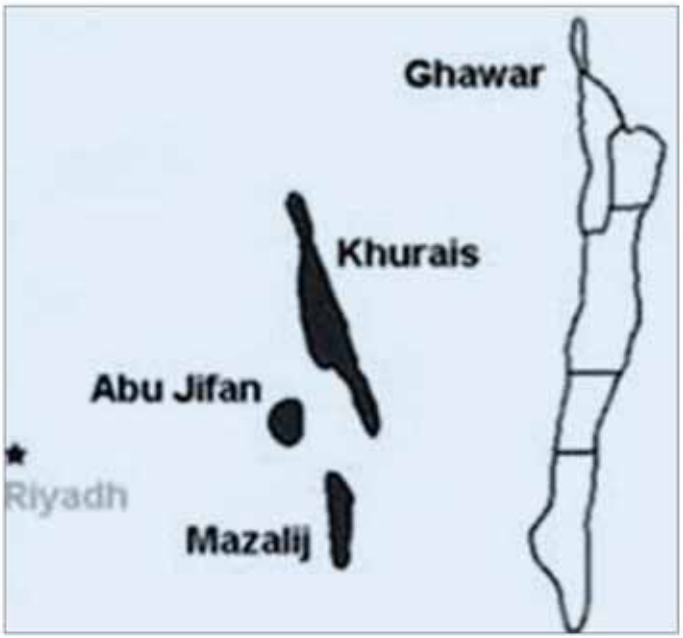

Fig. 5. Khurais complex location map.

Khurais, the main field discovered before the other two fields, represents the largest oil accumulation. It has two oil-bearing reservoirs (Arab-D and Hanifa) with an elongated, north-south trending, asymmetrical anticline structure and a tight aquifer as its lower limit. Both reservoirs consist of a carbonate formation that is a few hundred feet thick.

Surveillance Layer

The fields were developed using three types of wells: producer, observation and injector wells. The producer wells cover the entire body of the two reservoirs with a one-to-one ratio of data measurement, storage and control devices. Each well is equipped with a multiphase flow meter at the surface to measure three-phase fluid flow and with permanent downhole gauges installed thousands of feet underground to continuously measure reservoir pressure in real time. Additionally, all wells are equipped with electrical submersible pumps (ESPs) with variable speed drive and pressure sensors to measure discharge pressure. These ESPs facilitate the long-distance transport of the crude from the wells to a single central processing facility. At the surface, the wellhead is equipped with chokes, which can be adjusted remotely into variable settings. The choke upstream and downstream pressure can also be reported in real time. Each well is equipped with a remote terminal unit (RTU) to store real time data and transmit data to a supervisory control and data acquisition (SCADA) system.

As for observation wells, Khurais has a comprehensive strategic surveillance program where dedicated observation wells are placed to allow efficient sweep evaluation. They are mainly equipped with PDHMS to measure pressure and temperature in real time. The last type of development well is the injector. These are drilled in the periphery of the reservoir to provide the required pressure support and displacement efficiency. They are mainly equipped with chokes, flow meters and wellhead pressure sensors at the surface. It is imperative to emphasize that all equipment can be monitored and controlled remotely in real time, which is one of the major enablers of real time reservoir management concepts, as will be discussed later in this article.

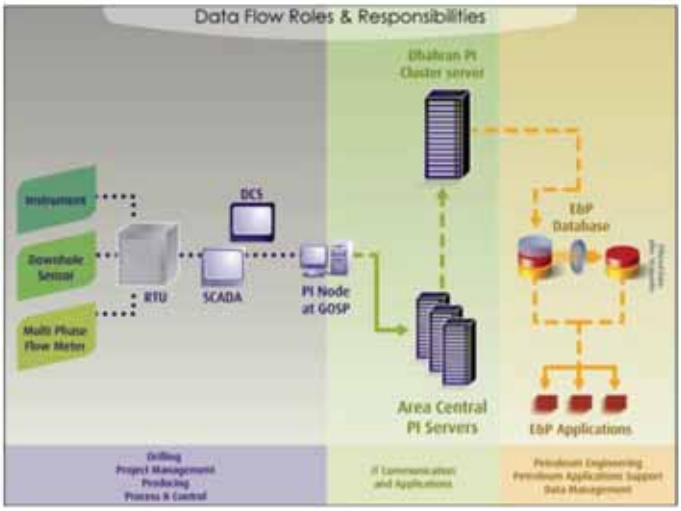

Fig. 6. Journey of real-time data[3]

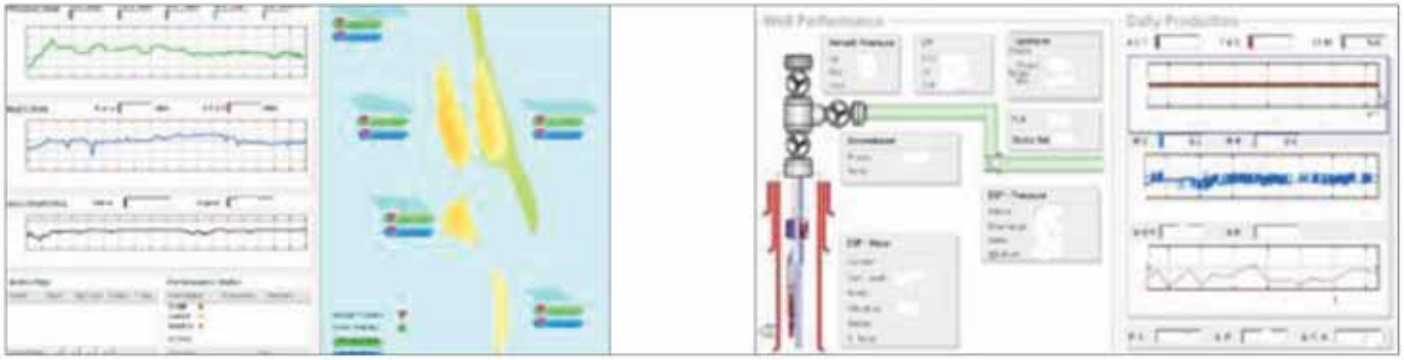

Fig. 7a. (Left) Data visualization example5, full asset overview.
Fig. 7b. (Right) A more detailed view of the data visualization example.

The journey of real time data from the field to the engineer's desktop navigates multiple stages of instruments, networks and productivity index (PI) servers, Fig. 6[3]. Each stage is managed by one or more organizations, as indicated by the color-shaded areas.

Data Visualization

On the desktop, the data visualization environment was built as a Web based application, starting from a full asset overview, Fig. 7a[5], where a dynamic Geographic Information Systems map of the fields is displayed. The map has the total production and injection rates, and displays the resources of the rigs in the field and the overall field status against set targets and conditions. Next to the map are field performance plots displaying production, injection and real time static reservoir pressure. The engineer can dive into more detailed views until reaching the well view, where actual well equipment and the real time data transmitted from the equipment are presented, Fig. 7b[5].

Data Validation and Ensuring Components Functionality

The first challenge that the team faced was dealing with the massive amount of data. Many issues related to data reliability were detected, such as the lack of data transmission from some intelligent field components, devices malfunctioning, etc. To overcome these difficulties, an integrated process and workflow was established to ensure data reliability and its availability at the engineer's desktop for proper utilization. Figure 8 illustrates the data flow process from the Khurais complex.

Unreliable data or equipment malfunctioning issues have been managed by integrating subsurface and surface dynamic data by component. Once data is integrated using the available real time data monitoring system, data with reliability issues can be detected for proper correction. Figure 9 shows the real time integration process to ensure data at the engineer's desktop is reliable.

This process has robust workflows with the capacity to validate huge amounts of data. This of course requires an efficient system capable of validating the massive real time data that keeps flowing to the engineer's desktop and of ensuring only valid and reliable data is fed into the specialized applications used by engineers to perform their tasks.

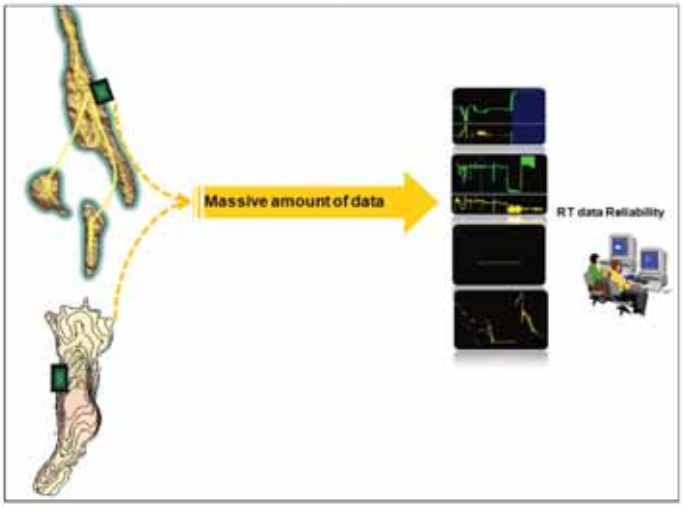

Fig. 8. Data flow process from the Khurais complex.

Fig. 9. Real time integration process on the desktop.

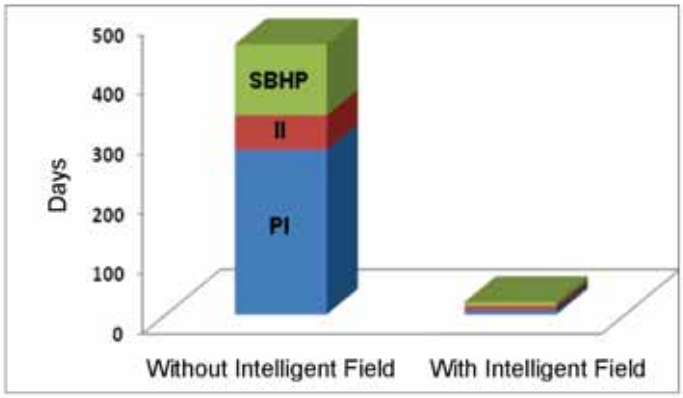

Fig. 10. Comparison of shut-in time needed to capture SBHP, II and PI requirements.

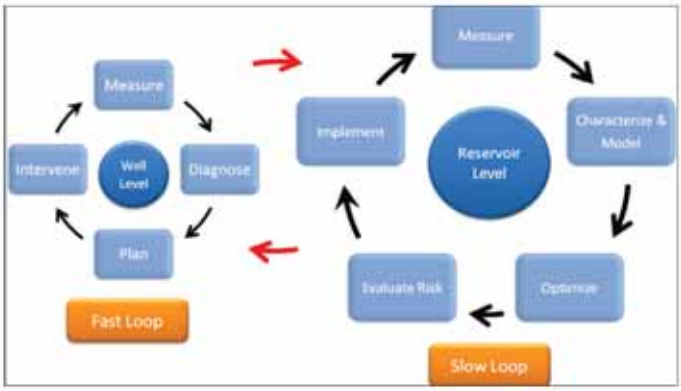

Fig. 12. Optimization loops at well and reservoir levels.

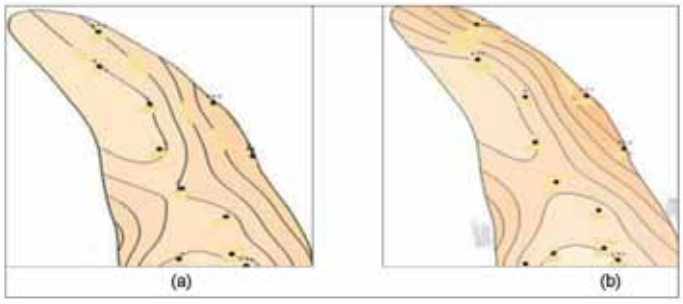

Fig. 11. Pressure maps.

Integration Layer

In early drilling of the development wells, real time data played a major role as it was used to geosteer drilling and efficiently place the wells[6]. At a later stage, the development wells were instrumental in meeting startup production targets. Prior to increment commencement, engineers were able to remotely control the well's rates and perform a capacity test. Project, facilities and production engineers were able to monitor the well's flow line data. Additionally, they were able to identify problems and set a timely mitigation plan. As for the reservoir engineers, the intelligent field played a major role by performing early tests to validate the development plan, assess productivity and injectivity, and optimize development requirements[5].

Advanced Data Collection

The power of utilizing the intelligent field data was demonstrated during a maintenance shutdown that lasted for 21 days. During this period, all static bottom-hole pressure (SBHP), and productivity and injectivity indices requirements were captured, eliminating the need for shutting in the wells in the future. Coordination among various organizations and the synergy enabled by intelligent field technology are the key factors to accomplishing such a major task in a short time. Despite the fact that there are more than 100 wells in the field, engineers were able to capture all productivity and injectivity indices along with the variation in SBHP across the whole reservoir, leading to a full reservoir understanding in 21 days. This is equivalent to a task of 455 days if intelligent field technology were not implemented, as illustrated in Fig. 10.

Reservoir Pressure Management

Managing the pressure propagation across the reservoir is an important task supported by reservoir management. Achieving a uniform reservoir pressure is an indication of a uniform flood front and efficient sweep. Figure 11 shows an example of using real time reservoir pressure data for generating models to assess pressure propagation. The engineers noticed that the pressure was unevenly propagating across the reservoir, Fig. 11a. Accordingly, the injection rate of the offset injectors was curtailed, leading to uniform pressure propagation, Fig. 11b.

Manage Communication between Reservoirs

Proactive management of communication between reservoirs is one of the major advantages realized with the adoption of intelligent field technology.

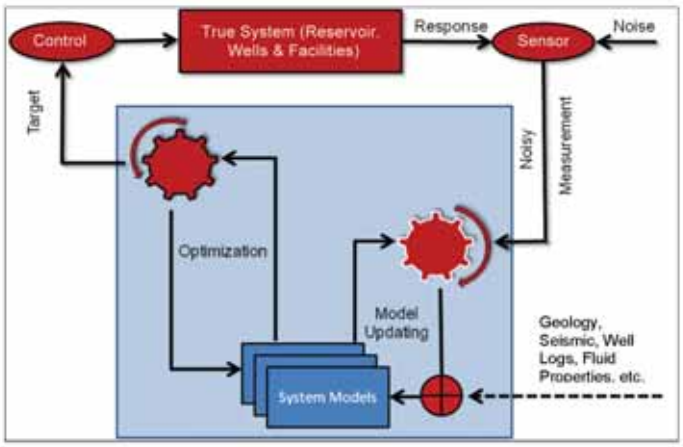

Fig. 13. Model based real-time reservoir management.

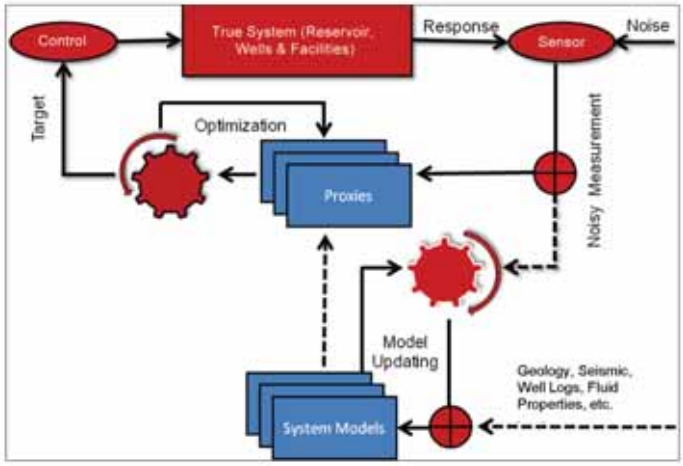

Fig. 14. Modified model based real-time reservoir management with proxies.

As mentioned earlier, this field consists of two main carbonate reservoirs. Those reservoirs are fractured, and some of those fractures form fairways extending through the impermeable formation between the reservoirs. Such communication is not surprising. In fact, similar experience from an analog field showed that communication should be anticipated in this field; however, the communication in the analog field, which lacked intelligent field technology, was not identified at an early stage in the field's life and took years to be understood. The communication in different areas of this field, in contrast, was identified, characterized, modeled and finally managed in three months, taking a huge step toward improving sweep efficiency from both reservoirs.

Optimization Layer

The optimization of field performance can be done at different stages within various time spans. It can be done at the well level when a fast intervention is needed to correct the well performance, such as adjusting the discharge pressure of the ESP or changing the choke settings. Normally, we refer to this level of optimization as a fast loop, because it can be performed very quickly when we can monitor and control the well in real time. A more challenging optimization stage is at the reservoir level, which is referred to as a slow loop. To perform this level of optimization efficiently, reservoir characterization and modeling becomes an integral part of the optimization loop. Performing the optimization at the reservoir level in real time can be extremely complicated, since it requires the integration of various disciplines, such as geology, geophysics and reservoir engineering. Optimization loops at the well and reservoir level, with their multiple stages, are illustrated in Fig. 12. The best way to ensure an optimal solution is to perform the optimization on both levels simultaneously.

Saudi Aramco has adopted a model-based real time reservoir management concept to change the reservoir management from sporadic action to a near

continuous process. Figure 13 shows the main elements of the model-based real time reservoir management process[7, 8]. The true system, which consists of the reservoir, wells and facilities, is indicated in the top of the figure. The simulated true system models are shown in the bottom of the figure. They include models that represent reservoir, well- bore and facility components. They can consist of multiple realizations to address the uncertainty associated with modeling the true system. Sensors indicated in Fig. 13 represent the stream of real time data measurements captured using various tools, such as the PDHMS and the multiphase flow meter. The measured data can be reconciled with the uncertain models through a model updating process, which may involve a computer assisted history matching technique. The reconciliation process is achieved by minimizing the difference between the measured and the simulated data, based on a predefined objective function. The second loop is the model-based optimization and decision making, which involves a numerical algorithm to reach an optimum solution to maximize the value of the true system. The last component is the control, which represents equipment used to control the well's performance, such as wellhead chokes and ICVs.

As illustrated earlier, the model-based real time reservoir management consists of two major loops: the model updating and optimization. The model updating might not be achieved in real time, since it requires integrating data from multiple disciplines. The complexity of this process is aggravated once it is performed on multiple models. Similarly, the optimization can be cumbersome when it is performed on the multiple realizations needed to address uncertainty. To overcome this difficulty, the model updating loop is replaced with proxies, which are simple models for fast intervention and optimization, Fig. 14. The proxies are generated based on the model updating loop, which will continue to take place offline. Those proxies should be updated frequently once there is an unacceptable difference between a measurement and the simulated data. The use of proxies is still a research area in Saudi Aramco and has not yet become fully operational.

Innovation Layer

To facilitate collaborative decision making and create an innovative environment around reservoir management processes and tasks, the concept of intelligent field centers (IFCs) was implemented in Saudi Aramco. The IFCs will provide continued emphasis on best-in-class reservoir management practices/tasks, but with a longer vision and a wider objective of optimizing the company's assets and operations.

An inclusive evaluation study was conducted to come up with the optimal design of these centers to ensure achieving the desired goals. The study identified several high priority workflows being performed by reservoir management that once implemented and integrated in the reservoir management analysis, will improve processes and efficiency. The result will be enhanced performance and eventually increased recoverable reserves.

The workflows and processes are summarized as follows:

- **Automation:** It provides a means to improve efficiency and reduce the time to perform "mundane" tasks. These tasks, along with data quality control and validation, are automated.

- **Integration:** It is necessary to provide systems that allow seamless integration of data and applications to workflows. The integration platform must allow integration even for complex reservoir engineering problems.

- **Collaboration:** Two main types of collaboration have been identified in the IFC environment. First, the IFC involves people in the review process, allowing professionals to exchange ideas as they review data in real time. Second, the professionals are free to interact, exchanging ideas about models, data, experiences and best practices.

- **Knowledge Capture:** The IFC environment allows the best knowledge capture of workflow steps, output and results. Historical solutions are included and used to guide the decision making, speed up the understanding and raise quality, which results in improved reservoir management.

- **Interoperability and Openness:** The IFC integrated system offers the ability to easily connect almost any application to the data. This allows the use of existing software applications, applications that are under development or those available from third party vendors.

Conclusions

Saudi Aramco has invested significantly in intelligent field technology. This article discusses Saudi Aramco's efforts to effectively implement this technology and maximize its value. Some specific conclusions can be summarized as follows:

- Realizing the benefits of intelligent field concepts

depends on the success of implementing real time reservoir management processes and workflows.

• Four major infrastructure layers, namely surveillance, integration, optimization and innovation, are built to support and facilitate real time reservoir management processes and workflows.

• The surveillance layer involves installing real time measurement and actuation devices. It also provides continuous maintenance and monitoring of these devices, and ensures full functionality.

• The integration layer involves building the required tools and workflows to constantly monitor reservoir performance. It facilitates the integration of various reservoir, wellbore and facility parameters.

• The optimization layer provides a comprehensive optimization system that covers the entire production system with its various processes, assets and recourses.

• The innovation layer provides the proper environment to capture experience and motivate cross-functional dialogue and thinking to generate innovative solutions and maximize the value of the intelligent field technology.

• The implementation of these layers is seen in field examples from the Khurais complex.

• Benefits realized from the intelligent field technology include advancing data collection and minimizing the time needed to understand the reservoir performance. Engineers were able to capture all productivity and injectivity indices along with the variation in SBHP across the whole reservoir in 21 days, compared to 455 days without intelligent field technology. The communication between the Arab-D and Hanifa reservoirs in Khurais field was identified, characterized, modeled and finally managed in three months, compared to several years spent to understand similar communication in an analog field without intelligent field technology.

Acknowledgements

The authors would like to thank Saudi Aramco management for their permission to present and publish this article.

This article was presented at the SPE Intelligent Energy International Conference and Exhibition, Utrecht, The Netherlands, March 27-29, 2012.

References

1. Mubarak, S.M.: "Real-time Reservoir Management from Data Acquisition through Implementation: Closed-Loop Approach," SPE paper 111717, presented at the Intelligent Energy Conference and Exhibition, Amsterdam, The Netherlands, February 25-27, 2008.

2. Abdul-Karim, A., Al-Dhubaib, T.A., Elrafie, E. and Alamoudi, M.O.: "Overview of Saudi Aramco's Intelligent Field Program," SPE paper 129706, presented at the SPE Intelligent Energy Conference and Exhibition, Utrecht, The Netherlands, March 23-25, 2010.

3. Al-Dhubaib, T.A.: "Intelligent Fields: Industry's Frontier and Opportunities," SPE paper 141874, presented at the SPE Middle East Oil and Gas Show Conference, Manama, Bahrain, September 25-28, 2011.

4. Al-Afaleg, N.I., Al-Garni, S., Rahmeh, B.A. and Al-Towailib, A.: "Successful Integration of Sparsely Distributed Core and Well Test Derived Permeability Data in a Viable Model of a Giant Carbonate Reservoir," SPE paper 77743, presented at the SPE Annual Technical Conference and Exhibition, San Antonio, Texas, September 29 - October 2, 2002.

5. Al-Mulhim, W.A., Faddagh, H.A., Shehab, M.A. and Shamrani, S.S.: "Mega I-Field Application in the World," SPE paper 128837, presented at the SPE Intelligent Energy Conference and Exhibition, Utrecht, The Netherlands, March 23-25, 2010.

6. Al-Ghamdi, A., Al-Bani, F. and Kragjcek, R.T.: "SS: Delivering the Largest Oil Increment in the World – Innovation Solutions and Rewards," OTC paper 20218, presented at the Offshore Technology Conference, Houston, Texas, May 4-7, 2009.

7. Alhuthali, A.H., Datta-Gupta, A., Yuen, B. and Fontanilla, J.P.: "Field Applications of Waterflood Optimization via Optimal Rate Control with Smart Wells," SPE paper 118948, presented at the SPE Reservoir Simulation Symposium, The Woodlands, Texas, February 2-4, 2009.

8. Jansen, J.D., Douma, S.D., Brouwer, D.R., et al.: "Closed Loop Reservoir Management," SPE paper 119098, presented at the SPE Reservoir Simulation Symposium, The Woodlands, Texas, February 2-4, 2009.

Biographies

Dr. Ahmed H. Al-Hutheli is a Reservoir Engineer in the Southern Area Reservoir Management Department. During his 13 years with Saudi Aramco, he has worked on multiple assignments concerning reservoir engineering aspects for four giant fields.

Ahmed is interested in reservoir and production system integration and optimization. He is also interested in risk management and decision making under uncertainty.

In 1998, Ahmed received his B.S. degree in Electrical Engineering from King Fahd University of Petroleum and Minerals (KFUPM), Dhahran, Saudi Arabia. In 2003, he received his M.S. degree in Petroleum Engineering from Texas A&M University, College Station, TX, and in 2011 Ahmed received his Ph.D. degree in Petroleum Engineering, also from Texas A&M University. He also earned a business certificate from Mays Business School at Texas A&M University in May 2008.

Ahmed is a member of the Society of Petroleum Engineers (SPE). He has published many technical papers on topics related to reservoir management.

Dr. Fahad A. Al-Ajmi is the General Supervisor for the Abqaiq Reservoir Management Division in Saudi Aramco. He has led the Khurais complex field development that came onstream in 2009, with production capacity of 1.2 million barrels per day, which makes it the largest oil field development in the company's history and perhaps the largest project of its kind in the world. Fahad has over 20 years of experience in reservoir management of Saudi Aramco's fields.

In 1988, he received his B.S. degree in Petroleum Engineering from King Fahd University of Petroleum and Minerals (KFUPM), Dhahran, Saudi Arabia. Fahad received his M.S. degree in Petroleum Engineering from the University of Southern California, Los Angeles, CA, in 1993, and in 1998 he received his Ph.D. degree from Texas A&M University, College Station, TX, also in Petroleum Engineering.

Fahad is an active member of the Society of Petroleum Engineers (SPE), where he has contributed to numerous technical papers and has served on several SPE forums and workshop committees. He was a SPE Distinguished Lecturer on the subject of reservoir management in 2008-9. Fahad is the recipient of numerous awards and recognitions for his successful completion of reservoir management projects and studies. He has published several papers.

Fahad also holds a faculty position at KFUPM, teaching formation evaluation and advanced water flooding.

Sultan S. Al-Shamrani is a Reservoir Engineer working in the Southern Area Reservoir Management Department. He has 8 years of industry experience, mainly in new field development and intelligent field implementation.

In 2004, Sultan received his B.S. degree in Petroleum Engineering from the University of Tulsa, Tulsa, OK.

Abdel Nasser Abitrabi B. is a Petroleum Engineer Specialist. He has more than 22 years of experience in oil and gas upstream and downstream operations. Abdel's experience involves reservoir management, integrated studies, production, drilling, data management and petroleum engineering consulting. He has been involved in the development of six new oil and gas fields, mainly in Venezuela and Saudi Arabia. Abdel has also worked on projects involving the minimization of formation damage while drilling, effective well placement in a heterogeneous clastic reservoir, intelligent field implementation and development of expert systems to manage intelligent fields.

Abdel received his B.S. degree from the University of Central Venezuela, Caracas, Venezuela, and a M.E. degree from Texas A&M University, College Station, TX, both in Petroleum Engineering.

World Oil and Gas Production

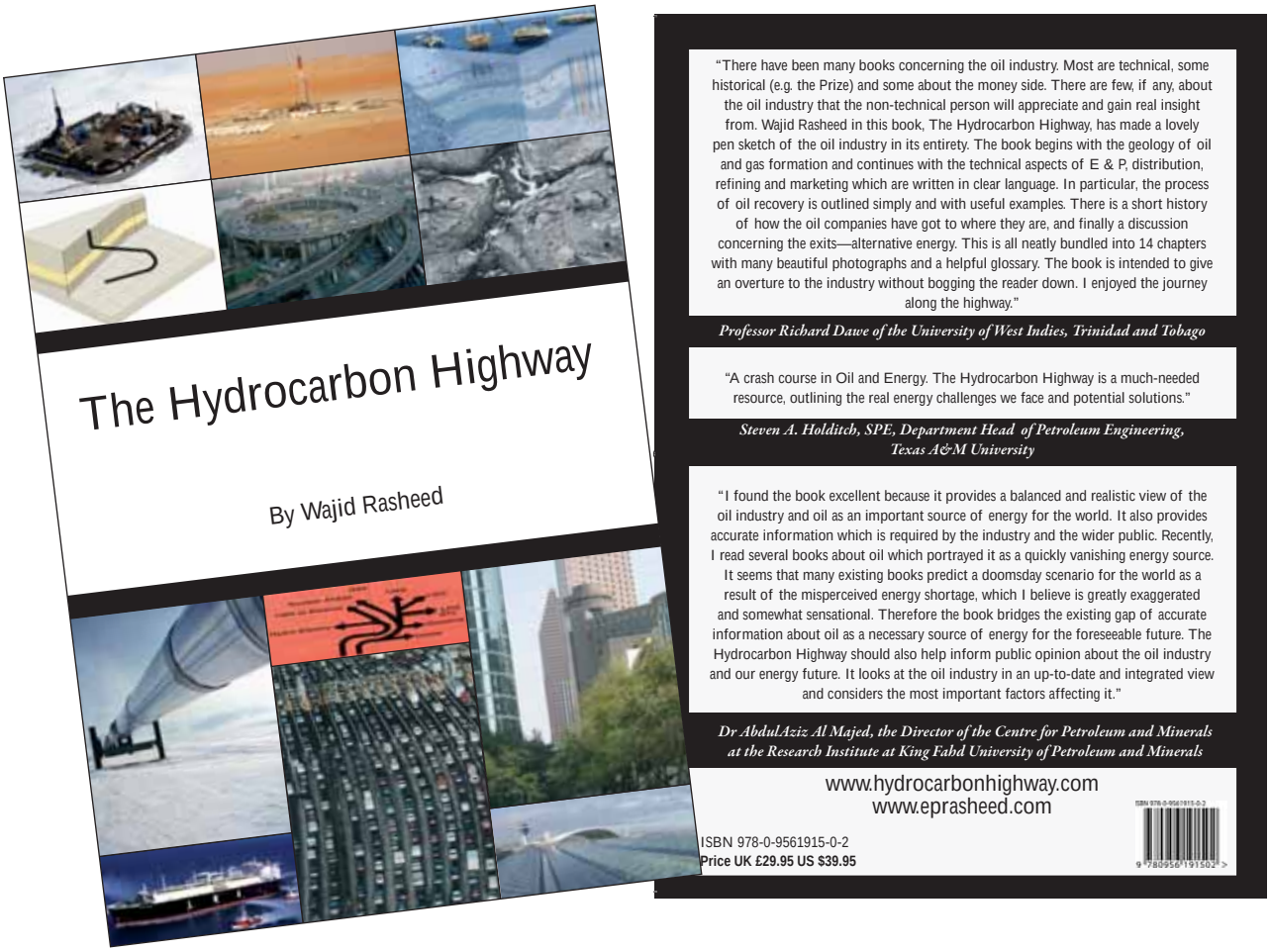

Here we focus on the worlds' oil and gas major producers (OPEC and non-OPEC) from an export perspective. We detail the dominant oil companies behind world exports as well as each country's production level, reserves and capacity.

Although conventional oil production and reserves are globally dispersed, the highest concentration is in the Middle East. Since the 1960s, this region averages nearly 30% of total global oil production and controls 61% of world oil reserves. OPEC itself produces 43% of world oil production and controls 75% of proved oil reserves. Of the 15 countries worldwide that produced 2 MMbbl/d or more of total liquids for export, seven were OPEC members[1].

The Oil Is Ours

Any consideration of OPEC must begin with its importance as a reserves holder and major oil exporter. From this perspective, only producers that export more than 1 MMbbl/d to the global markets are considered (net of any imports for national refining or consumption). Net exporters play an extremely important role in satisfying demand in global markets because their oil supplies are real exports over and

“The combined population of OPEC countries is just over half a billion people and most are dependent on oil revenues for sustaining their economies.”

above their domestic needs and are therefore known sources of future oil supply.

Every Move You Make

Undoubtedly, every move made by OPEC gets as much headline ink around the world as any Central Bank decision. It is watched by the major press agencies who have assigned some of their brightest minds to cover the decisions that usually come out of the Austrian capital. Sitting permanently as an inter-governmental organization, OPEC has 11 members: Algeria, Indonesia, the Islamic Republic of Iran, Iraq, Kuwait, the Socialist People's Libyan Arab Jamahiriya, Nigeria, Qatar, Saudi Arabia, United Arab Emirates and Venezuela. The combined population of OPEC countries is just over half a billion people and most are dependent on oil revenues for sustaining their economies. For these countries, oil is the platform for economic, social and political growth[2].

OPEC currently produces about 43% of the world's crude oil, but that is forecast to grow to more than 50% in the next quarter of a century. OPEC has 75% of the world's oil reserves and this will enable it to expand oil production to meet the growth in demand. In order to expand OPEC output, the oil industry needs the oil price to remain at a profitable level. Oil producers invest billions of dollars in exploration and infrastructure (drilling and pumping, pipelines, docks, storage, refining, staff housing, etc.) and a new oil field can take three to ten years to locate and develop. Commercialisation and profitability are complex issues which are dealt with—in the next Chapter[3].

All OPEC countries are sensitive to oil-price fluctuations because of the large contribution oil revenues make to state coffers. As one would expect, high oil prices yield larger gains in revenues from oil exports; the opposite is also true.

Before getting into detail about the major OPEC exporters of oil, it is worth mentioning the Gas Exporting Countries' Forum (GECF). This forum was formed in Teheran, Iran in 2001 with a view to managing global gas reserves and providing a stable and transparent energy market. The GECF consists of 15 gas-producing countries: Algeria, Bolivia, Brunei, Egypt, Equatorial Guinea, Indonesia, Iran, Libya, Malaysia, Nigeria, Qatar, Russia, Trinidad and Tobago, the United Arab Emirates and Venezuela. Five of these countries – Russia, Iran, Qatar, Venezuela and Algeria – control nearly two-thirds of the world's gas reserves and account for 42% of its production. The GECF has a liaison office in Qatar which is 'formulating a gas-trading model to share knowledge of supply and demand and create a level playing field in negotiations

“Famous for its ability to ‘swing’ world markets into ‘equilibrium’, Saudi Arabia is commonly recognised as the world’s leading oil exporter.”

with international operators’. It is likely that the GECF will become a gas OPEC. Russia has offered to permanently host the organisation at the most recent meeting in Moscow where Equatorial Guinea and Norway were attending as observers[4].

Saudi Arabia

Saudi Arabia produced a daily average of 10.4 million barrels of oil (MMbbl) in 2007, consumed 2.15 MMbbl/d and exported 8.25 MMbbl/d.

Famous for its ability to ‘swing’ world markets into ‘equilibrium’, Saudi Arabia is commonly recognised as the world’s leading oil exporter. It sits atop a quarter of world oil reserves, a fifth of international exports and more than a tenth of total world production. It has a refining capacity of 3 MMbbl/d. One of the Kingdom’s goals is to maintain sufficient spare production capacity so that it can stabilise the market in a given situation. Leaving production capacity idle, and therefore forfeiting revenues, is commendable on the part of Saudis. Whether such ability continues to exist, and averts the energy crises resulting from supply level, will be dependent on investment in refining capacity and technology.

Geology

The Saudi Geographical Survey identifies the Phanerozoic cover as the geologic range of interest for oil and gas reserves. The Phanerozoic ranges from the Saudi Arabian Paleozoic (540-250 millions of years ago [Ma]) to the Cenozoic (65 Ma to recent) and it crops out as relatively flat beds of sedimentary rocks such as sandstone, siltstone, limestone, evaporites (salt deposits), and volcanic rocks. The youngest deposits in the region include coral limestone and unconsolidated sand, silt, gravel and sabkhah, which accumulated in the sand seas of the Rub al Khali and An Nafud and were deposited on to dried-up lake beds, valleys (wadis) and coastlines.

Reserves

Estimates place Saudi Arabia’s proven reserves by the end of 2007 as at least 264.2 billion barrels including new finds and the mega-projects listed below. This is a consensus figure based on the inclusion of probable and possible reserves based on the Society of Petroleum Engineers (SPE) reserves criteria[5].

Although there has been recent speculation of a lower volume of reserves primarily due to watercut, this is a red-herring as the occurrence of increased water production and re-injection are standard reservoir conditions and secondary recovery mechanisms. This is discussed more fully in *Chapter 9: Mature Fields*. Based on current reserves data, it is fair to say that the last barrel of oil will likely be from Saudi Arabia.

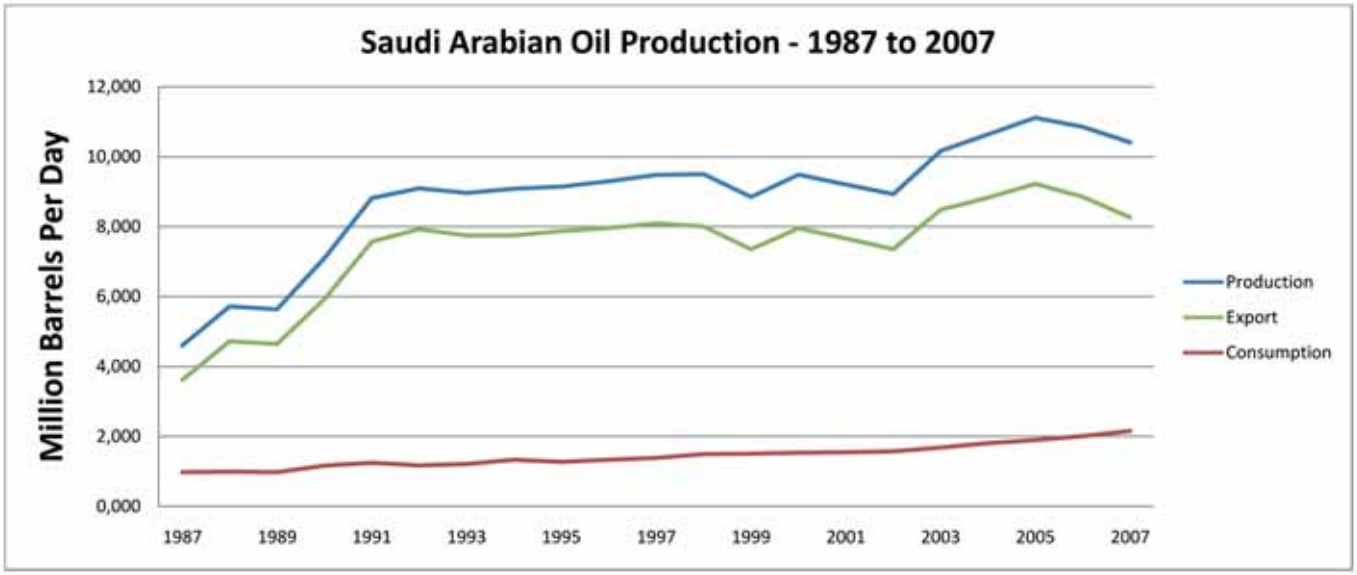

Table 1 - Saudi Arabian Oil Production (1987 to 2007)

Saudi Aramco

Saudi Aramco is the modern day legacy of the Arab American Company. It is as technically sophisticated and diverse as any major oil company with approximately 86% of its staff as Saudis and the remaining 14% employees from more than 50 countries. Saudi Aramco has invested heavily in reservoir and E & P technology and runs one of the world's largest carbonate research centres encompassing reservoir modelling, dynamics and visualisation. Contrary to the popular belief that low-cost onshore environments have limited technology applications, Saudi Aramco runs the latest in downhole drilling and completions technology such as rotary steerables, high-end logging and formation evaluation tools as well as maximum reservoir contact wells (see *Chapter 7: Pregnant Ladies and Fish Bones*). The company's flagship Research and Development Centre (R&DC) employs 350 research staff working on seismic, drilling, completion and production projects[6].

In spite of the recent surge in its oil income, stabilisation funds and foreign investments, Saudi Arabia is seeking to diversify its industrial and financial base beyond petroleum and has initiated several knowledge and industry based projects such as the King Abdullah University of Science and Technology[7].

Iran

Iran produced 4.4 MMbbl/d through 2007. It still made net oil exports of 2.78 MMbbl/d considering that Iranian domestic oil consumption was 1.62 MMbbl/d[8].

Iran's oil and gas sector is dominated by the National Iranian Oil Company (NIOC). Foreign companies are active in Iran and include Gazprom, Japanese National Oil Company (JNOC), PETRONAS, StatoilHydro and Total. Oil and gas ventures are subjected to 'buy-back' arrangements whereby ownership is retained by the Iranian state. NIOC has made several large discoveries, notably the Azadegan field which is yet to be developed and has recoverable reserves of 9 billion barrels (bbls). Other noteworthy fields include Ferdowsi (30.6 billion bbls), Moud (6.63 billion bbls), Zagheh (1.3 billion bbls), Bangestan (600 MMbbls) and Kushk. Iran relies heavily on oil export revenues for approximately 80% of total export earnings and 40% of the government budget[9].

Venezuela

Venezuela produced 2.63 MMbbl/d in 2007 and consumed 596,000[10] MMbbl/d, therefore it exported 2.03 MMbbl/d[11].

Petróleos de Venezuela S.A. or PdVSA is the state-owned oil company of the Bolivarian Republic of Venezuela and it is responsible for the majority of oil production. Although IOCs such as ConocoPhillips,

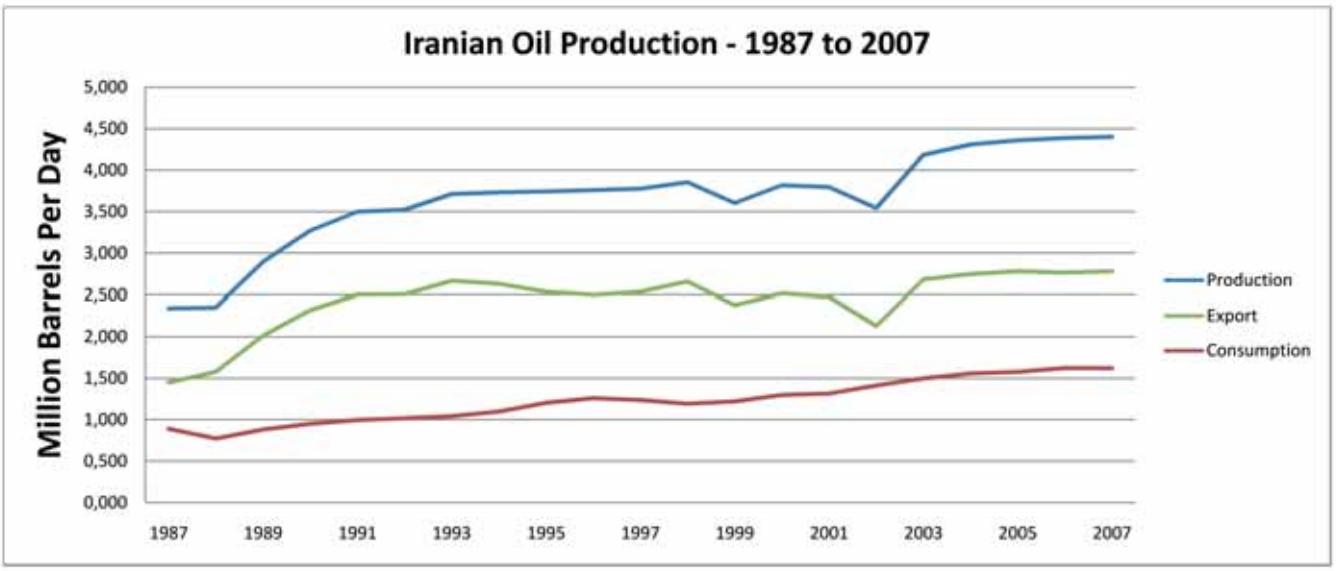

Table 2 - Iranian Oil Production (1987 to 2007)

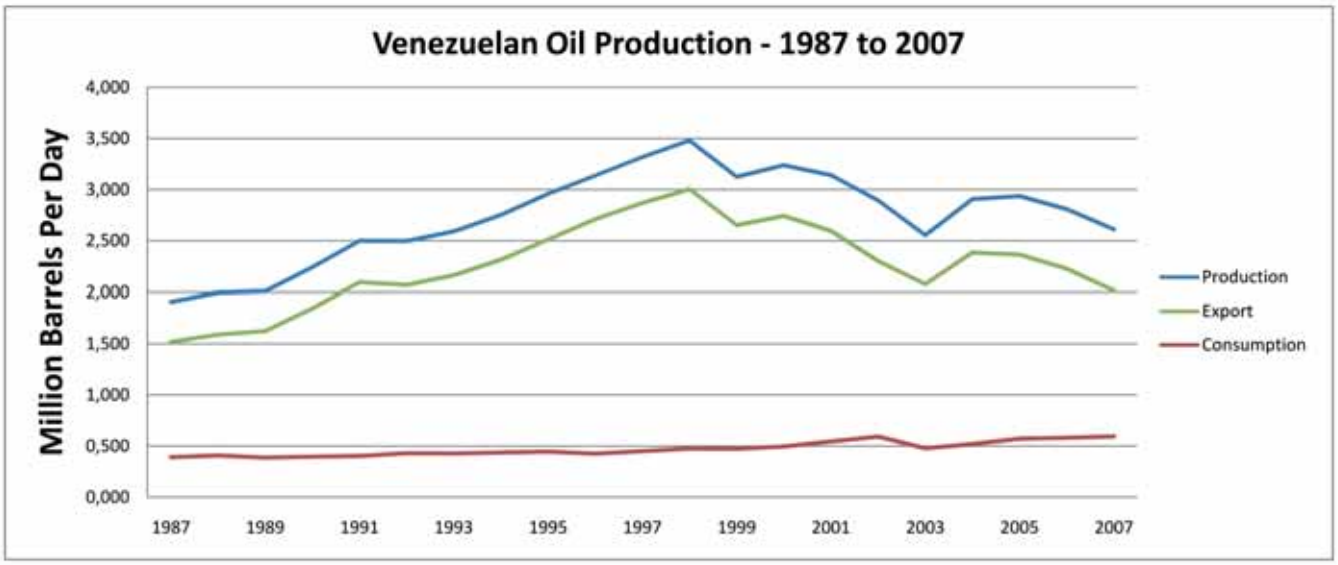

Table 3 - Venezuelan Oil Production (1987 to 2007)

Chevron and Petrobras are present, they must work with PdVSA.

The country is split into two oil provinces: Maracaibo in the West and the 'Oriente' (Spanish for East), both of which share the same prolific source rock. Oil accumulations are found in Cretaceous limestones and in overlying tertiary sandstones. The East Venezuela Basin is asymmetrical with a long, gently-dipping, southern flank. Oil has migrated up this flank to shallow depths where it has been weathered and has generated sizeable heavy oil and bitumen deposits at depths of 1640 to 4921 ft (500 to 1500 m) along the Orinoco River[12].

Oil export revenues are important for Venezuela because as much as 45% of government revenues come from oil[13].

Based on company figures, PdVSA aims to raise

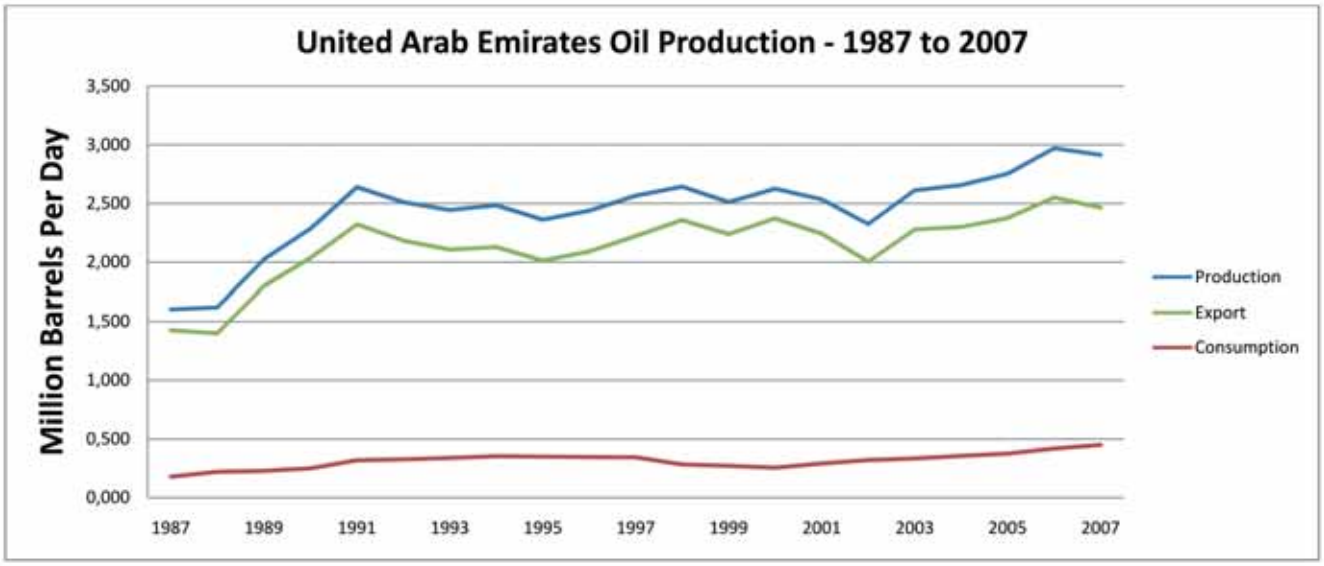

Table 4 - UAE Oil Production (1987 to 2007)

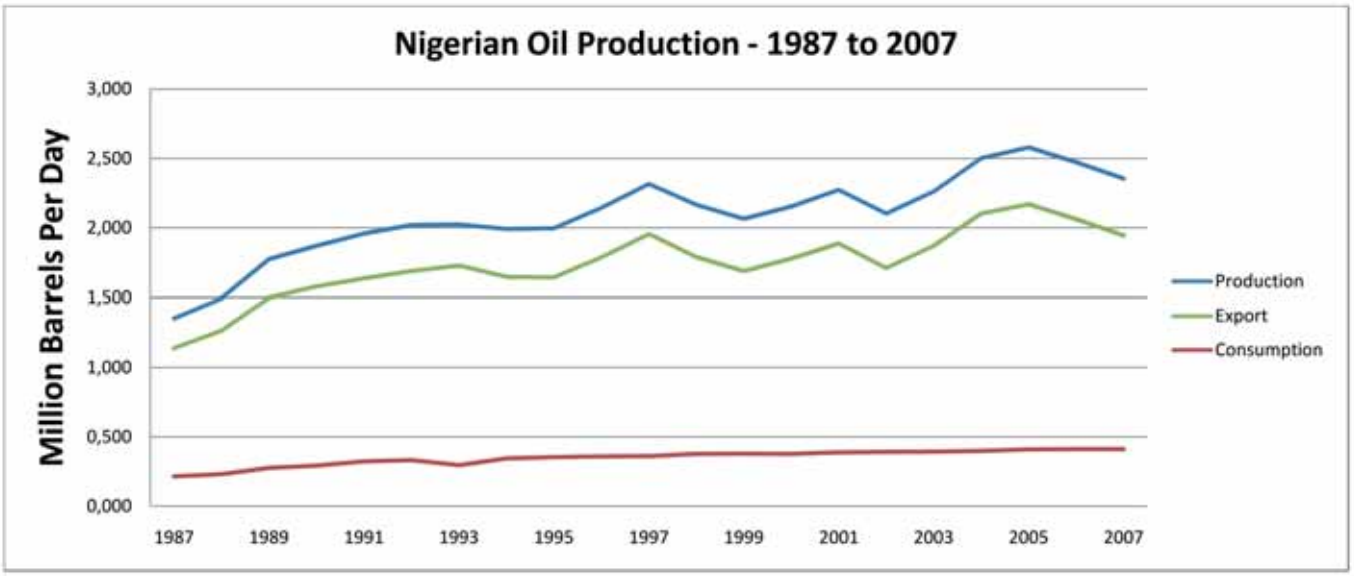

Table 5 - Nigerian Oil Production (1987 to 2007)

the country's crude oil production capacity to 5.5 MMbbl/d by 2010[14].

UAE

In 2007, the United Arab Emirates or UAE produced 2.9 MMbbl/d, consumed 0.45 MMbbl/d and exported a total of 2.45 MMbbl/d[15].

The Abu Dhabi National Oil Company (ADNOC) is the major oil and gas producer in the UAE. It is responsible for all operations in Abu Dhabi and owns the Abu Dhabi Company for Onshore Oil Operations (ADCO), which operates in onshore and shelf waters in the Emirates.

ADCO produces oil from five main fields: Asab, Bab, Bu Hasa, Sahil and Shah. The Zakum Development Company (ZADCO) is responsible for oil development and production from the Upper Zakum field. It also operates Umm Al Dalkh and Satah on behalf of its

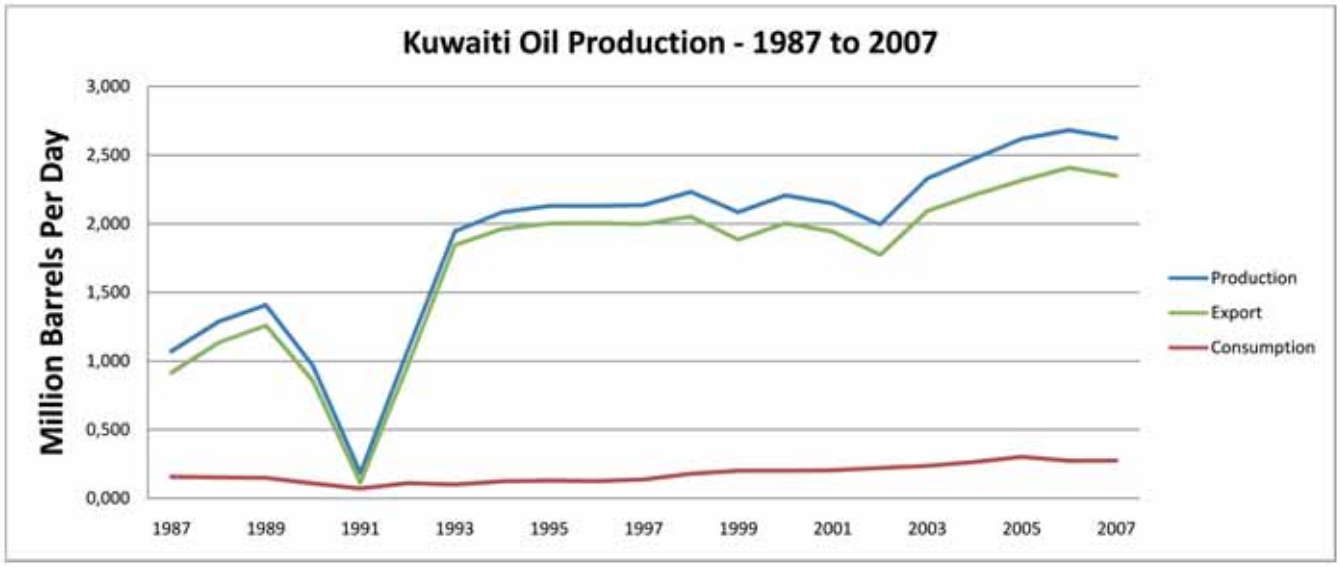

Table 6 - Kuwaiti Oil Production (1987 to 2007)

partners. There is also the National Drilling Company (NDC) for onshore and offshore drilling. As with other OPEC countries, relatively strong oil prices and revenues in recent years have helped to significantly improve the UAE's economic, trade, and budgetary situations[16].

The UAE economy is relatively diversified and is in transition from a purely oil-based economy to one that is increasingly moving towards services such as tourism, banking, re-exports, information technology, etc. Privatisation has moved ahead relatively quickly, and the country has set up various Free Zones to encourage foreign trade and investment. These moves have helped to moderate the effects of fluctuating oil prices and revenues[17].

Nigeria

Nigeria produced 2.36 MMbbl/d in 2007 and is estimated to have consumed 0.4 MMbbl/d, hence exporting approximately 1.96 MMbbl/d[18].

Most of Nigeria's crude oil production, comprising ten major crude streams (including condensate), is light sweet crude, API grades 21°-45°, with a low sulphur content. Nigeria's marker crudes on the international oil market are Bonny Light and Forcados. Numerous fields are known across the Niger Delta, and some of the more marginal fields have become the focus of redistribution with the debate favouring private local companies[19].

Nigeria's oil and gas industry is funded through Joint Ventures (JVs), with the National Petroleum Corporation (NPC) as a major shareholder and each oil company holding a share. The largest JV is operated by the Shell Petroleum Development Company (SPDC) and produces nearly half of Nigeria's crude oil, with an average daily output of approximately 1.1 MMbbl/d. Other companies working with the NPC, include ExxonMobil, Chevron, ConocoPhillips, Total and Agip. The remaining funding arrangements comprise Production Sharing Contracts (PSCs), which are mostly confined to Nigeria's deep offshore development programme.

A number of the oil companies prospecting in the offshore blocks in the Niger Delta, have built up considerable deepwater experience in the Gulf of Mexico (GOM), the Gulf of Guinea (particularly in Angola), and the North Sea. Technology developments have reduced the cost of exploration and production, although profitability is reckoned at levels exceeding 5,000 bbl/d per well.

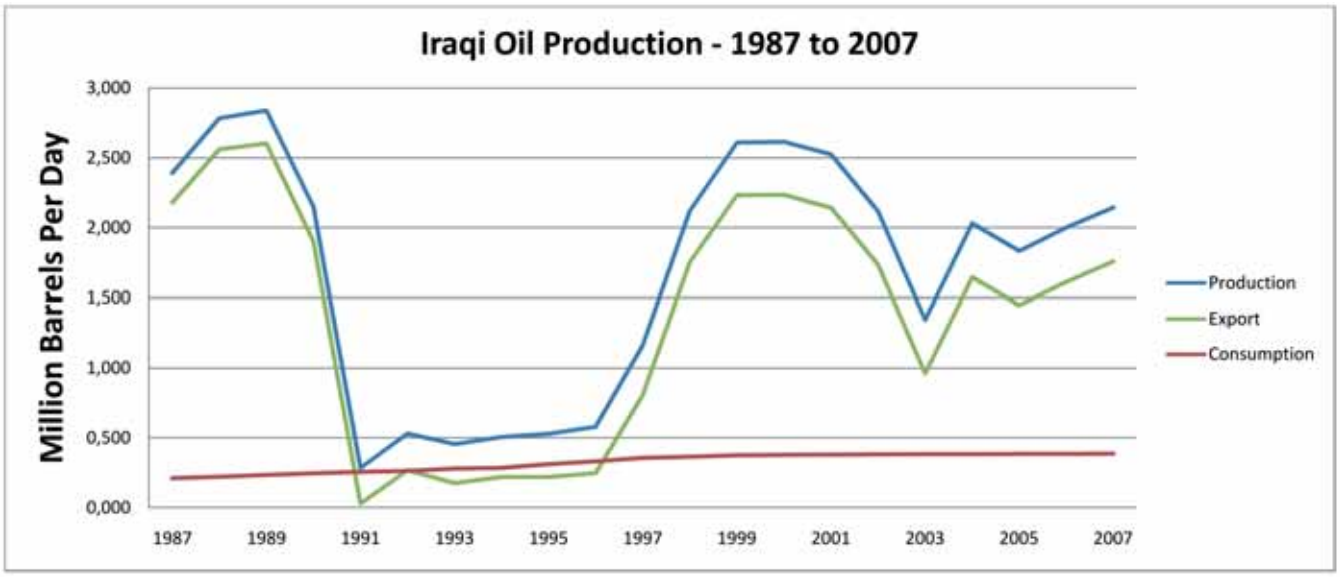

Table 7 - Iraqi Oil Production (1987 to 2007)

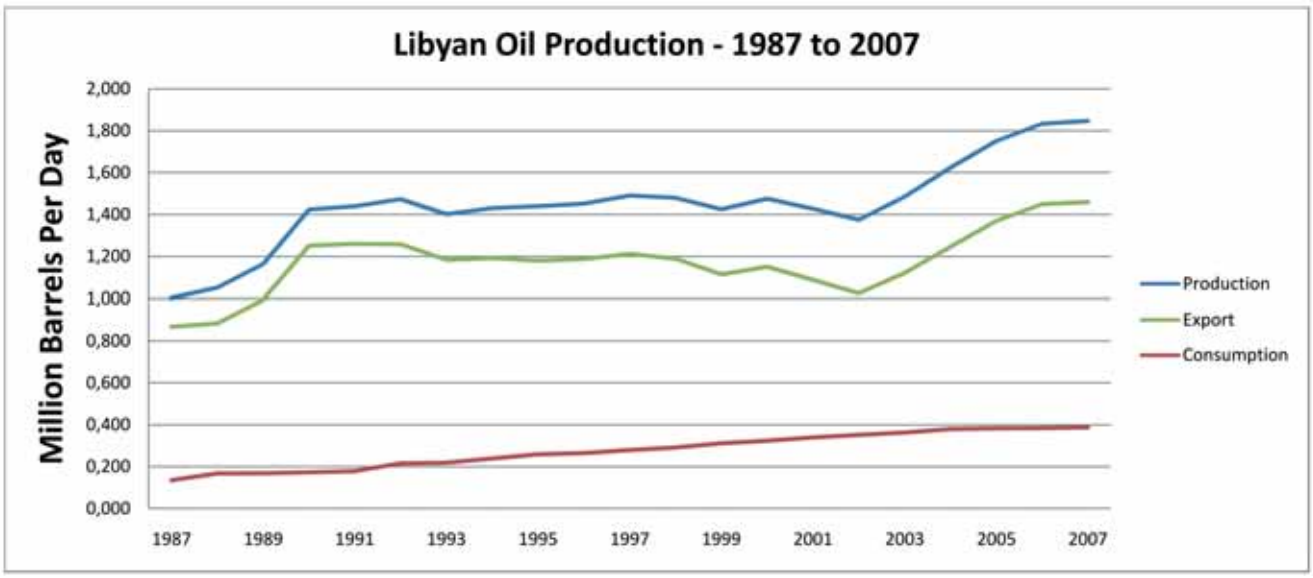

Table 8 - Libyan Oil Production (1987 to 2007)

A number of major discoveries have been recorded with Shell's Bonga and Chevron's Agbami field both estimated to hold one billion barrels each. These successes have turned the focus of Nigerian exploration into deep waters which remains a highly prospective area[20].

Kuwait

Kuwait produced 2.62 MMbbl/d in 2007 and consumed 0.28 MMbbl/d allowing it to export 2.34 MMbbl/d.

The Kuwait Petroleum Corporation (KPC) was founded in 1980 with the Government of Kuwait as its sole owner. It owns most of the oil and gas concerns in Kuwait such as the Shuaiba, Al Ahmadi and Mina Abdulla refineries. It is a shareholder, along with BP, of the Kuwait Oil Company (KOC) which produces approximately 2 MMbbl/d. KOC aims to increase production by developing more of the country's light oil and gas reserves in the Jurassic and Paleozoic formations respectively[21].

Iraq

Iraq's oil production fell severely from 2000, from 2.61 MMbbl/d to a low in 2003 of 1.34 MMbbl/d. Iraq's oil production, however, has regained capacity and it is worth noting that Iraqi E & P costs are amongst

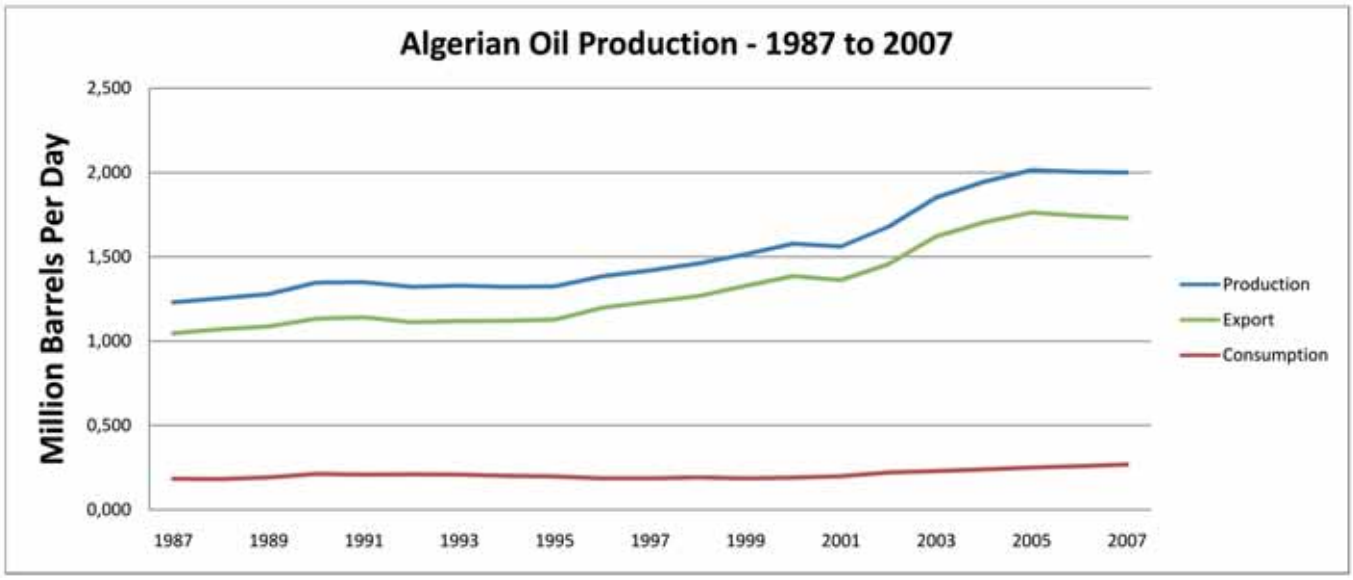

Table 9 - Algerian Oil Production (1987 to 2007)

the lowest in the world and, given the application of commonly available technology, the country has the potential to produce at far higher levels.

During 2007, Iraq produced 2.145 MMbbl/d and is estimated to have consumed 0.38 MMbbl/d. It is therefore estimated that Iraq exported 1.76 MMbbl/d[22]. Iraq has 115 billion barrels of proven oil reserves, placing it third worldwide after Saudi Arabia and Iran. Oil production in Iraq is concentrated in two oilfields: Rumaila which has 663 producing wells and Kirkuk which has 337 producing wells.

Libya

In 2007, Libya produced 1.85 MMbbl/d and was estimated to have consumed 0.30 MMbbl/d, thereby exporting 1.5 MMbbl/d[23].

Exploration onshore is concentrated in the Sirte, Murzuq and Ghadames Basins as well in the areas of Kufra and Cyrenaica.

Among Libya's largest onshore fields are the Amal field and the Gialo field, both with reserves of over four billion barrels of oil. Other large fields occur in the Sarir complex in southern Cyrenaica which is in the southeastern margin of the Upper Cretaceous-Tertiary Sirte Basin, which is one of the most highly productive oil basins in North Africa[24].

The majority of Libya's oil and gas is found onshore in three geological trends of the Sirte Basin. In the West, the known fields are Samah, Beida, Raguba, Dahra-Hofra and Bahi. In the north-centre of the country, there are the giant oilfields of Defa-Waha and Nasser and also the large Hateiba gas field and an easterly trend containing Sarir, Messla, Gialo, Bu Attifel, Intisar, Nafoora-Augila and Amal[25].

In early 2005, Libya held its first round of licences with Occidental, Woodside Petroleum, the UAE's Liwa and Petrobras gaining licences. The country continues to attract foreign investment and now has a relatively diverse E & P sector.

Algeria

In 2007, Algeria produced 2.0 MMbbl/d, consumed 0.27 MMbbl/d, and exported 1.73 MMbbl/d. Additionally, Algeria is an established Liquefied Natural Gas (LNG) exporter serving European and US markets.

The petroleum sector is dominated by the NOC Sonatrach which is owned by the Algerian government. Through its subsidiaries, the company has a domestic monopoly on oil production, refining, and transportation. Upstream activities, how-ever, are open to foreign companies, who must work in partnership with Sonatrach, with the company in question usually holding majority ownership in production-sharing agreements. The most notable of these companies are Anadarko, BHP, BP and Repsol[26]. Algeria's

> "OPEC decisions can equally affect oil exporting countries. OPEC decisions can influence oil price trends (other things remaining equal), which can affect the revenues realised by oil exporters."

Saharan Blend oil is a preferred sweet and light crude approximately 46° API. As of 2007, Algeria had 160 trillion cubic feet (Tcf) of proven natural gas reserves. Hassi Messaoud is the country's largest oilfield and is owned by Sonatrach with average production of 0.350 MMbbl/d of sweet and light 46° API crude. The Hassi Messaoud complex is reckoned to hold six billion barrels and is expected to provide approximately 0.7 MMbbl/d over the next five years. Sonatrach also operates the Hassi R'Mel field, which produced 0.18 MMbbl/d of 46.1° API crude. Anadarko produces approximately 0.5 MMbbl/d from the Hassi Berkine and Ourhound fields in eastern Algeria and is also developing further assets.

Major non-OPEC Producers

Major non-OPEC producer countries are the US, Russia, Mexico, China, Canada and Norway. The focus here, however, should be on producers that make significant oil exports after allowing for their national consumption: for example, in 2007 the US produced 6.9 MMbbl/d (8% of world crude oil) and China produced 3.7 MMbbl/d (4.8%. of world crude oil)[27]. These countries , however, consume far more than they produce. In 2007, oil consumption for the US was 20.7 MMbbl/d and for China 7.89 MMbbl/d, making these two countries the world's largest net oil importers. In the case of Canada, the oil produced was 3.30 MMbbl/d and consumption was 2.30 MMbbl/d, making net exports 1.0 MMbbl/d in 2007[28].

Consequently, after stripping out domestic consumption, significant non-OPEC* net oil exports lie in the hands of four countries: Russia, 7.28 MMbbl/d; Norway, 2.34 MMbbl/d; Mexico, 1.45 MMbbl/d; and, Kazakhstan, 1.27 MMbbl/d.

Considering net exports, the importance of OPEC exports becomes strikingly clear as ten of the world's major oil exporters (more than one MMbbl/d) belong to OPEC, a total which is roughly double that of the combined non-OPEC exports[29,30,31].

Non-OPEC and OPEC Major Net Exporters of Oil 2007

Non-OPEC oil production has risen in the past few years, notably from Russia which briefly displaced Saudi Arabia as the world's foremost crude oil producer in 2006 and from rising exports from central Asian states such as Kazakhstan[32]. It is recognised, however, that only Saudi Arabia retains the existing spare capacity required to meet the predicted total

> Non-OPEC reserves-to-production ratio – an indicator of how long proven reserves will last at current production rates – is approximately 26 years for non-OPEC.

world oil demand growth over the next five years. Other areas such as Offshore West Africa (Angola) and Offshore East Brazil are increasing production, with Brazil reaching a narrow margin of self-sufficiency in April 2006. Neither, however, is likely to make a major impact on world oil exports over the next decade especially considering the high costs associated with these deepwater developments[33].

A Wider OPEC?

It is often reported that the ripples of OPEC decisions are always most keenly felt by consumers 'at-the-pump' in importing countries; however, OPEC decisions can equally affect oil exporting countries. OPEC decisions can influence oil price trends (other things remaining equal), which can affect the revenues realised by oil exporters. This has been noted by certain non-OPEC countries which may see certain advantages of some degree of co-ordinated production policies with OPEC. Russia and Norway are two examples, although they have not always actually carried out co-ordination.

While the stated volumes of non-OPEC production (or export) restrictions have usually been small, the participation of these non-member countries can lead to accentuated effects as market analysts attribute value to such actions and can lead to even greater cohesion with OPEC in restricting output. In this way, the effect of wider co-ordination with OPEC policies is not often recognised[34]. High or increasing oil prices since 2000, however, have led non-OPEC to maximise production rather than restrict output. Whether intended or not, since 2000 there have been similar actions from OPEC and non-OPEC exporters. Since 2003, Mexico, Norway, Russia, Oman and Angola have all pushed to maintain or increase production in the high price environment. The peak prices of mid 2008 of US $147 and the subsequent collapse of oil prices to US $35 by the end of 2008 prompted dramatic production cuts from OPEC. Russia participated as an 'observer' in OPEC meetings, but made no production cuts.

World Oil Consumption

Of the 85.22 MMbbl/d of oil consumed worldwide in 2007, OPEC countries together consumed approximately 7.6 MMbbl/d, which again shows their importance in sustaining production. Of the world's top ten oil consumers in 2007, only Russia has significant net oil exports. The remaining top consumers are listed as the world's largest oil importers, with the exception of Brazil, which reached oil self-sufficiency in April 2006[35].

Estimates of proven oil reserves vary, but the essential fact remains that most of the world's proven oil reserves are held by OPEC. According to OPEC

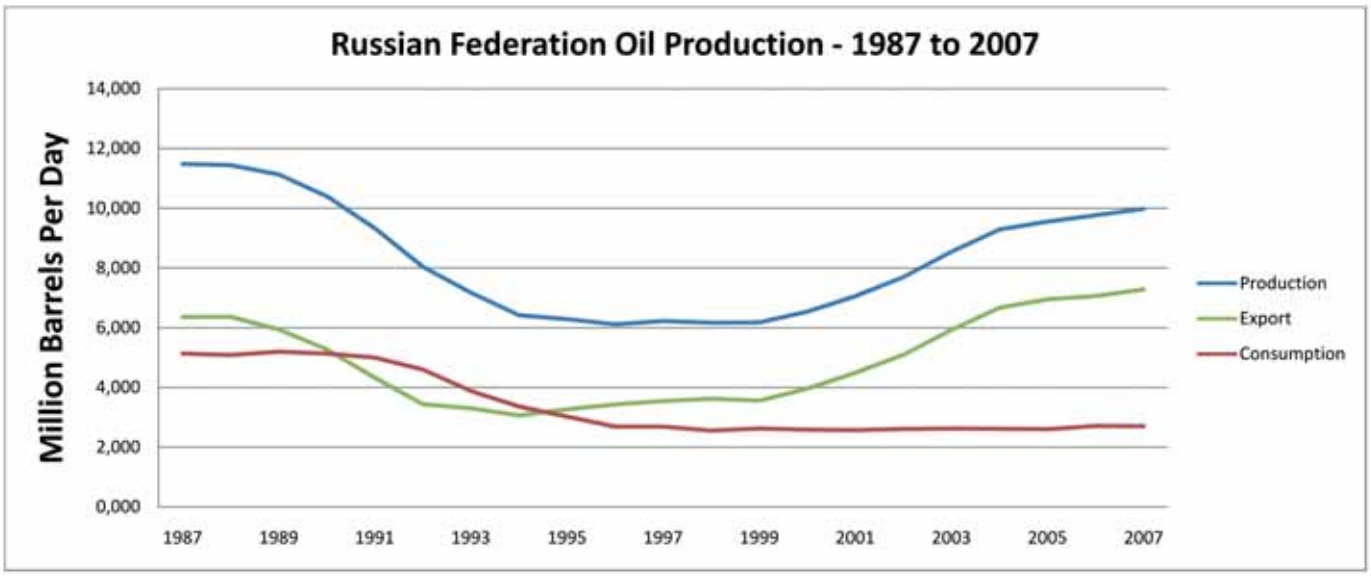

Table 10 - Russian Federation Oil Production (1987 to 2007)

statistics, world proven reserves are 1.15 trillion barrels of proven reserves, of which OPEC holds 0.9 trillion barrels[36]. According to BP's statistical review, world proved reserves are 1.2 trillion barrels, of which 0.9 trillion are held by OPEC[37] and 0.30 trillion are held by non-OPEC members. According to the US Energy Information Association (EIA) which bases it figures on the Oil and Gas Journal, total reserves are 1.3 trillion of which 0.85 trillion are held by OPEC[38]. The remaining reserves are split between Russian, the Former Soviet Union (FSU) and Canada.

Non-OPEC reserves include Canadian unconventional reserves which have higher production costs[39]. In the future, the inclusion of unconventional oil reserves for other countries may positively affect OPEC member Venezuela, as well as non-OPEC countries such as Canada, Brazil and Australia. The reserves of non-OPEC countries are being depleted more rapidly than OPEC reserves. Non-OPEC reserves-to-production ratio – an indicator of how long proven reserves will last at current production rates – is approximately 26 years for non-OPEC. OPEC reserves-to-production is 73 years based on 2007 crude oil production rates. Combining the longer reserves life and the high net oil exports figures, it is clear to see just how important OPEC production is over the long term[40].

Refinery Capacity

Countries that have high petroleum demand tend to have large refinery capacities due to proximity to end consumers. Exemplifying this, the US is the world's largest consumer and has the highest refinery capacity in the world, with 20% of the world's crude oil refinery capacity (17.59 MMbbl/d of a total 87.91 MMbbl/d).

Russia's refinery capacity stands at an estimated 5.58 MMbbl/d. Japan (4.56 MMbbl/d) and China (7.5 MMbbl/d) are the only remaining countries with refinery capacities exceeding 3 MMbbl/d[41]. There are several countries that are important to world trade in refined petroleum products despite very low (or non-existent) levels of crude oil production. For instance, Caribbean nations (including US and European territories) have very limited oil production (233,000 bbl/d in 2007), but a refinery capacity of about 2.6 MMbbl/d. Much of this refined product is exported to the US[42].

Review of Major Non-OPEC Oil Exporters

Russia

Russia produced 9.98 MMbbl/d in 2007 and consumed 2.7 MMbbl/d in the same period. The country therefore exported 7.28 MMbbl/d during 2007 making it the second largest oil exporter after Saudi Arabia.

> Central to Rosneft's cash flow and portfolio is Yuganskneftegaz, which represents approximately two thirds of the company's annual oil production and over 70% of its proved SPE oil reserves.

After the break-up of the Soviet Union in the early 1990s, the nature of the Russian oil industry changed dramatically. From being geographically dispersed and technically fragmented with numerous state-owned entities, the State set about vertically integrating these companies in the likeness of IOCs. Behind the scenes inter-related forces were at work. Central Asian states such as Kazakhstan became sovereign nations and were developing their respective oil and gas industries rapidly and independently. These Central Asian Republics had succeeded in attracting and retaining oil and gas investment capital. The Russian government acted to restructure its own industry, not only to attract investment, but also to integrate its NOCs so that they could compete both at home and overseas. It also acted to counter market volatility by channelling windfall oil revenues into a stabilisation fund that came into effect in 2004[42].

Today, several Russian oil companies compete globally and the stabilisation fund is believed to be worth almost US $60 billion—approximately 7.5 percent of the country's Gross Domestic Product (GDP). Taxes on oil exports have been raised significantly and private oil companies complain that the higher export taxes are hindering efficient allocation of profits into exploration and development[43].

The decision to develop Shtokman without foreign partners is a signal as strong as any of Russia's move toward nationalisation and emergence as an independent energy power. IOCs such as Chevron, ConocoPhilips, Total and Norwegian company StatoilHydro were excluded from the development and this came as a surprise as it was commonly thought that partnership with a foreign company would occur, especially one with technical expertise, in the harsh conditions of the Barents Sea[44].

Major Russian oil companies that have majority state holdings are Rosneft, Gazprom, Transneft and Rosgas. Other privately-owned companies such as Lukoil are locally owned, while TNK is a BP owned venture and Sakhalin Energy is a consortium of major oil companies.

Rosneft

Rosneft's E & P efforts have been growing steadily and were strengthened by the US $9.3 billion acquisition of Yuganskneftegaz (ex-Yukos), which established the company's proved oil and gas reserves at 21.69 billion barrels of oil equivalent (boe) in 2007 (including gas condensates and gas). Rosneft is also the world's seventh largest producer (in comparison to publicly traded oil companies) and Russia's second largest producer. Average daily output in 2007 was 2 MMbbl/d[45].

Central to Rosneft's cash flow and portfolio is Yuganskneftegaz, which represents approximately two

> Gazprom and its producing subsidiaries hold more than 40 oilfield exploration and development licences in the West Siberian petroleum basin, as well as in Omsk and Tomsk in Chukotka.

thirds of the company's annual oil production and over 70% of its proved SPE oil reserves. Purneftegaz is Rosneft's second largest production asset. With large non-associated natural gas reserves at the Kharampur field, it is likely to increase in importance as Rosneft seeks to further monetise its gas reserves. Additional exploration in the Timano-Pechora oil province and expanded export capacity at the Arkhangelsk terminal have helped Rosneft grow[46].

Rosneft holds more than a third of Sakhalin's total offshore oil and gas resources. It holds sizeable stakes in all five stages of development. While still at the early stages of exploration, it holds stakes in the Sakhalin-3, Sakhalin-4 and Sakhalin-5 of 49.8%, 51% and 51%, respectively. Rosneft holds a stake in the Sakhalin-1 project, which is currently being developed under a Production Sharing Agreement (PSA) implemented in 1996 with ExxonMobil and Sodeco of Japan (and, since 2001, with India's ONGC). Sakhalin-1 began oil and gas production in late 2005 and is anticipated to experience substantial growth over the next several years[47].

Rosneft also holds interests in Eastern Siberia, in the form of the Vankor field in Krasnoyarsk and with TNK-BP, the Verkhnechonsk field in the Irkutsk. Other resources on the Black Sea shelf, Sea of Azov and the Kurmangazy structure in Kazakhstan could help the company's future plans for growth[48].

Gazprom

In 2007, GazpromNeft's oil production was 660,000 bbl/d. It comprises nearly half a million shareholders with the Russian Federation controlling a majority of 50.002%. According to the company, it employs some 300,000 people in different operations[49]. Gazprom and its producing subsidiaries hold more than 40 oilfield exploration and development licences in the West Siberian petroleum basin, as well as in Omsk and Tomsk in Chukotka. It acquired Sibneft which has 80% of its reserves concentrated in Noyabr'sk with four large fields – Sugmutskoye, Sutorminskoye, Vyngapurovskoye and Sporyshevskoye – accounting for nearly 50% of Sibneft's reserves. Sibneft was also active in upstream oilfield services and is active in the geophysical arena through OJSC Noyabr'skneftegazgeophysica – a geophysical services company that offers borehole logging, perforation and seismic data preparation[50]. During recent years, Sibneft has spun-off several service companies that were formerly production divisions including Service Drilling Company LLC and Well Workover Service Company LLC. These service companies compete with

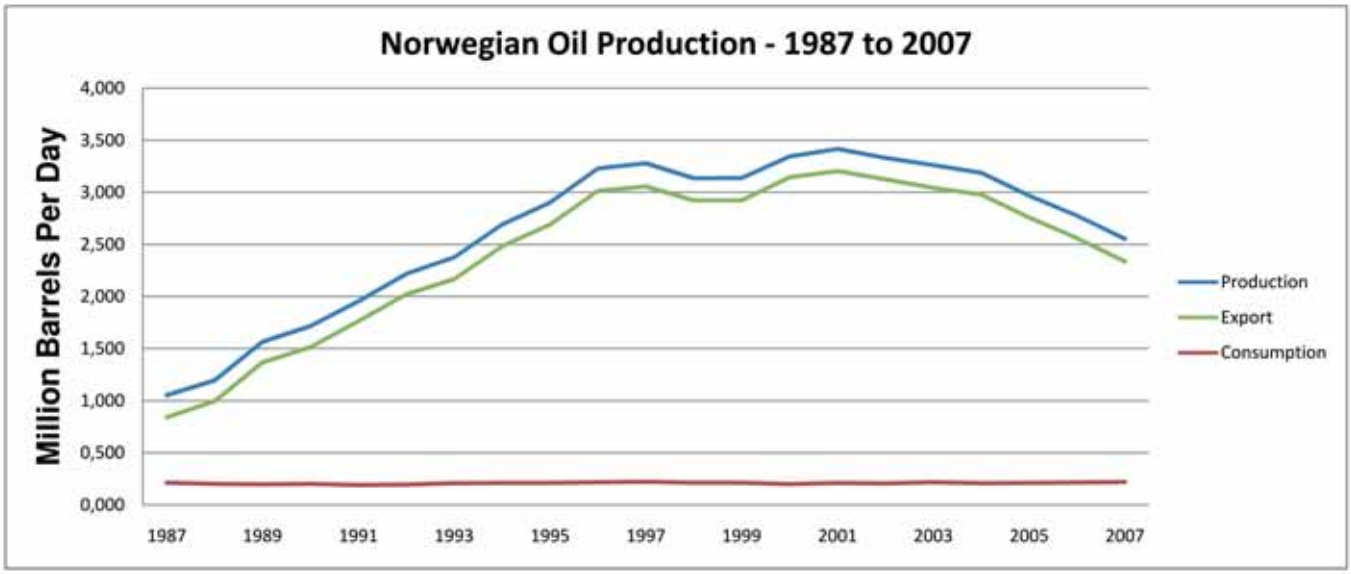

Table 11 - Norwegian Oil Production (1987 to 2007)

other Russian and international drilling and service contractors, providing drilling and well work over services[51].

Gazprom – Natural Gas

Russia has the largest natural gas reserves in the world, 1.58 trillion cubic feet (Tcf). In 2007, Russia was the world's largest natural gas producer (58.8 billion cubic feet [Bcf]), as well as the world's largest exporter (16.3 Bcf)[52].

Russia's natural gas infrastructure, however, needs updating and its natural gas industry has not experienced the success of its oil industry, with limited growth in gas production and consumption[53].

Three major fields in Western Siberia – Urengoy, Yamburg, and Medvezh'ye – comprise more than 70% of Gazprom's total natural gas production, but these fields are now in decline. Although the company projects increases in its natural gas output between 2008 and 2030, most of Russia's natural gas production growth will come from independent gas companies such as Novatek, Itera and Northgaz. Barents Sea Exploration of the Russian Barents Sea began in the 1970s and to date discoveries in the area consist of ten significant gas and condensate fields, as well as a total of 125 identified fields or potential structures. Total reserves are estimated between five and ten trillion cubic metres[54].

The largest deposit is the Shtokman (Shtockmanovskoye) gas and condensate field, discovered in 1988, with total reserves of 3 trillion m^3, and with estimated recoverable reserves (C1+C2) of 2.5 trillion m^3. Gazprom plans to develop the Shtokman field on its own and expects it to become the resource base for the export of gas to Europe through the Nord Stream pipeline (which is currently under construction)[55]. The energy resources of north-west Russia remain largely unexploited. The total hydrocarbon resources of the Russian Arctic shelf are estimated at about 100 billion tonnes of oil equivalent (toe). The natural gas reserves in north-west Russia form the most important strategic energy resource in the region. Estimates placed on Barents Sea reserves vary from 2 trillion m^3 to 5 trillion m^3. In any event, these reserves offer a major supply contribution to European energy needs. In addition, it is expected that there are also oil deposits in the eastern and northern areas of the Barents Sea. Furthermore, the so-called 'grey zone', formed by the sea boundary claims of Norway and Russia, is considered a promising gas or oil province.

The Timan-Pechora oil and gas region has estimated total oil resources of over 4,800 million tonnes, of

> The United Kingdom is the largest importer of Norway's oil and gas having imported 814,500 bbl/d from Norway, or 34 % of Norway's 2007 total exports.

which over 1,400 million tonnes is estimated to be recoverable. The Republic of Komi has 520 million tonnes of oil resources. Perhaps the most significant deposit found in the Pechora Sea is the Prirazlomnoye oil field, with estimated reserves of 56-62 million tonnes. The licence for the development of the field is held by JSC Rosshelf, and the Australian company BHP is participating in the development of this field. The exploration of Barents Sea oil resources is still at an early stage[56].

The Timan-Pechora province is considered the third most important oil producer of the Russian Federation, and there is a significant development potential in the area. If the above-mentioned oil reserves are compared world-wide, they are equivalent to Norway's North Sea reserves; however, most of the approximately 200 fields in the region are quite small. Gas reserves are rather small compared to the Barents Sea reserves, for example, which means that they are mainly of local importance[57].

Transneft Russia needs to expand export capacity for its oil and gas in order to monetise growing production. Crude oil exports via pipelines, however, are under the jurisdiction of Russia's state-owned Transneft. The Transneft system cannot meet export needs with an excess of approximately three million barrels of its total seven million barrels transported by road, rail and river routes[58]. This means substantial investments must be made to ensure growing levels of production can reach the markets, especially foreign ones.

Several proposed oil pipeline routes and pipeline expansion projects are planned including the Baltic Pipeline System (BPS), which carries crude oil from Russia's West Siberian and Timan-Pechora oil provinces westward to the newly completed port of Primorsk in the Russian Gulf of Finland[59].

Sakhalin Island

Several IOCs entered into PSAs to develop the resources in Sakhalin Island, Okhotsk Sea (see *Chapter 8: Extreme E & P*). Oil reserves in the area are estimated at around 14 billion barrels, and natural gas reserves at approximately 2.6 trillion cubic metres[60].
The Sakhalin-1 project was led by Exxon Neftegaz, in conjunction with consortium members SODECO, ONGC Videsh, Sakhalinmorneftegaz and RN Astra. The Sakhalin-2 project was developed by Shell, Mitsubishi and Mitsui, and entails the development of Russia's first LNG facility to be built on the southern tip of the island. Sakhalin-2 will also be used to supply natural gas to the United States, Korea and Japan in 2008. Sakhalin 3-6, North and South East of Sakhalin Island, are at the planning stages of development[61].

> Most of the Barents Sea is unexplored and activity there will always be subject to high costs associated with a harsh offshore area and environmental concerns as the seas have abundant fish stocks and are considered unpolluted.

Norway

Norway had 8.2 billion barrels of proven oil reserves at the end of 2007, the largest in Western Europe. Norway's oil reserves are located offshore on the Norwegian Continental Shelf (NCS), which is divided into the North Sea, the Norwegian Sea and the Barents Sea[62].

Oil and Gas Exports

Norway produced 2.56 MMbbl/d in 2007 and consumed 221,000 bbl/d in the same period. The country therefore exported 2.34 MMbbl/d during 2007. Norway has significantly increased its natural gas production; in 2007 it produced 8.7 bcf and consumed 0.4 bcf[63].

The United Kingdom is the largest importer of Norway's oil and gas having imported 814,500 bbl/d from Norway, or 34 % of Norway's 2007 total exports.

In contrast to its maritime neighbour, the UK, Norway's government holds a dominant stake in the oil sector and controls 66.42% of StatoilHydro (the remainder of the shares are owned by international, institutional and private stockholders)[64].

StatoilHydro itself holds more than 80% of Norway's oil and gas production. Additionally, Norway's government owns approximately 40% of the country's total oil production through the State Direct Financial Interest (SDFI). State-owned Petoro administers these ownership interests, while StatoilHydro is responsible for managing actual production from SDFI assets[65].

IOCs do have a sizeable presence in the NCS, but they must act in partnership with StatoilHydro. The largest private oil producers in Norway are ConocoPhillips, ExxonMobil and BP. Petoro is the state limited company which is responsible for managing, on behalf of the government, SDFI[66].

While the state has the ownership of the SDFI's assets, Petoro acts as the licencee in production licences, pipelines and land-based plants on behalf of the government. The primary objective of Petoro's administration of the SDFI portfolio is to achieve the highest possible income for the state. The SDFI arrangement involves the state paying a share of all investments and operating costs in projects which correspond to its direct financial interest. On the same terms as the other owners, the government then

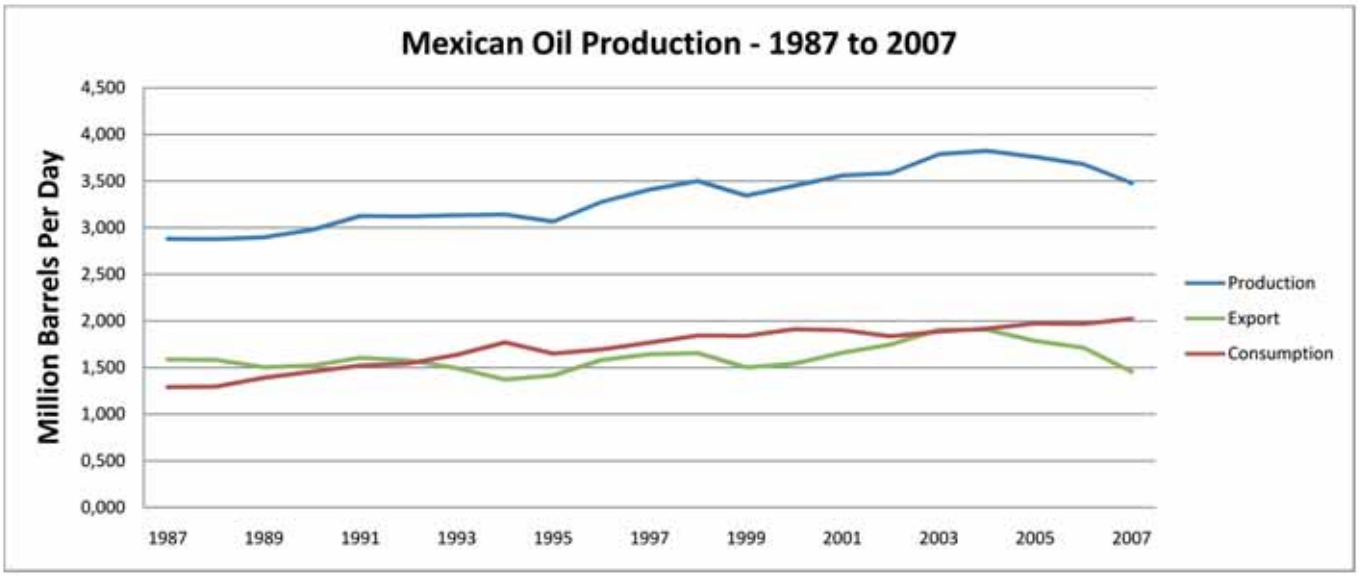

Table 12 - Mexican Oil Production (1987 to 2007)

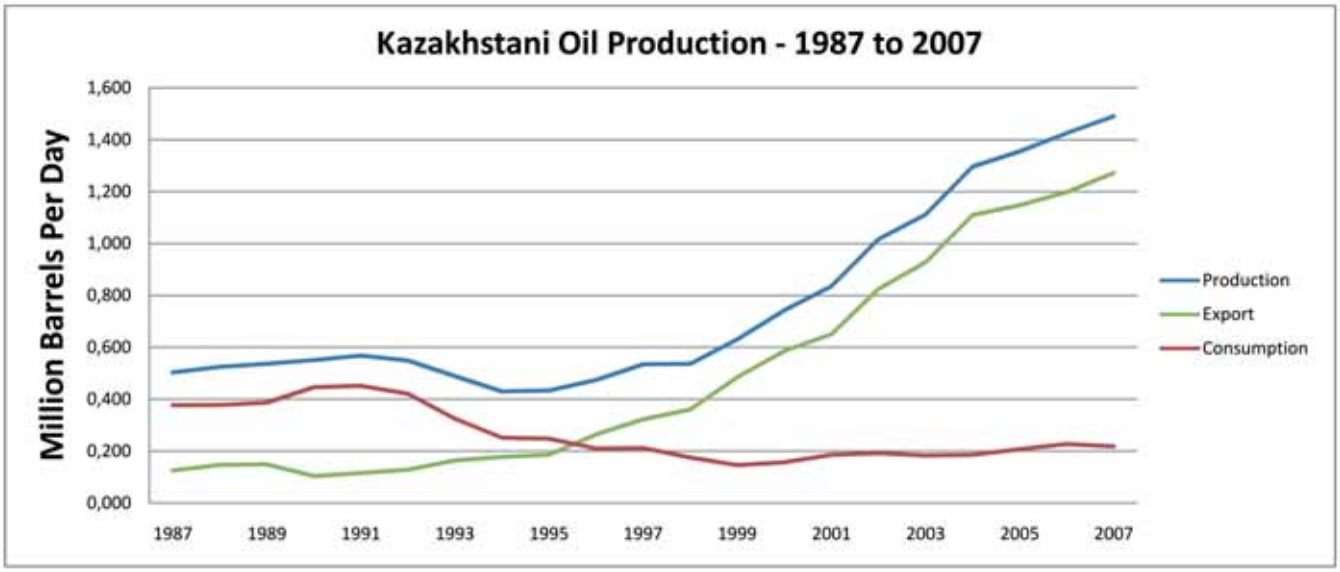

Table 13 - Kazakhstani Oil Production (1987 to 2007)

receives a matching share of revenues from the sale of production and other income sources.

The licencees, and in particular the operator, are responsible for developing discoveries which are made within the boundaries of a licence. Should there be a need for research and technology development to overcome technological challenges in developing the discovery, the tax system provides favourable conditions to ease the burden of such efforts. Relevant expenditures on research are fully deductible against tax and there is a special tax scheme aimed at stimulating research and development in industry ('Skattefunn').

Due to the nature of oil exploration and production in the NCS, the region has traditionally been accessible only by international oil majors. Because of harsh weather and operating conditions, projects in the NCS require sizable initial investments. Further, the structure of Norway's petroleum taxes means that smaller, marginal fields often are not profitable. Finally, stringent environmental, safety, and labour regulations further increase operating costs[67].

Technology Development

The Ministry in Norway funds petroleum-related research programmes which are administered by the

> The Caspian Sea contains six separate hydrocarbon basins and has attracted much foreign investment as most of its oil and natural gas reserves are undeveloped and unexplored with the notable exception of Kashagan, which is the flagship project in the North Caspian Sea.

Norwegian Research Council. The two most important programmes are called Petromaks and Demo 2000. Petromaks deals with basic and applied research and Demo 2000 covers the demonstration/application of new technology. The main aim of both programmes is to increase value creation on the Norwegian Continental Shelf and to increase the export of Norwegian oil and gas technology. The Ministry has also established OG 21, 'Oil and Gas in the 21st Century', which provides overall guidance on priorities for the public research and technology programmes, as well as for related activities in universities, research institutes and industry through a comprehensive national R & D strategy. The OG 21 board consists of members from oil companies, the supply industry, research institutions and academia. The implementation of the OG 21 strategy is largely based on the activities of the Petromaks and Demo 2000 programmes and on joint industry projects[68].

As with any development project on the Norwegian Continental Shelf, the Ormen Lange and Snøhvit developments have been driven by commercial interests. The Ministry's role in development projects is to coordinate the administrative procedures and approval processes, ensuring that the projects comply with sound resource management practice, as well as balancing all interests with regard to value creation, environmental concerns and the fisheries. With regard to Snøhvit, minor tax regime adjustments were made to facilitate the development of the LNG projects[69].

Production

The bulk of Norway's oil production occurs in the North Sea, with smaller amounts in the Norwegian Sea. In 2007, LNG production of the Snøhvit field was scheduled to commence which brought development to Hammerfest. Most of the Barents Sea is unexplored and activity there will always be subject to high costs associated with a harsh offshore area and environmental concerns as the seas have abundant fish stocks and are considered unpolluted. The Barents Sea is likely to contain oil and gas reserves, but the

> Kazakhstan's reserves are very much a work-in-progress as the country is relatively unexplored and untapped.

question remains one of delineation. To this end, the Norwegian government has restarted licensing in the Barents Sea and companies such as StatoilHydro are looking keenly to what some consider as a new frontier for the Norwegian Petroleum Industry[70].

Exploration and Production

Norwegian oil production rose dramatically from 1980 until the mid-1990s, remained flat since (see Table 11) and has now started to decline. During the first six months of 2005, for example, Norway's oil production averaged 2.95 MMbbl/d, while in 2007 the average figure was 2.55 MMbbl/d. As North Sea fields continue to mature, Norwegian oil production will focus on mature fields, though it is expected that new developments in the Barents Sea will offset some of this decline.

One of the largest oil fields in Norway is the Troll complex operated by StatoilHydro. Other important fields include Ekofisk (ConocoPhillips), Snorre (StatoilHydro), Oseberg (StatoilHydro), and Draugen (Shell). ConocoPhillips, ExxonMobil and BP operate oilfields in Norway. There is a great emphasis on increasing production from existing projects, including the incorporation of smaller satellite fields that will take advantage of the existing infrastructure[71].

As was the case with the United Kingdom, however, many oil majors have begun to withdraw from the NCS in order to pursue projects in high-growth regions. StatoilHydro have begun to sell NCS interests in order to pursue projects in Latin America and Africa.

Mexico

Pemex (Petróleos Mexicanos) was created as a result of the 1938 Mexican President Cardenas' nationalisation of the oil industry.

Today, the company is responsible for all petroleum production in Mexico which is 3.48 MMbbl/d (2.02 MMbbl/d consumption) and 4.5 bcf of gas production (5.2 bcf consumption). The United States is the destination of over 70% of Mexico's 1.46 MMbbl/d exports[72].

A highly prospective area for Mexico are the Mexican waters of the 'Gulf of Mexico' or GOM which to date have only been developed within the US territorial jurisdiction. Mexico's reservoirs are mostly high permeability limestone reservoirs, while the US tends to be lower permeability sandstones. This in part accounts for the higher average Pemex production well rates of approximately 6000 bbl/d per well. The onshore Burgos Basin on the Mexico-U.S. border shares similar gas prone characteristics with its onshore South Texas neighbours[73].

Mexico must prove its deeper GOM trends and in recent times has issued new discoveries such as Noxal. It has been said that it could be a difficult and longwinded task for Mexico to develop its own deepwater expertise,

but this argument fails to recognise that many service provisions could be made by service and supply companies rather than oil companies. However, by bringing in reputed deepwater oil companies, the best development strategies could be applied to the GOM Mexican deepwaters.

Kazakhstan

The Caspian Sea contains six separate hydrocarbon basins and has attracted much foreign investment as most of its oil and natural gas reserves are undeveloped and unexplored with the notable exception of Kashagan, which is the flagship project in the North Caspian Sea. High prospectivity is the cause of interest in the Caspian Sea region, but for net oil exports Kazakhstan alone is relevant (although Azerbaijan and Turkmenistan are worth noting for future production growth)[74].

Kazakhstan produced 1.49 MMbbl/d in 2007 and consumed 219,000 bbl/d in the same period. The country therefore exported 1.27 MMbbl/d during 2007.

Proven Kazakhstani oil reserves are 39.8 billion barrels (defined as oil and natural gas deposits that are considered 90% probable) and gas reserves are 67.2 Tcf. The figure for the Caspian sea is much higher but is split between several states. Kazakhstan's reserves are very much a work-in-progress as the country is relatively unexplored and untapped. Even relatively high-profile Kashagan does not have any final proven oil reserves figures as it is still undergoing appraisal and exploratory well drilling. After Russia, Kazakhstan was the largest oil-producing republic in the Soviet Union and has successfully attracted foreign investment in its oil sector to increase oil production to 1.49 MMbbl/d in 2007, most of which came from two large onshore fields (Tengiz, and Karachaganak) and the offshore complex of Kashagan which is still under appraisal and first oil is not expected before 2011. The Tengiz oil field is estimated to contain recoverable oil reserves of six to nine billion barrels. The Kashagan complex has an unitisation agreement that covers the Kalamkas, Aktoty and Kairan blocks[75]. North Caspian Operating Company (partners include ExxonMobil, Shell, Total, Eni, ConocoPhillips, Inpex and National Oil Company KazMunaiGas) is developing the Kashagan complex. The field was discovered in June 2000, when the first exploration well (KE-1) was drilled with 13 billion tonnes of oil potentially recoverable with the use of gas re-injection[76].

Now that we have in-depth knowledge of where our oil and gas resources are located, we need to think about how one actually gets access to these resources. Does one need to buy the land from those who own it? Are there procedures and policies in place that need to be followed? What are the legal requirements? Who can actually acquire oil or gas fields? Who are the major players in this area?

References

1. BP Statistical Review 2008 page 8.

2. Considering the contributions oil revenues make to GDP

3. Concerns regarding commercialisation and profitability are the main reasons why insufficient refining capacity.

4. The GECF was widely covered in the press.

5. BP Statistical Review 2008 defined as proved reserves.

6. Saudi Aramco Annual Report 2008. For specifics of technologies see editions of Saudi Aramco Journal of Technology.

7. King Abdullah University of Science and Technology (KAUST) is being built in Saudi Arabia as an international, graduate-level research university dedicated to inspiring a new age of scientific achievement in the Kingdom that will also benefit the region and the world. KAUST will be merit-based and will recruit men and women from around the world.

8. BP Statistical Review 2008 page 8.

9. EIA/IEO www.eia.doe.gov/pub/oil_gas/petroleum/analysis_publications/oil_market_basics/supply

10. BP Statistical Review 2008 page 8.

11. BP Statistical Review 2008 page 11.

12. Rice University Energy Study: Latin America the Orinoco Heavy Oil Belt in Venezuela (Heavy Oil To The Rescue?) Manik Talwani Schlumberger Professor of Earth Science.

13. EIA/IEO www.eia.doe.gov/pub/oil_gas/petroleum/analysis_publications/oil_market_basics/supply

14. PdVSA Annual Report 2008.

15. BP Statistical Review 2008 page 8.

16. Oil wealth has undoubtedly helped the UAE especially Abu Dhabi secure commercial growth.

17 See Dubai's Strategic Plan

18. BP Statistical Review 2008 page 8.

19 See Niger Delta Development Commission Master Plan 2001 which states 'There have been many attempts and many plans made in the past to improve the lives of the people of the Niger Delta Region of Nigeria. Sadly, each ended with very little to show for the time and resources spent. Therefore it is understandable that the people of the Niger Delta are quite disillusioned with 'plans' at this time. The disenchantment of the people not withstanding, it must be stated that the Niger Delta Master Plan is different in its goals, focus and approach, and will not suffer the fate of the others before it'.

20. Depositional Control on Hydrocarbon Accumulations in Deepwater Nigeria By Xijin (CJ) Liu Conoco Phillips Search and Discovery Article #40226 (2006)

21. Kuwait Petroleum Corporation (KPC) Annual Report 2008.

22. Any number for consumption will be controversial for those who require an explanation see "Scramble to carve up Iraqi oil reserves lies behind US diplomacy," Observer, October 6, 2002.

23. BP Statistical Review 2008 page 8.

24. Sarir, Sirte Basin, Desert Surprise Then and Now Some Keys to Revisit of Libya Compiled from articles by C. J. Lewis (1990) and R. M. Sanford (1970).

25. Framework for the Exploration of Libya: An Illustrated Summary Compiled by Jingyao Gong.

26. Sonatrach Annual Report 2007.

27. BP Statistical Review 2008 page 8.

28. Idem.

29. Idem.

30. OPEC Annual Statistical Bulletin 2008.

31. EIA IEO 2008 outlook.

32. EIA IEO 2008 outlook states Kazhakstan as exporter to note.

33. The deepwater developments are particularly susceptible to the low oil price environment.

34. Perhaps wider co-ordination is simply due to market forces.

35. See Brazil Oil and Gas Issue 3 – Petrobras and Self Sufficiency (www.braziloilandgas.com/issue3).

36. BP Statistical Review 2008 page 8.

37. OPEC Annual Statistical Bulletin 2008.

38. EIA IEO 2008.

39. This is a well known fact regarding Canadian Tar Sands.

40. There is no doubt regarding OPEC's future importance.

41. BP Statistical Review 2008 page 18.

42. Idem.

43. The Stabilization fund of the Russian Federation was established on January 1, 2004 as a part of the federal budget to balance the books in the event of the oil price falling below a cut-off price, currently set at US $27 per barrel. Furthermore, the Fund is to serve as an important tool for absorbing excessive liquidity, reducing inflationary pressure and insulating the economy from the volatility of export earnings.

44. Widely reported in the press.

45. Rosneft Annual Report 2008 converted from tonnes.

46. Ditto above.

47. Sakhalin Report 2006.

48. Rosneft Annual Report 2008.

49. GazpromNeft Annual Report 2008.

50. OJSC Noyabrskneftegazgeophysica—Company

Profile 2006.

51. Sibneft Annual Report 2005.

52. GazpromNeft Annual Report 2008.

53. Recently Russia is investing more in its Gas infrastructure.

54. Offshore Magazine Feb 1997 RUSSIA Barents Sea still languishing in political limbo Gazprom, Rosshelf, and partners predicting production post-2000 Dev George Managing Editor.

55. Nordstream Facts Newsletter Issue 9/1—2009.

56. Barents Sea field delineated 2008-12-08 StatoilHydro.

57. Idem.

58. CGES Pipeline Advisory Service bulletin No. 23 2006 6th November 2006.

59. Baltic Pipeline System (BPS) was built to transport the crude from fields in Western Siberian, Timan-Pechora and Volga-Urals petroleum provinces to a terminal on the coast of the Gulf of Finland for export. The system includes an existing oil pipeline, which links Haryaga and Usa, trunk pipelines from Usa to Ukhta to Yaroslavl to Kirishi, new trunk pipelines between Haryaga and Usa and between Kirishi the coast of the Gulf of Finalnd, and finally the new oil export terminal in the city of Primorsk.

60. The Federation of Russian States Oil and Gas Activity and Concession Map—2nd Edition —2007.

61. Sakhalin-1 Project Receives Award for Excellence from International Petroleum Technology Conference Kuala Lumpur, December 3, 2008.

62. The Norwegian Petroleum Directorate is administratively subject to the Ministry of Petroleum and Energy, and advises the Ministry on matters concerning the management of the petroleum resources on the Norwegian continental shelf. The Directorate holds all the important data in connection with the petroleum activity in Norway, including a complete, up-to-date survey of resources, production, costs and other relevant information.

63. BP Statistical Review 2008 page 8.

64. Norway StatoilHydro shareholders.

http://www.statoilhydro.com/en/InvestorCentre/Share/Shareholders/Top20/Pages/default.aspx

65. Petter Osmundsen Commitment at home and abroad 30.4.2007 Merging Statoil and Hydro's petroleum business will benefit the international involvement of the new company, since size is significant in this business. But any reduction in activity on the NCS would be a very poor socio-economic outcome for Norway.

66. See Petoro Perspective Sveinun Sletten. The Norwegian government has been involved as an owner from the early days of the country's oil adventure – through Statoil and Hydro. And from 1985 also through the State's Direct Financial Interest (SDFI).

67. The Norwegian Petroleum Directorate shall contribute to creating the greatest possible values for society from the oil and gas activities by means of prudent resource management based on safety, emergency preparedness and safeguarding of external environment.

68. The Research Council for Norway, Funding for Petroleum Research Adviser Tor-Petter Johnsen PETROMAKS.

69. Offshore Magazine April 2002 Norway: NKr 46 billion Snøhvit scheme brings LNG to northern Norway By Nick Tedre, Contributing Editor.

70. StatoilHydro Annual Report 2008.

71. 2000 NWECS Report by Wajid Rasheed.

72. BP Statistical Review 2008 page 8.

73. US Country Analysis Brief of Mexico http://www.eia.doe.gov/emeu/cabs/mexico.html

74. US EIA DOE Caspian Sea Analysis Report January 2007.

75. Authors discussion with Kazhak expert.

76. See www.eia.doe.gov/emeu/cabs/Kazakhstan/pdf

Saudi Arabia oil & gas

www.saudiarabiaoilandgas.com

Contribute to Saudi Arabia Oil & Gas during 2012

EPRasheed is looking for editorial submissions on the topics outlined in the editorial calendar. This can provide your company with the opportunity to communicate EP technology to the wider oil and gas community.

Please send abstracts or ideas for editorial to **wajid.rasheed@eprasheed.com**

Preference is given to articles that are Oil Company co-authored, peer reviewed or those based on Academic research.

Editorial 2012 Calendar

Jan/Feb	Mar/Apr	May/Jun	Jul/Aug	Sep/Oct	Nov/Dec
Ad Closing: 2 Jan 2011 **Materials Closing:** 9 Jan 2011	**Ad Closing:** 6 March 2012 **Materials Closing:** 13 March 2012	**Ad Closing:** 21 April 2012 **Materials Closing:** 28 April 2012	**Ad Closing:** 4 July 2012 **Materials Closing:** 11 July 2012	**Ad Closing:** 30 August 2012 **Materials Closing:** 31 August 2012	**Ad Closing:** 6 October 2012 **Materials Closing:** 13 October 2012
• New Stimulation Technology • Advances in Drilling Technology • Smart Reservoirs • Deep Diagnostics & Reservoir Mapping • Geosciences • E&P Software Solutions for Asset, Field and Well Management	• Intelligent Fields • Oil Field Automation and Optimization • Extreme Reservoir Contact • Seismic • Near Surface • Wide Azimuth • Near Surface Resolution	• Integration in Upstream • Shale Gas Developments • Shale Gas Technology Challenges • Real Time Operations • I Field • Drilling Automation	• Deep Water Red Sea Challenges • Assessment of KSA & IOCs Gas Exploration Initiatives • KSA Upstream Research & Development • KFUPM Techno Valley • Tight Gas Technology Development	• KSA Offshore Gas Development Projects (Karan, Wasit, Arabia, etc....) • Smart Water Chemistry in Carbonate Recovery	• Maximizing Sweep Efficiency in Heterogeneous Carbonate Reservoir Using Advanced Intelligent Completion Technology • Red Sea Salt Challenges
Issue 24 *'Deep Diagnostics'*	**Issue 25** *'The Intelligent Field'*	**Issue 26** *'Shale Gas'* '	**Issue 27** *'Red Sea Challenges'*	**Issue 28** *Offshore Gas'*	**Issue 29** *'Maximising Sweep Efficiency'*
BONUS CIRCULATION					
10th Middle East Geosciences Conference & Exhibition* 4-7 March 2012 Bahrain	**SPE/IADC Drilling Conference** 6-8 March 2012 San Diego California USA **SPE/DGS Annual Technical Symposium & Exhibition*** 8-11 April 2012 Khobar Saudi Arabia **Offshore Technology Conference** 30 April - 3 May 2012 Houston, Texas USA	**The 8th Middle East Refining & Petrochemicals Conference & Exhbition** 20-23 May 2012 Manama Bahrain			**SPE Annual Technical Conference and Exhibition** 8-10 October 2012 San Antonio Texas, USA
SPECIAL PUBLICATIONS					
* Official Technical Magazine	** Official Saudi Magazine	* Official Technical Magazine			* Media Partner

Dielectric Scanner

MULTIFREQUENCY DIELECTRIC
DISPERSION SERVICE

It Speaks **Volumes**

about Carbonates, Shaly Sands, and Heavy Oil

Radial profiling identifies an additional 150 ft of movable heavy oil in Orinoco thinly bedded sands and shales that was not visible with resistivity-based interpretation.

Get the full story about this and other case studies at **www.slb.com/ds**

Global Expertise
Innovative Technology
Measurable Impact

Schlumberger